

学位論文

Study on New Reduction Methods of Graphene Oxide
(酸化グラフェンの新しい還元手法に関する研究)

平成25年12月 博士（理学）申請

東京大学大学院理学系研究科

化学専攻

田中 弘成

Abstract

Graphene is a one-atom thick sheet composed of sp^2 carbon atoms arranged in a regular hexagonal lattice. Graphene has been paid much attention for their remarkable properties and various applications of graphene have been expected. However, mass production of graphene has not been established yet. At present, reduction of graphene oxide (GO) is a promising method of mass production of graphene but this method has a problem that defects, which were formed in oxidation process, and some functional groups remained after reduction. To solve this problem I developed three new reduction methods of GO.

First, I reduced GO by annealing GO on a Ni foil. According to Raman spectra, this sample was restored but most of GO sheets disappeared with Ni evaporation. Then, to avoid the disappearance of GO sheets, I annealed GO sheets by annealing GO at the interface of a Ni overlayer and SiO_2 substrate. As a result, large area graphene and threadlike graphene were formed. Then I changed the quantity of GO, the kind of metal overlayer and annealing temperature. When all carbon atoms dissolved into metal overlayer, threadlike graphene was formed. In contrast, when not all carbon atoms dissolved, thick large area graphene was formed. To fabricate thin graphene sheet, the thickness of Ni film and cooling rate were changed. In the case of thin Ni film, graphene with the similar shape of GO was formed. On the other hand, in the case of thick Ni film, graphene with the different shape of GO was formed.

Second, I reduced GO by radical treatment in solution process. I used CH_3I , C_2H_5Br , BrC_2H_4Br and $PhCH_2Br$ as radical sources. From Raman spectra, improvement of the crystallinity were achieved as following order; $CH_3I > BrC_2H_4Br > C_2H_5Br > PhCH_2Br$.

Third, I conducted sulfuration and reduction of GO by using $(NH_4)_2S_x$. From XPS spectra, the existence of sulfur was confirmed and S/C was 3.8 atom%. From Raman spectra, the crystallinity of GO was improved by treatment with $(NH_4)_2S_x$.

In conclusion, I developed three reduction methods, which are cost effective and suitable for industrial application. These reduction methods open up the opportunity for mass production of graphene from graphene oxide.

Contents

Chapter 1 Introduction	1
1.1 Graphene	1
1.2 Fabrication Methods of Graphene	5
1.3 Structure of Graphene Oxide	11
1.4 Preparation Methods of Graphene Oxide	14
1.5 Reduction Methods of Graphene Oxide	17
1.6 The Aim of This Thesis	20
References	21
Chapter 2 Experimental Equipment	25
2.1 Metal Deposition Chamber	25
2.2 Raman Spectroscopy	27
2.3 Infrared Heating Furnace	28
2.4 Conductivity Measurement Chamber	29
2.5 Other Equipment	30
References	33
Chapter 3 Graphene Preparation from Graphene Oxide	
by Annealing on Metal Surfaces	34
3.1 Introduction	34
3.2 Annealing Graphene Oxide on Metal Foil	36
3.2.1 Experimental Method	36
3.2.2 Results and Discussion	40
3.3 Annealing Graphene Oxide between a Ni Layer and SiO ₂	43
3.3.1 Experimental Method	43
3.3.2 Results and Discussion	44

3.4 Dependence of the Shape of Graphene on the Quantity of Graphene Oxide, the Kind of Metal Overlayer and Annealing Temperature	49
3.4.1 Experimental Methods	49
3.4.2 Results and Discussion	51
3.5 Dependence of the Shape of Graphene on the Thickness of Ni Film and Cooling Rate	64
3.5.1 Experimental Method	64
3.5.2 Result and Discussion	65
3.6 Conclusions	75
References	77
Chapter 4 Reduction of Graphene Oxide by Radical Treatment	80
4.1 Introduction	80
4.2 Experimental Method	81
4.2.1 Radical Treatment of GO Suspension	81
4.2.2 Sample Preparation for Raman Spectroscopy	83
4.3 Results and Discussion	84
4.4 Conclusions	91
References	92
Chapter 5 Reduction and Sulfuration of Graphene Oxide by Solution Process	94
5.1 Introduction	94
5.2 Experimental Methods	95
5.2.1 Preparation of Sulfurated Graphene	95
5.2.2 Sample Preparation for Raman Spectroscopy	96
5.3 Results and Discussion	97
5.4 Conclusions	102

References	103
Chapter 6 Concluding Remarks	105
Acknowledgement	107

Chapter 1

Introduction

1.1 Graphene

Graphene is a one-atom thick sheet of graphite and composed of sp^2 carbon atoms arranged in a regular hexagonal pattern (Figure 1.1) [1]. By A. K. Geim and K. S. Novoselov, Graphene was first isolated in 2004 by using mechanical cleavage (Scotch tape method) [2]. They won the Nobel Prize in Physics for graphene research in 2010. Since then, Graphene has been investigated for various applications in wide field due to its excellent properties such as high carrier mobility [3], high thermal conductivity [4], high Young's modulus [5], high transparency and so on. High carrier mobility was reported by Bolotin *et al.* According to their report, mobilities of suspended graphene which was fabricated by a combination of electron beam lithography and etching was in excess of $200,000 \text{ cm}^{-1} / \text{V} \cdot \text{s}$ at electron density of $\sim 2 \times 10^{11} \text{ cm}^{-2}$ at $\sim 5 \text{ K}$. This mobility is larger than any other semiconductors or semimetals. Alexander A. Balandin *et al.* reported high thermal conductivity of graphene. By using a noncontact optical-based

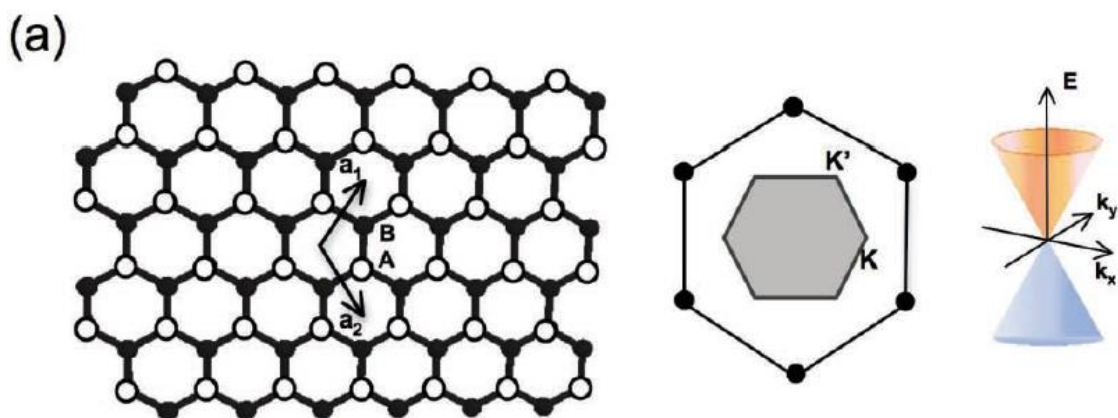


Figure 1.1 Schematics of the crystal structure, Brillouin zone and dispersion spectrum of graphene. Reproduced with permission from [1]. Copyright: 2010 WILEY-VCH Verlag GmbH & Co. KGaA, Weinheim.

technique, they discovered that thermal conductivity of graphene was up to $(5.30 \pm 0.48) \times 10^3$ W/mK. For these properties, applications of graphene have been expected such as field effect transistor (FET) device, touch panel display and transparent electrode.

However, applications of graphene to electronic devices have some problems. One problem is that graphene has zero band gap (Figure 1.1). If graphene is applied to FET devices, on/off ratio is too low due to zero band gap. To solve this problem, some promising approaches have been reported. One is fabrication of graphene nanoribbon. By theoretical calculation, it is predicted that band gap will open with increase of the width of graphene nanoribbon (Figure 1.2) [6]. In experiment, Melinda Y. Han *et al.* fabricated graphene nanoribbon with widths ranging from 10-100 nm and length of 1-2 μm by lithographic processes and investigate its electronic transport [7]. Similar to the theoretical calculations, the narrower the wide of graphene nanoribbon was, the larger the band gap opened. Though band gap is opened by lithographic processes, lithography system is very expensive and these processes are not suitable for mass production. James M. Tour's group developed a mass production method of graphene nanoribbon [8]. They produced graphene nanoribbon by oxidizing MWCNTs in concentrated sulfuric acid with KMnO_4 . By oxidation, C=C bonds are broken and dione are formed (Figure 1.3). Graphene nanoribbon produced by oxidation of MWCNTs was functionalized with oxygen groups such as carbonyls, carboxyls and hydroxyls. Though these functional groups can be removed mostly by reduction with aqueous hydrazine in the presence of ammonia, a little oxygen groups remained and made electronic characteristics inferior. Thus, graphene nanoribbon with large band gap can be produced in large quantities by this method but the quality of graphene nanoribbon was not good. Another method to open the band gap is hetero atom doping such as nitrogen. Dacheng Wei *et al.* produced N-doped graphene by CVD process [9]. They used CH_4 gas and NH_3 gas as the C source and N source respectively. The N content in graphene can be controlled from 1.2-3.2 % by changing NH_3/CH_4 ratio. N-doping in graphene network change the electrical structure of graphene and open the band gap. Thus, N-doped graphene show improved on/off ratio (Figure 1.4). Another problem is mass production

of high quality graphene. This problem is explained in the section 1.2.

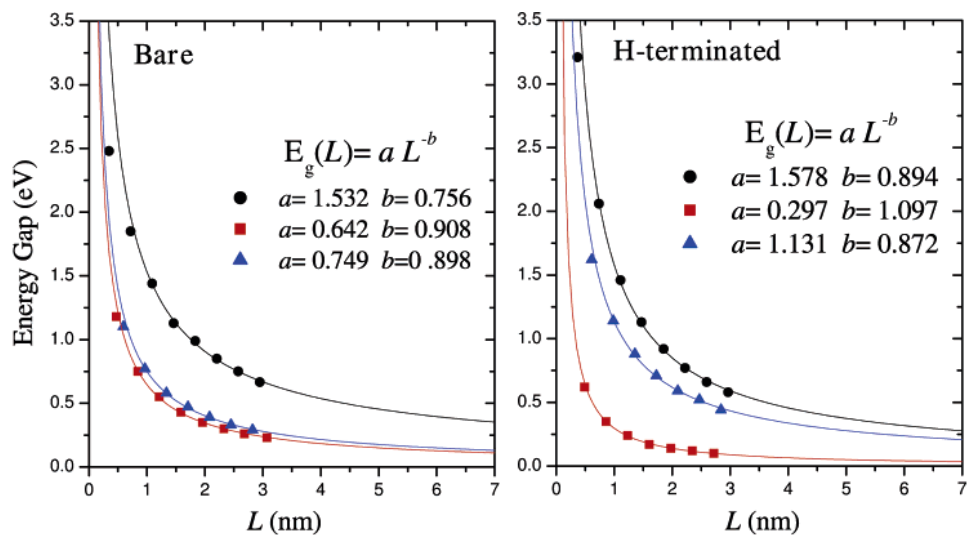


Figure 1.2 Extrapolation of the band gap oscillation to large CNRs width for bare (left panel) and hydrogen terminated (right panel) CNRs. Reproduced with permission from [6]. Copyright: 2006, American Chemical Society.

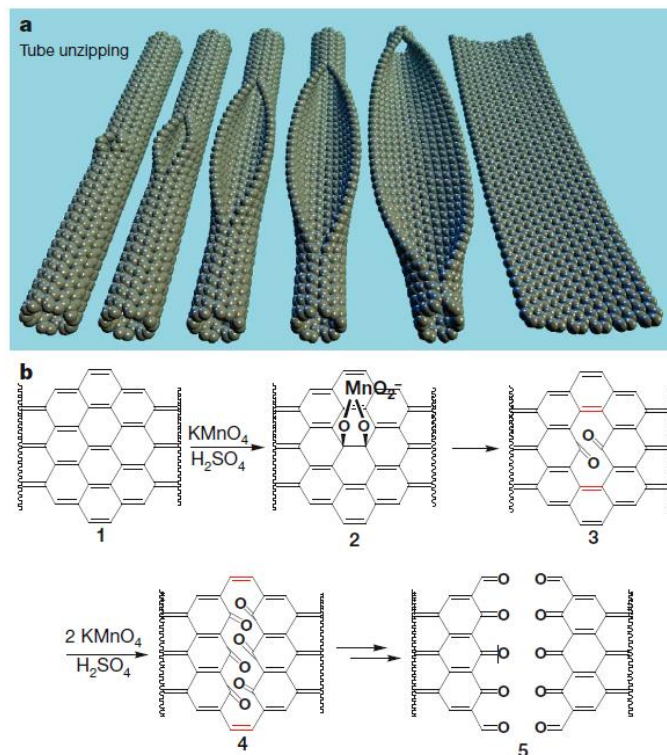


Figure 1.3 a, Representation of the gradual unzipping of one wall of a carbon nanotube to form a nanoribbon. Oxygenated sites are not shown. b, The proposed chemical mechanism of nanotube unzipping. Reproduced with permission from [8]. Copyright 2009, Nature Publishing Group.

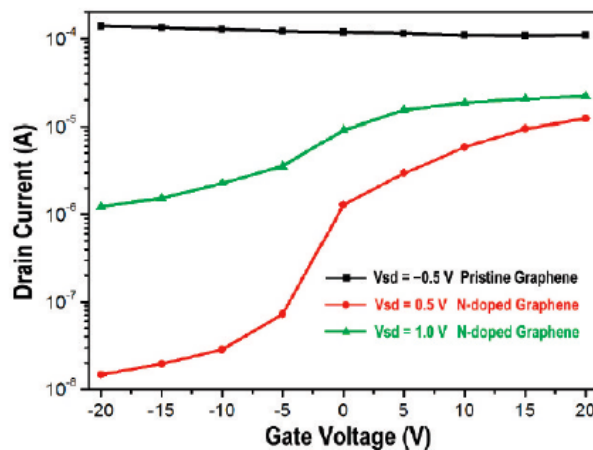


Figure 1.4 Transfer characteristics of the pristine graphene (V_{ds} at -0.5 V) and the N-doped graphene (V_{ds} at 0.5 and 1.0 V). Reproduced with permission from [9]. Copyright 2009, American Chemical Society.

1.2 Fabrication Methods of Graphene

Graphene has been fabricated in various methods. The method to fabricate the highest quality graphene is mechanical exfoliation method (Scotch tape method). Mechanical exfoliation method is cleaving of HOPG (Highly Oriented Pyrolytic Graphite) by using Scotch tape. As mentioned in section 1.1, graphene was first isolated by this method. Graphene produced by this method is high quality; almost defect free and single crystal. So, this method is suitable for measurement of physical properties of graphene but not suitable for mass production. Another method to fabricate high quality graphene is CVD method. In CVD process, graphene is grown on a metal substrate (e.g. Cu, Ni, Pt, etc.) by flowing carbon source gas (e.g. methane, ethylene, benzene, etc.) with hydrogen gas and heating at high temperature. In the case of Ni, the carbon atoms dissolve into Ni and segregate. Alfonso Reina *et al.* fabricated graphene by using Ni substrate [10]. They obtained 1 to 10 layers graphene film by exposure of a polycrystalline Ni film to a highly diluted CH₄ gas under ambient pressure at 900-1000 °C. Figure 1.5 shows (a) graphene grown on a patterned Ni film and (b) graphene transferred onto SiO₂ substrate.

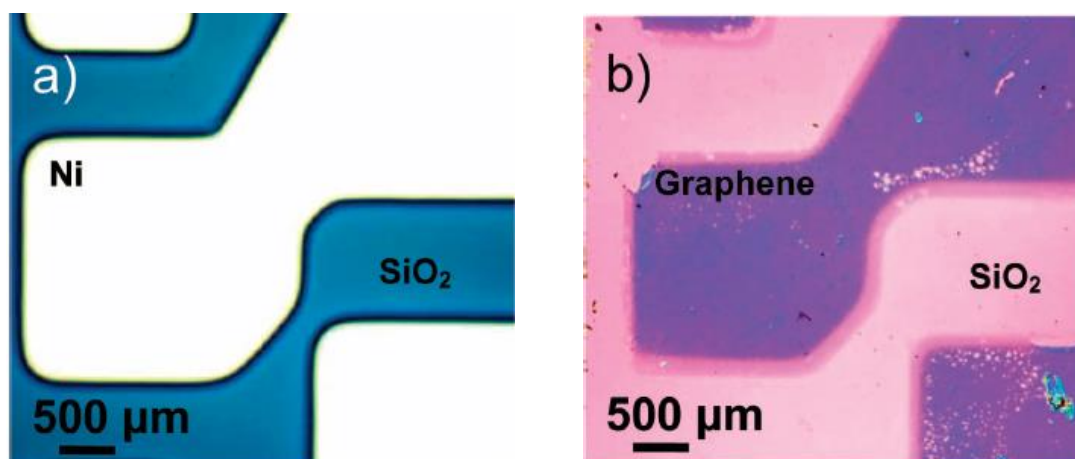


Figure 1.5. (a) Optical image of a prepatterned Ni film on SiO₂/Si. (b) Optical image of the grown graphene transferred from the Ni surface in panel a to another SiO₂/Si substrate.

Reproduced with permission from [10]. Copyright: 2009, American Chemical Society.

Graphene is formed by carbon segregation, so not only monolayer graphene but also few layer or multilayer graphene are grown in this method. Most of few layer or multilayer graphene are formed at grain boundaries. Thus graphene grown on a Ni film is inhomogeneous.

In the case of Cu, monolayer graphene is formed uniformly. Xuesong Li *et al.* fabricated graphene on Cu foil by CVD using methane and hydrogen mixed gas [11]. Methane molecules or carbon radicals diffuse on Cu surface and graphene is formed by catalysis of Cu. Monolayer graphene covered the surface of Cu and formation of secondary layer rarely occurs. Thus only monolayer graphene is formed. Figure 1.6 (A) and (B) show SEM image and optical microscope image of graphene transferred from Cu foil to SiO₂ substrate respectively. Figure 1.6 (C) shows Raman spectra of spots with corresponding colored circle in Figure 1.6 (A) and (B). According to these results, more than 95 % of graphene is monolayer. Bilayer is ~3 to 4 % and trilayer or few-layer (<10) is less than 1 %.

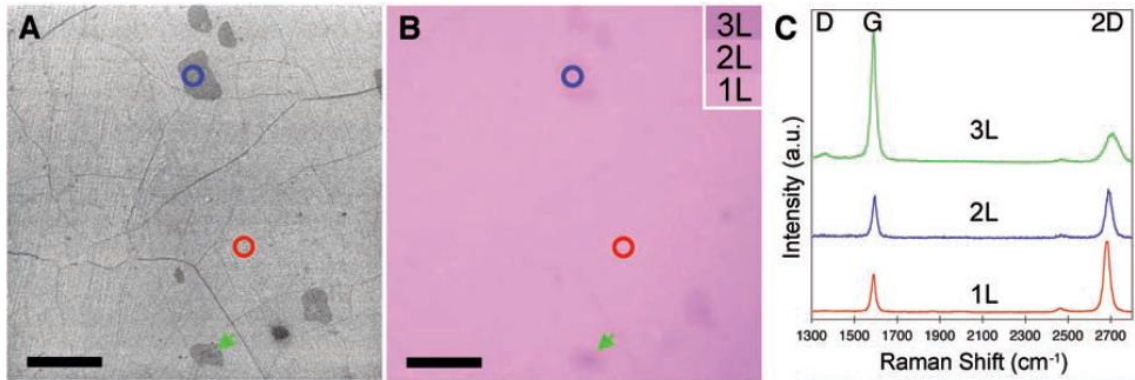


Figure 1.6. (A) SEM image of graphene transferred from Cu foil to SiO₂ substrate. (B) Optical image of graphene of the same regions as in (A). (C) Raman spectra from the marked spots with corresponding colored circles. Scale bars, 5 μm . Reproduced with permission from [11].

Copyright: 2009, American Association for the Advancement of Science.

Recently, based on the method of graphene growth on Cu foil by CVD process, roll-to-roll production method was developed [12]. Sukang Bae *et al.* fabricated 30-inch graphene films by roll-to-roll process. The roll-to-roll step consists of 3 steps as shown

in Figure 1.7: (i) attachment of a thermal release tape to graphene film on copper foil, (ii) etching of the copper foil with copper etchant such as $(\text{NH}_4)_2\text{S}_2\text{O}_8$ and (iii) transfer of the graphene films with a thermal release tape onto any kind of substrates. By mild heat ($\sim 90\text{-}120\text{ }^\circ\text{C}$), the thermal release tape is detached from graphene films and substrates. By this roll-to-roll process, it is possible to produce graphene at large scale but this process is not suitable for industrial applications because flammable gases such as methane and hydrogen are dangerous and this process costs money due to etching copper foil and vacuum equipment.

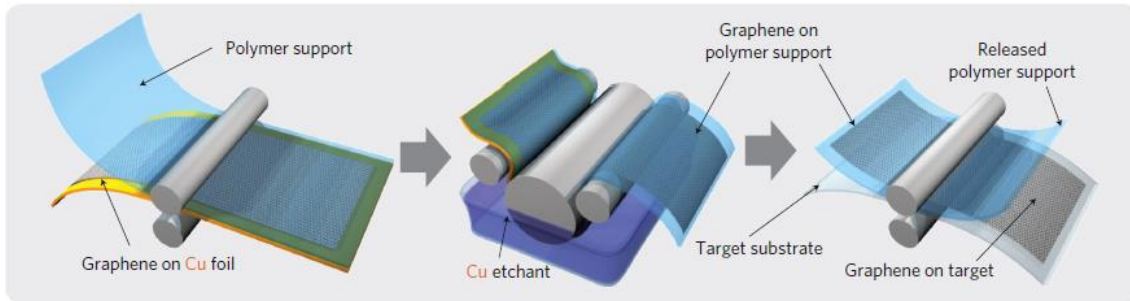


Figure 1.7. Schematic of the roll-to-roll production of graphene films on copper foil. Reproduced with permission from [12]. Copyright: 2010, Nature Publishing Group.

To avoid using carbon feedstock gases, graphene growth from carbon solid sources was developed [13]. Zhengzong Sun *et al.* obtained graphene by depositing a poly(methyl methacrylate) (PMMA) thin film on a copper foil and annealing at $800\text{-}1000\text{ }^\circ\text{C}$ for 10 min with a reductive gas flow (H_2/Ar). The hole mobility of PMMA derived graphene was about $410\text{ cm}^2/\text{V}\cdot\text{s}$ at room temperature and the D band intensity was noise level. These results indicate that few defects presented and PMMA derived graphene was high quality. Instead of PMMA, graphene can be obtained from other solid carbon sources such as fluorene ($\text{C}_{13}\text{H}_{10}$) and sucrose ($\text{C}_{12}\text{H}_{22}\text{O}_{11}$). In addition to these solid carbon sources, graphene can be obtained from melamine ($\text{C}_3\text{N}_6\text{H}_6$). By using mixture of melamine and PMMA as solid carbon sources, N-doped graphene was formed. As mentioned in section 1.1, band gap of N-doped graphene is opened and on/off ratio is high, so N-doped graphene is expected for application of FET devices.

The N contain ratio confirmed by XPS spectra was 2-3.5 %. However, the on/off ratio was not improved because N atoms were incorporated randomly. Thus, it is required that preparation of N-doped graphene by this method is improved.

These CVD methods have a problem that transfer process is needed. To solve this problem, graphene preparations by transfer-free method have been researched. For example, Sun-Jung Byun *et al.* achieved transfer free graphene growth on SiO₂ substrate by depositing a Ni thin film on a polymer (e.g. PMMA, polystyrene and polyacrylonitrile) film which was deposited on a SiO₂ substrate and annealing at 1000 °C with Ar and H₂ gas flow as shown in Figure 1.8 [14]. By this method, graphene was formed on a SiO₂ substrate and transfer process was needless. However this method is not suitable for industrial applications because hydrogen gas and high temperature of 1000 °C is needed.

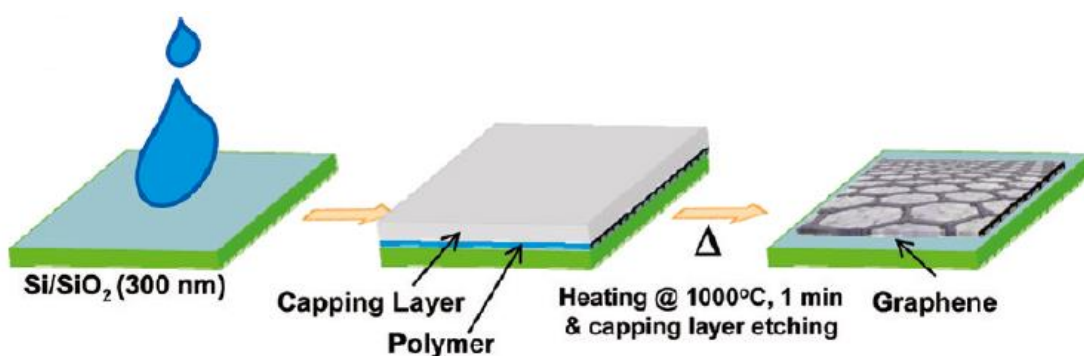


Figure 1.8. Schematic of the transfer free graphene growth process by using a Nickel capping layer. Reproduced with permission from [14]. Copyright: 2011, American Chemical Society.

Another method to produce high quality and large area graphene is decomposition of the (0001) surface of 6H-SiC [15]. Problems of this method are that high temperature of 1250 °C to 1450 °C is required and formed graphene cannot be transferred to any desirable substrate. Additionally, SiC substrate is itself expensive.

Cost-effective and scalable process to fabricate graphene is liquid phase exfoliation of graphite. Yenny Hernandez *et al.* obtained graphene by sonication of graphene dispersed in various solvents [16]. The concentration of graphene depends on the kind

of solvent and exfoliation can only occur when the energetic cost is very small. The enthalpy of mixing (per unit volume) can be calculated as equation (1.1).

$$\frac{\Delta H_{mix}}{V_{mix}} \approx \frac{2}{T_{flake}} (\delta_G - \delta_{sol})^2 \phi \quad (1.1)$$

$\delta_i = \sqrt{E_{sur}^i}$ is the square root of the surface energy of phase i , T_{flake} is the thickness of graphene flake and ϕ is the graphene volume fraction. Nanotube and graphite surface energy is about 70-80 $\text{mJ} \cdot \text{m}^{-2}$. Thus, solvent whose surface energy is close to 70 -80 $\text{mJ} \cdot \text{m}^{-2}$ is expected to exfoliate graphite flake effectively. In fact, the dispersed concentration shows the peak at around surface energy of 70-80 $\text{mJ} \cdot \text{m}^{-2}$ as shown in Figure 1.9. Concentration of graphene was more than 8 % when the solvent was benzyl benzoate (surface tension; 45.95 $\text{mJ} \cdot \text{m}^{-2}$). However, the yield of monolayer graphene was about 1 wt% and the lateral size of dispersed graphene is only a few micrometers.

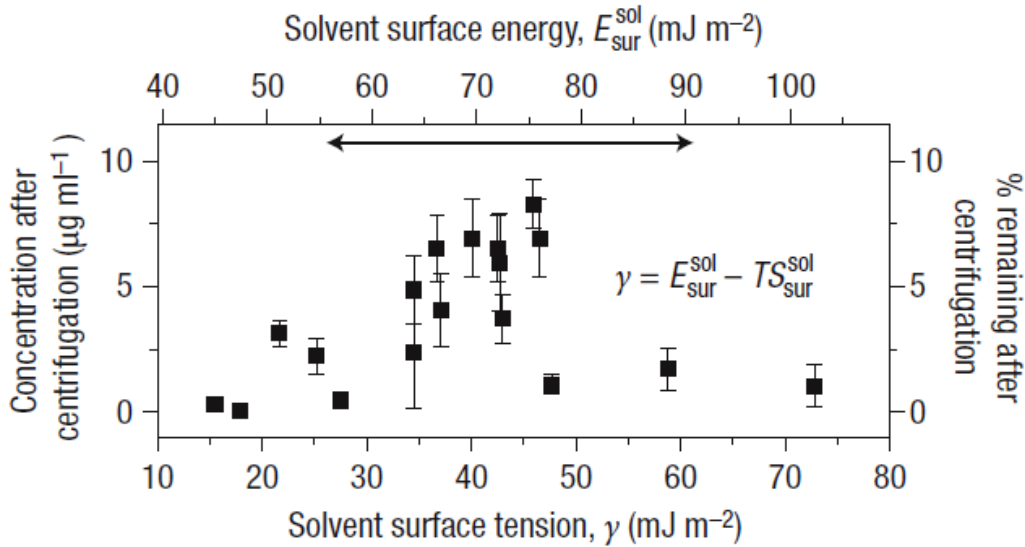


Figure 1.9 Graphene concentration plotted versus solvent surface tension or solvent surface energy. Reproduced with permission from [16]. Copyright: 2008, Nature Publishing Group.

The graphene preparation method most suitable for industrial application is reduction of graphene oxide (GO). GO is the oxidized form of graphene and functionalized with oxygen functional groups (e.g. hydroxyl, epoxy and carboxyl acid groups) as shown in Figure 1.10. Due to these hydrophilic functional groups, GO can be dispersed in various

solvents and exfoliated by electrostatic repulsion of these functional groups. Most of functional groups of GO can be removed by chemical treatment or thermal annealing. Thus, graphene can be obtained at large scale as shown in Figure 1.11, but graphene produced from GO is disordered due to remained functional groups and defects which are formed in oxidation process. The disordered structure of graphene results in the inferior performance of graphene devices. The details of GO are mentioned in following sections.

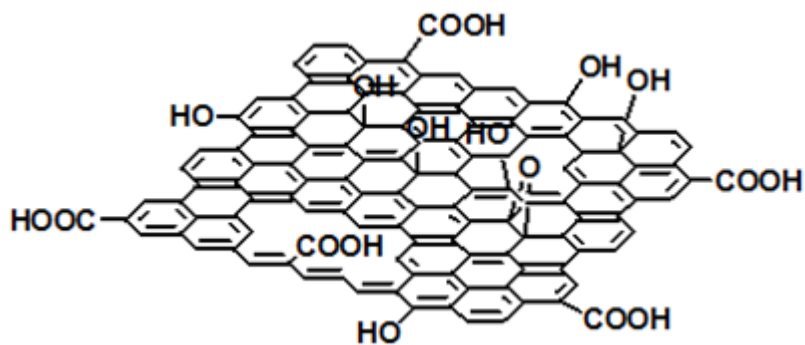


Figure 1.10 Structure of graphene oxide (Lerf- Klinoski model).

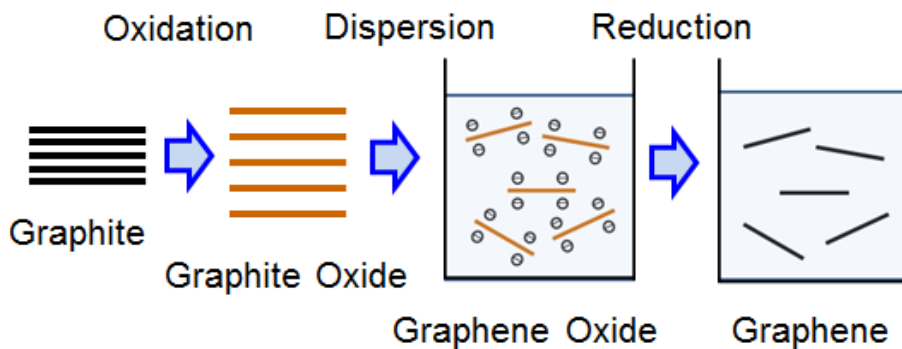


Figure 1.11 Graphene preparation process via reduction of graphene oxide.

1.3 Structure of Graphene Oxide

Graphite oxide was first synthesized about 150 years ago but the exact structure is still ambiguous. The reasons are that graphite oxide is nonstoichiometric and its chemical composition depends on oxidation condition. To date, many structure models of graphite oxide have been reported (Figure 1.12) [17]. In Hofmann model, graphite oxide is hexagonal structure plane functionalized with only epoxy groups. The chemical composition is C_2O . In Ruess model, in addition to epoxy groups, hydroxyl groups are also incorporated into graphite oxide. This model first explained the existence of hydrogen in graphite oxide. In contrast to Hofmann model, Ruess model consists of cyclohexane chair. Scholz-Boehm suggested the structure functionalized with hydroxyl and carbonyl groups and contained quinoidal species without epoxy groups. Nakajima and Matsuo proposed a step 2 type model analogous to that of poly(carbon monofluoride), $(CF)_n$. At present the structure presented by Lerf and co-workers is the most advocated. In Lerf- Klinoski model, flat aromatic regions with unoxidized benzene rings and sp^3 carbon atoms are distributed randomly.

In 2009, Wei Gao *et al.* proposed a new model of graphite oxide, which contains five- and six-membered-ring lactols in addition to epoxy and hydroxyl groups (Figure 1.13) [18]. Based on the solid state ^{13}C NMR spectroscopy of graphite oxide, they proposed the presence of lactols.

The atomic structure of GO and reduced graphene oxide (rGO) was observed by Kris Erickson *et al.* [19]. Figure 1.14 shows TEM images of (A) suspended monolayer graphene, (B) suspended monolayer GO sheet and (C) suspended monolayer rGO sheet. On the right images, holes are indicated in blue, graphitic regions in yellow and areas with remaining functionalities in red. In Figure 1.14 (A), graphitic area is almost 100 %. On the other hand, in Figure 1.14 (B), holes, graphitic regions and high contrast disordered regions, which is highly oxidized area are approximate area percentages of 2%, 16%, and 82%, respectively. Thus, GO sheet is almost disordered and the graphitic area which is not oxidized area is between 1 to 6 nm^2 . Holes are formed because CO and CO_2 are released from GO sheet. When GO was reduced, the graphitic area increase to 70 % and holes increase to 5 %. The increase of holes is due to release of CO and

CO₂ in annealing process. This result indicates that disorder region remains in rGO despite of reduction.

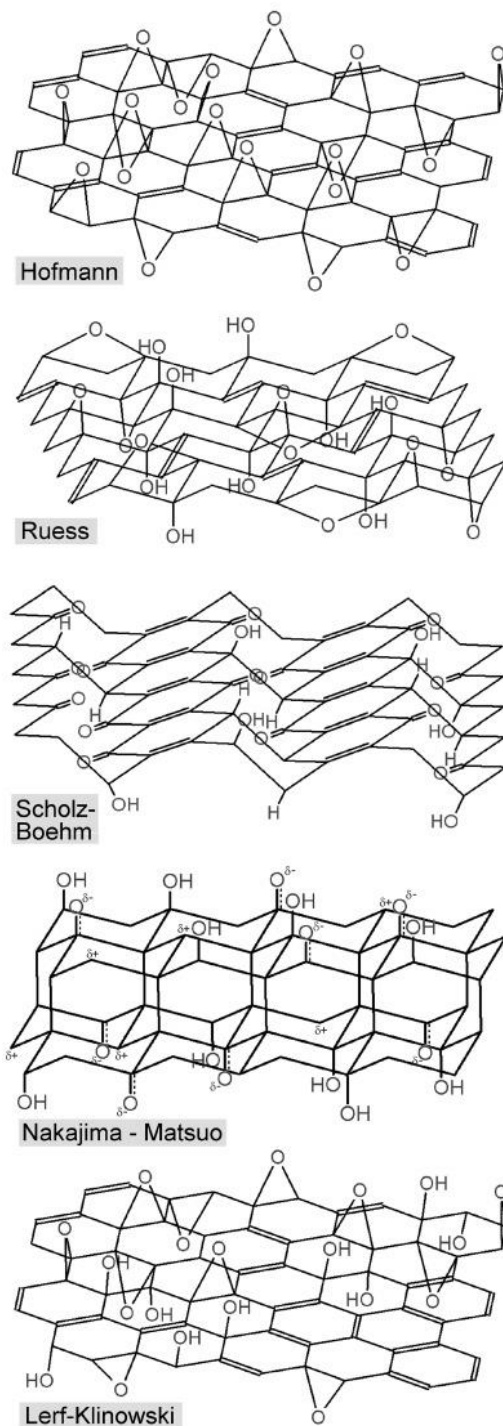


Figure 1.12 Several older structural model of graphene oxide. Reproduced with permission from [17]. Copyright: 2006, American Chemical Society.

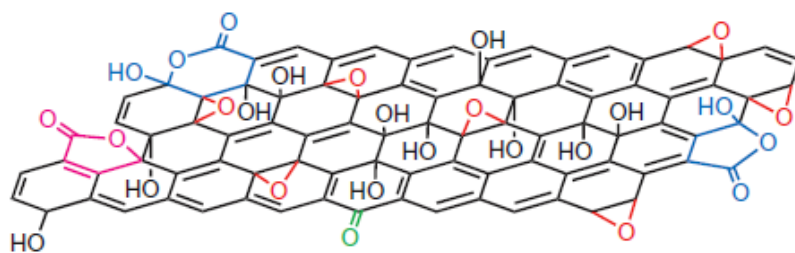


Figure 1.13 New structural model of graphite oxide. Reproduced with permission from [18].

Copyright: 2009, Nature Publishing Group.

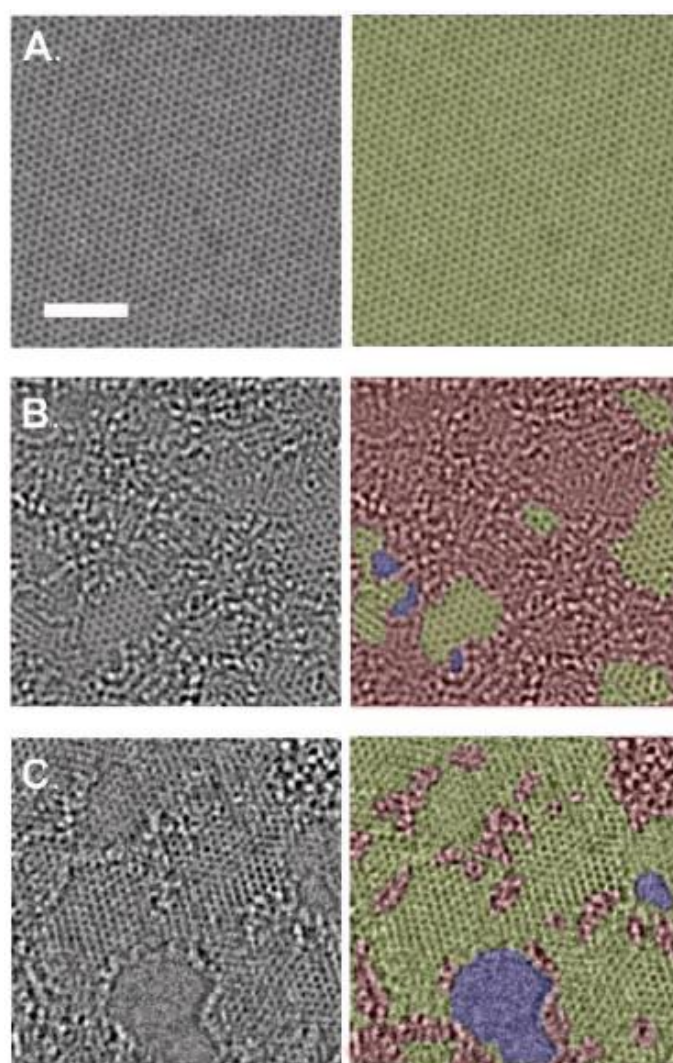
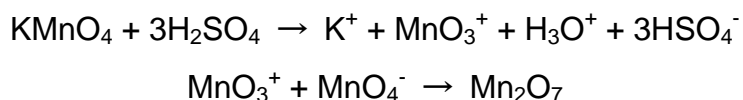


Figure 1.14. TEM images of (A) single suspended graphene, (B) single suspended GO sheet and (C) suspended monolayer of rGO. Reproduced with permission from [19]. Copyright: 2010 WILEY-VCH Verlag GmbH & Co. KGaA, Weinheim.

1.4 Preparation Methods of Graphene Oxide

GO has been synthesized by various methods and the chemical structure depends on the synthesis method. Graphite oxide was first prepared by Brodie in 1855 [20]. The preparation of graphite oxide by Brodie method is as follows. First, fuming nitric acid is added into a flask and cooled to 0 °C. Then, graphite powder is added into the flask and stirred to avoid aggregation. Next, potassium chlorate is slowly added for 1h and the reaction mixture is stirred for 21 h at 0 °C. Finally, the mixture is diluted in distilled water and filtered. L. Staudenmaier improved Brodie method by adding concentrated sulfuric acid [21]. Hummers and Offeman oxidized graphite by using KMnO_4 as follows [22]. First, concentrated sulfuric acid is added to a flask. Then graphite powder and sodium nitrate are added into the flask. The solution is cooled at 0 °C in ice bath and potassium permanganate is added slowly. Next, the ice bath is removed and distilled water is added slowly. This process causes increase of temperature to 98 °C. After that, 3% hydrogen peroxide is added to reduce the residual permanganate and manganese dioxide. Finally, the mixture is filtrated and graphite oxide is obtained. As scheme 1.1, potassium permanganate react with sulfuric acid and dimanganese heptoxide forms.



Scheme 1.1. Formation of dimanganese heptoxide by reaction of potassium permanganate with sulfuric acid.

Hummers method is safer than Brodie method and Staudenmaier method. So graphite oxide is prepared by Hummers method or modified Hummers method commonly.

Recently, new oxidation methods of graphite have been developed. For instance, Daniela C. Marcano and co-workers improved Hummers method by increasing the amount of potassium permanganate and adding phosphoric acid [23]. The advantage of this method is that the improvement of yield. When 3 g of graphite was used as precursor of GO, graphite oxide which was not exfoliated was 6.7 g in the case of Hummers method, on the other hand, that was 0.7 g in the case of this improve method.

In addition to this, reaction produces no toxic gas and not a large exotherm in this method. Ching-Yuan Su *et al.* obtained ultra-large GO sheet by modified Hummers method, where they replaced first step with a bath sonication process in sulfuric acid [24]. Pre-oxidation and pre-exfoliation make it easier to exfoliate graphite sheets and ultra-large GO sheets with the lateral size of up to 3 mm (Figure 1.15). In addition to these modified Hummers method, GO have been synthesized by other oxidants. Sourov Chandra *et al.* alter potassium permanganate to potassium dichromate as oxidant [25]. Though toxic gas is generated by reaction of hydrogen peroxide with the residual permanganate and manganese dioxide in Hummers method, this problem can be overcome by using K_2CrO_7 . Jianfeng Shen *et al.* used benzyl peroxide as oxidant and solvent [26]. This method is only heating of graphite powder with benzyl peroxide at 110 °C and any other solvent are not needed. This oxidation method is fast and facile but there is the potential that benzyl peroxide may explode. By these preparation methods, GO can be obtained at large scale but rGO is disordered because oxidation is harsh and many defects are generate. Thus, mild oxidation process which suppress the generation of defects is demanded. Recently, Siegfried Eigler *et al.* developed a wet chemical synthesis method of high-quality graphene [27]. Though their procedure was based on Hummers method, they oxidized graphite flake below 10 °C and added cold water continuously. According to their previous report, GO is not stable at 50 °C and hole defects are formed by CO_2 generation [28]. So, by cooling below 10 °C in oxidation process, hole defects are suppressed and relatively high-quality GO is obtained. Figure 1.16 A)-C) show the pictures and SEM image of graphite and GO. Figure 1.16 D)-E) show Raman spectra of graphite, GO and rGO respectively. rGO was reduced by hydriodic/trifluoroacetic acid. In Figure 1.16 D), D band intensity is high, FWHM of D band and G band are broad and 2D band intensity is low. On the other hand, in Figure 1.16 E), D band intensity is low, FWHM of D band and G band are sharp and 2D band intensity is high. This Raman spectrum indicates that this rGO is relatively high-quality. However in this procedure, yield is lower compared to conventionally prepared GO.

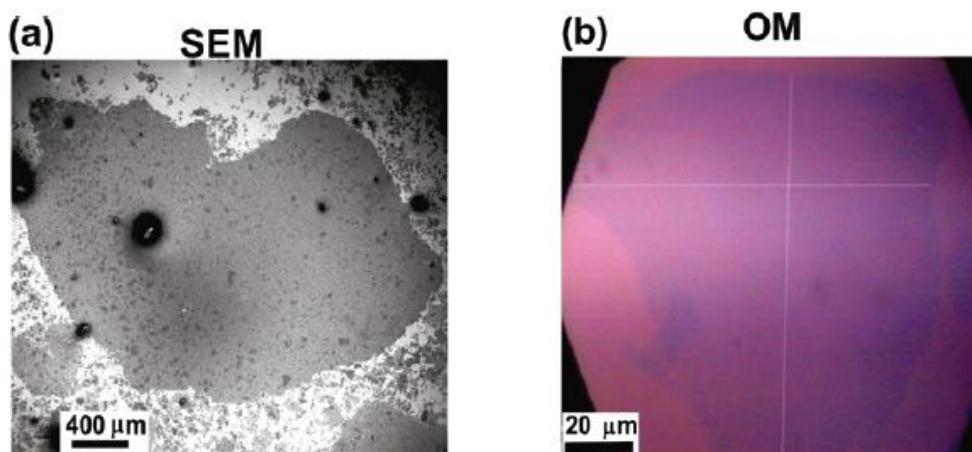


Figure 1.15 (a) SEM image and (b) optical microscope image of GO produced by pre-oxidation method. Reproduced with permission from [24]. Copyright: 2009, American Chemical Society.

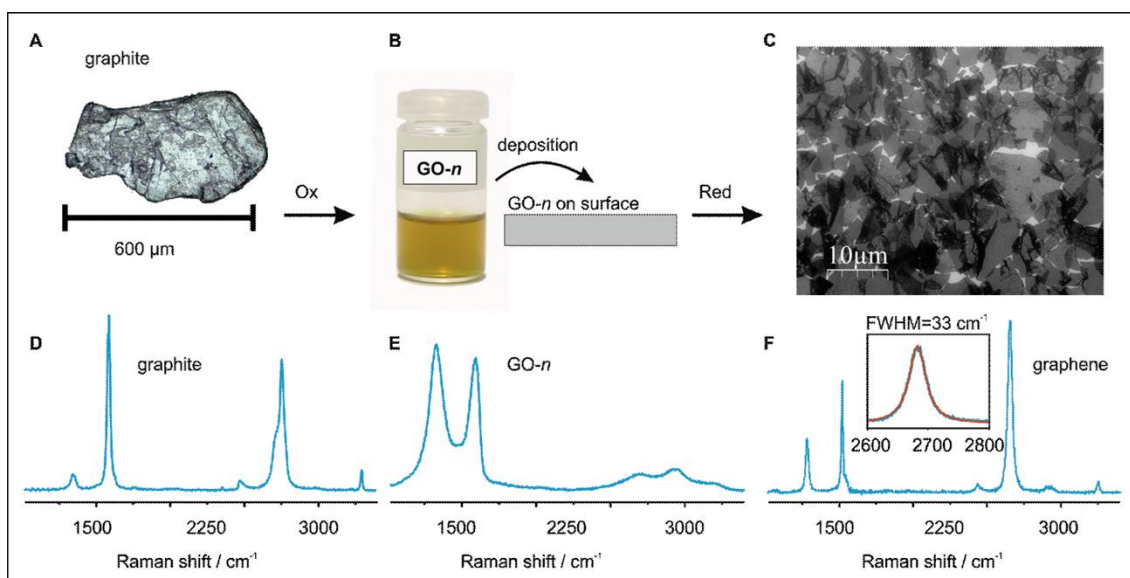


Figure 1.16 (A) reflected light microscope image of natural graphite. (B) aqueous dispersion of GO. GO-n means new form of graphene oxide. (C) SEM image of GO film. (D)-(E) Raman spectra of natural graphite, GO and rGO respectively. Reproduced with permission from [27]. Copyright: 2013 WILEY-VCH Verlag GmbH & Co. KGaA, Weinheim.

As mentioned above, preparation of high-quality graphene at large scale is very difficult. Harsh oxidation is necessary for mass production of GO but mild oxidation is necessary to produce high-quality GO or graphene. Thus in oxidation process, the quality and yield are in relation of trade-off. So, for mass production of high-quality graphene, improvement of reduction process is more hopeful than that of oxidation process. Reduction method is mentioned in the next section.

1.5 Reduction Methods of Graphene Oxide

To obtain graphene from GO, reduction process is needed. Most of functional groups of GO can be removed by thermal annealing or chemical treatment. In the case of thermal annealing at 1000 °C, functional groups are removed by generation of CO or CO₂ as shown in Figure 1.17 [29]. Carbon atoms are also removed with oxygen atoms, so hole defects are formed in annealing process. In Figure 1.14, hole defects in rGO are larger than that in GO and this result indicates CO or CO₂ generation. Thus, to reduce GO without forming hole defects, chemical reduction is desirable. Hydrazine is commonly used to reduce GO. Hydrazine reduction of GO was reported by Sasha Stankovich *et al.* [30]. In their method, hydrazine hydrate was added to the GO aqueous solution and heated at 100 °C. GO is reduced and convert to rGO by the mechanism shown in Scheme 1.2. During reduction of GO, the brown color of GO turns black. Due to elimination of oxygen groups, hydrophilic property is lost and rGO has a hydrophobic property and aggregation occurs. So, reduction without aggregation of rGO sheets is necessary in order to obtain monolayer or few-layer graphene sheets. Another problem of hydrazine reduction is that defects which are formed in oxidation process remain in rGO after reduction. Various kind of defect exist in oxidation process (e.g. hole defects, five-membered ring, seven-membered ring and sp³ carbon atoms). Though most of sp³ carbon atoms functionalized with oxygen groups convert to sp² carbon atoms and π -networks is restored by reduction reaction, other defects and a few functional groups remain. These defects decrease electron properties such as electrical conductivity and carrier mobility. The electric conductivity of rGO reduced with

hydrazine is $\sim 2400 \pm 200$ S/m, which is two orders magnitude less than that of natural graphite ($\sim 1 \times 10^5$ S/m) and five orders magnitude better than that of GO (~ 0.02 S/m). Additionally, hydrazine is toxic and dangerous. These problems impede the mass production of high-quality graphene. Therefore, the problems of GO reduction that we should solve for industrial applications are summarized as follows; i) GO sheets aggregate during reduction process due to elimination of hydrophilic functional groups. ii) Defects and a few functional groups remain, which degrade the electrical properties. iii) Hydrazine, which is commonly used as a reducing agent of GO reduction, is toxic and dangerous and unsuitable for industrial applications.

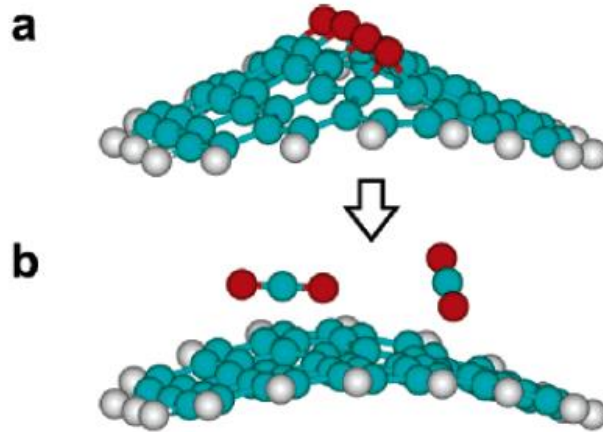
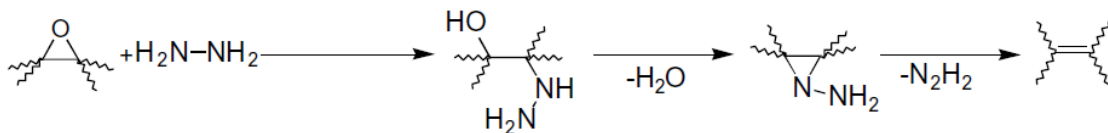


Figure 1.17 a) Atomic model of graphene oxide. b) Release of carbon dioxide during thermal treatment. Reproduced with permission from [29]. Copyright: 2006, American Chemical Society.



Scheme 1.2. Proposed reaction pathway for epoxide reduction with hydrazine. Reproduced with permission from [30]. Copyright: 2007, Elsevier Ltd.

Recently, alternative reducing agents have been reported. For example, sodium borohydride (NaBH_4) [31], sodium hydroxide (NaOH) or potassium hydroxide (KOH) [32] and vitamin C [33] were used as reducing agent of GO reduction. By adding these reagents into GO aqueous solution and heating, GO is reduced. These reducing agents are safer than hydrazine and have reducing ability comparable to hydrazine (Table 1.1). The reduction mechanisms are still unclear but it is possible that epoxy rings open and hydroxyl groups are eliminated by dehydration in the case of NaOH or KOH . In fact, GO is reduced not only under alkaline condition but also under acid condition [34]. These results indicate that epoxy and hydroxyl groups are removed via dehydration under alkali or acid condition. More efficient reducing agent than these reagent is hydroiodic (HI) acid [34]. The conductivity of rGO reduced with HI is ~ 29800 S/m. The C/O ratio and electric conductivity; σ of each reduction method are summarized in Table 1.1. By any reduction method, defects and a few functional groups remain and rGO is disordered. Thus, defect healing and complete removing of functional groups are challenging problems.

Table 1.1. Comparison of reduction method.

Ref. No.	Reduction method	C/O ratio	σ S/m
30	Hydrazine hydrate	10.3	~ 2400
31	15-150 mM NaBH_4 solution, 2h	8.6	max. 45
32	8 M NaOH or KOH 90 °C, 5 h	Not available	Not available
33	Vitamin C	12.5	max. 7700
34	H_2SO_4 or H_3PO_4 90 °C 2h then 120 °C 2h	Not available	~ 6900
35	55% HI solution	>14.9	~ 29800

1.6 The Aim of This Thesis

As mentioned above, graphene preparation by reduction of GO, which is suitable for mass production of graphene, has a problem that some defects and functional groups remain in GO after reduction. These defects and functional groups degrade the electrical and mechanical properties of graphene. Thus, effective reduction method is needed for graphene application such as electric devices. Various reduction methods of GO have been reported but this problem has been unsolved. So, the aim of this thesis is development of effective GO reduction methods, which are suitable for mass production of graphene, to solve this problem. In this thesis, I developed three effective reduction methods of GO; annealing on metal surfaces, reaction with free radicals and treatment with $(\text{NH}_4)_2\text{S}_x$.

References

- [1] Zhu, Y.; Murali, S.; Cai, W.; Li, X.; Suk, J. W.; Potts, J. R.; Ruoff, R. S. *Adv. Mater.* **2010**, 22, 3906–24.
- [2] Novoselov, K. S.; Geim, A. K.; Morozov, S. V; Jiang, D.; Zhang, Y.; Dubonos, S. V; Grigorieva, I. V; Firsov, A. A. *Science* **2004**, 306, 666–9.
- [3] Bolotin, K. I.; Sikes, K. J.; Jiang, Z.; Klima, M.; Fudenberg, G.; Hone, J.; Kim, P.; Stormer, H. L. *Solid State Commun.* **2008**, 146, 351–355.
- [4] Balandin, A. A; Ghosh, S.; Bao, W.; Calizo, I.; Teweldebrhan, D.; Miao, F.; Lau, C. N. *Nano Lett.* **2008**, 8, 902–7.
- [5] Lee, C.; Wei, X.; Kysar, J. W.; Hone, J. *Science* **2008**, 321, 385–8.
- [6] Barone, V.; Hod, O.; Scuseria, G. E. *Nano Lett.* **2006**, 6, 2748–54.
- [7] Han, M.; Özyilmaz, B.; Zhang, Y.; Kim, P. *Phys. Rev. Lett.* **2007**, 98, 206805.
- [8] Kosynkin, D. V; Higginbotham, A. L.; Sinitskii, A.; Lomeda, J. R.; Dimiev, A.; Price, B. K.; Tour, J. M. *Nature* **2009**, 458, 872–6.
- [9] Wei, D.; Liu, Y.; Wang, Y.; Zhang, H.; Huang, L.; Yu, G. *Nano Lett.* **2009**, 9, 1752–8.
- [10] Reina, A.; Jia, X.; Ho, J.; Nezich, D.; Son, H.; Bulovic, V.; Dresselhaus, M. S.; Kong, J. *Nano Lett.* **2009**, 9, 30–5.

- [11] Li, X.; Cai, W.; An, J.; Kim, S.; Nah, J.; Yang, D.; Piner, R.; Velamakanni, A.; Jung, I.; Tutuc, E.; Banerjee, S. K.; Colombo, L.; Ruoff, R. S. *Science* **2009**, 324, 1312–4.
- [12] Bae, S. K.; Kim, H.; Lee, Y. B.; Xu, X. F.; Park, J. S.; Zheng, Y.; Balakrishnan, J.; Lei, T.; Kim, H. R.; Song, Y.; Kim, Y. J.; Kim, K. S.; Özyilmaz, B.; Ahn, J. H.; Hong, B. H.; Iijima, S. *Nat. Nanotechnol.* **2010**, 5, 574.
- [13] Sun, Z.; Yan, Z.; Yao, J.; Beitler, E.; Zhu, Y.; Tour, J. M. *Nature* **2010**, 468, 549–52.
- [14] Byun, S.-J.; Lim, H.; Shin, G.-Y.; Han, T.-H.; Oh, S. H.; Ahn, J.-H.; Choi, H. C.; Lee, T.-W. *J. Phys. Chem. Lett.* **2011**, 2, 493–497.
- [15] Berger, C.; Song, Z.; Li, T.; Li, X.; Ogbazghi, A. Y.; Feng, R.; Dai, Z.; Marchenkov, A. N.; Conrad, E. H.; First, P. N.; de Heer, W. A. *J. Phys. Chem. B* **2004**, 108, 19912.
- [16] Hernandez, Y.; Nicolosi, V.; Lotya, M.; Blighe, F. M.; Sun, Z.; De, S.; McGovern, I. T.; Holland, B.; Byrne, M.; Gun'ko, Y. K.; Boland, J. J.; Niraj, P.; Duesberg, G.; Krishnamurthy, S.; Goodhue, R.; Hutchison, J.; Scardaci, V.; Ferrari, A. C.; Coleman, J. N. *Nat. Nanotechnol.* **2008**, 3, 563–8.
- [17] Szabó, T.; Berkesi, O.; Forgó, P.; Josepovits, K.; Sanakis, Y.; Petridis, D.; Dékány, I. *Chem. Mater.* **2006**, 18, 2740–2749.
- [18] Gao, W.; Alemany, L. B.; Ci, L.; Ajayan, P. M. *Nat. Chem.* **2009**, 1, 403–8.
- [19] Erickson, K.; Erni, R.; Lee, Z.; Alem, N.; Gannett, W.; Zettl, A. *Adv. Mater.* **2010**, 22, 4467–72.

- [20] Brodie, B. *Ann. Chim. Phys.* **1855**, 45, 351–353.
- [21] Staudenmaier, L. *Ber. Dtsch. Chem. Ges.* **1898**, 31, 1481–1487.
- [22] Hummers, W. S.; Offeman, R. E. *J. Am. Chem. Soc.* **1958**, 80, 1339.
- [23] Marcano, D. C.; Kosynkin, D. V.; Berlin, J. M.; Sinitskii, A.; Sun, Z.; Slesarev, A.; Alemany, L. B.; Lu, W.; Tour, J. M. *ACS Nano* **2010**, 4, 4806–14.
- [24] Su, C.-Y.; Xu, Y.; Zhang, W.; Zhao, J.; Tang, X.; Tsai, C.-H.; Li, L.-J. *Chem. Mater.* **2009**, 21, 5674–5680.
- [25] Chandra, S.; Sahu, S.; Pramanik, P. *Mater. Sci. Eng., B.* **2010**, 167, 133–136.
- [26] Shen, J.; Hu, Y.; Shi, M.; Lu, X.; Qin, C.; Li, C.; Ye, M. *Chem. Mater.* **2009**, 21, 3514–3520.
- [27] Eigler, S.; Enzelberger-Heim, M.; Grimm, S.; Hofmann, P.; Kroener, W.; Geworski, A.; Dotzer, C.; Röckert, M.; Xiao, J.; Papp, C.; Lytken, O.; Steinrück, H.-P.; Müller, P.; Hirsch, A. *Adv. Mater.* **2013**, 25, 3583–7.
- [28] Eigler, S.; Dotzer, C.; Hirsch, A.; Enzelberger, M.; Müller, P. *Chem. Mater.* **2012**, 24, 1276–1282.
- [29] Schniepp, H. C.; Li, J.-L.; McAllister, M. J.; Sai, H.; Herrera-Alonso, M.; Adamson, D. H.; Prud'homme, R. K.; Car, R.; Saville, D. A.; Aksay, I. A. *J. Phys. Chem. B* **2006**, 110, 8535–9.
- [30] Stankovich, S.; Dikin, D. a.; Piner, R. D.; Kohlhaas, K. A.; Kleinhammes, A.; Jia, Y.; Wu, Y.; Nguyen, S. T.; Ruoff, R. S. *Carbon* **2007**, 45, 1558–1565.

- [31] Shin, H.-J.; Kim, K. K.; Benayad, A.; Yoon, S.-M.; Park, H. K.; Jung, I.-S.; Jin, M. H.; Jeong, H.-K.; Kim, J. M.; Choi, J.-Y.; Lee, Y. H. *Adv. Funct. Mater.* **2009**, 19, 1987–1992.
- [32] Fan, X.; Peng, W.; Li, Y.; Li, X.; Wang, S.; Zhang, G.; Zhang, F. *Adv. Mater.* **2008**, 20, 4490–4493.
- [33] Fernández-Merino, M. J.; Guardia, L.; Paredes, J. I.; Villar-Rodil, S.; Solís-Fernández, P.; Martínez-Alonso, A.; Tascón, J.M. D. *J. Phys. Chem. C* **2010**, 114, 6426–6432.
- [34] Chen, J. L.; Yan, X. P. *J. Mater. Chem.* **2010**, 20, 4328–4332.
- [35] Pei, S.; Zhao, J.; Du, J.; Ren, W.; Cheng, H.-M. *Carbon* **2010**, 48, 4466–4474.

Chapter 2

Experimental Equipment

2.1 Metal Deposition Chamber

Figure 2.1 shows the metal deposition chamber. A metal film (Ni or Pd) is deposited on a substrate in this chamber. As shown in Figure 2.2, a piece of metal wire is heated by Knudsen cell and evaporated. In the case of Ni deposition, a piece of Ni wire is heated at 1300 °C and in the case of Pd deposition, a piece of Pd wire is heated at 1250 °C. The base pressure is about 1×10^{-6} Pa but pressure increase to about 1×10^{-4} Pa during metal deposition. To avoid the deposition of impurity, the shutter is closed and protects a substrate. The shutter is opened after 30 min of reaching desirable temperature. The distance from metal wire to a substrate is about 15 cm. The thickness of deposited metal film is measured by quartz crystal microbalance (QCM) method. In this condition, deposition rate of Ni and Pd is ~ 0.67 nm/min and 0.13 nm/min respectively. A substrate is fixed by titanium plate as shown in Figure 2.3. So, a metal film is not deposited on the area where the titanium plate is set.



Figure 2.1 Picture of the metal deposition chamber

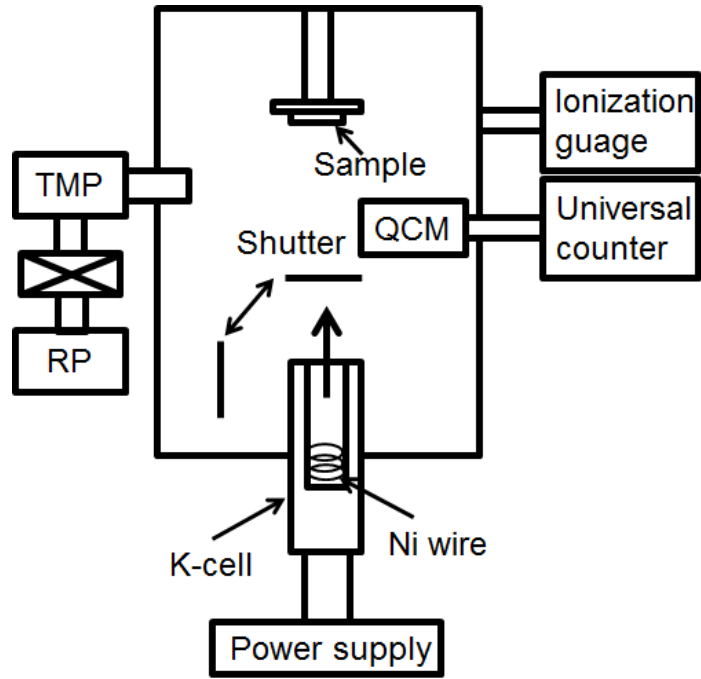


Figure 2.2 Model of metal deposition chamber.

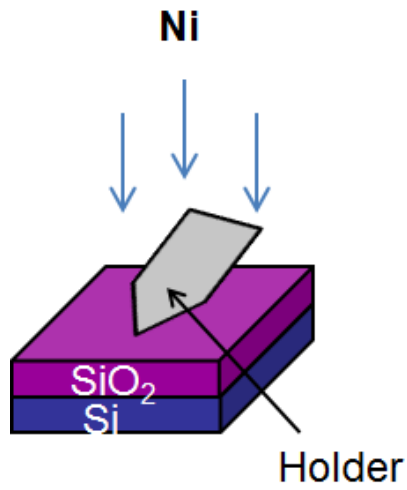


Figure 2.3 Illustration of a sample fixed by a titanium holder.

2.2 Raman Spectroscopy

Raman spectroscopy provides beneficial information about graphite, graphene and other carbon materials. Figure 2.4 a) shows a typical Raman spectrum of graphite. In a Raman spectrum of graphite or graphene, 3 peaks are observed. The peaks observed at ~ 1350 , 1580 and 2700 cm^{-1} correspond to D, G and 2D bands. The G band comes from graphite lattice [1]. The narrow FWHM of G band indicates that graphene is high quality. The D band originates of defects or edges. The 2D band is overtone of the D band. The intensity ratio of D band and G band; I_D/I_G is used to evaluate the quality of graphene or graphite. The intensity ratio of 2D band and G band; I_{2D}/I_G is used to evaluate the layer number of graphene or graphite. The I_{2D}/I_G ratio of monolayer, bilayer and few-layer graphene are more than 2, about 1 and less than 1 respectively. Additionally, the 2D band intensity drops in the case of defective graphene [2]. Thus, the I_{2D}/I_G intensity also can be used as an index of crystallinity of graphene or graphite. These are summarized in Figure 2.4 b). It was reported that down-shifting of the G band occurred by laser induced heat [3]. So, evaluation of the quality of graphene from G band shift is difficult.

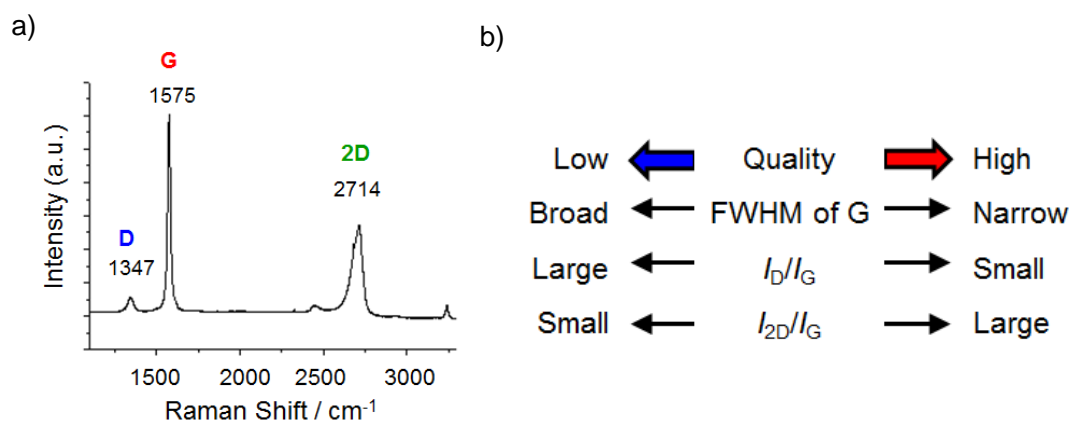


Figure 2.4 a) Typical Raman spectrum of graphite. b) Evaluation index of graphene quality.

Raman spectra were measured by NRS-3000/ Jasco Ltd. Figure 2.5 shows the picture of apparatus of Raman spectroscopy.



Figure 2.5 Picture of apparatus for Raman spectroscopy NRS-3000.

2.3 Infrared Heating Furnace

The samples were heated by using infrared heating furnace. When the samples were heated in Ar atmosphere, MILA-5000-P-N/ULVAC-RICHO Inc. was used (Figure 2.6a). The furnace is connected to an argon gas cylinder and Ar gas can be flowed in heating process. When the samples was heated in vacuum, MILA-5000-UHV/ULVAC-RICHO Inc. was used (Figure 2.6b). The base pressure was $\sim 5.0 \times 10^{-4}$ Pa. These 2 types of infrared heating furnaces can control the heating rate and cooling rate.

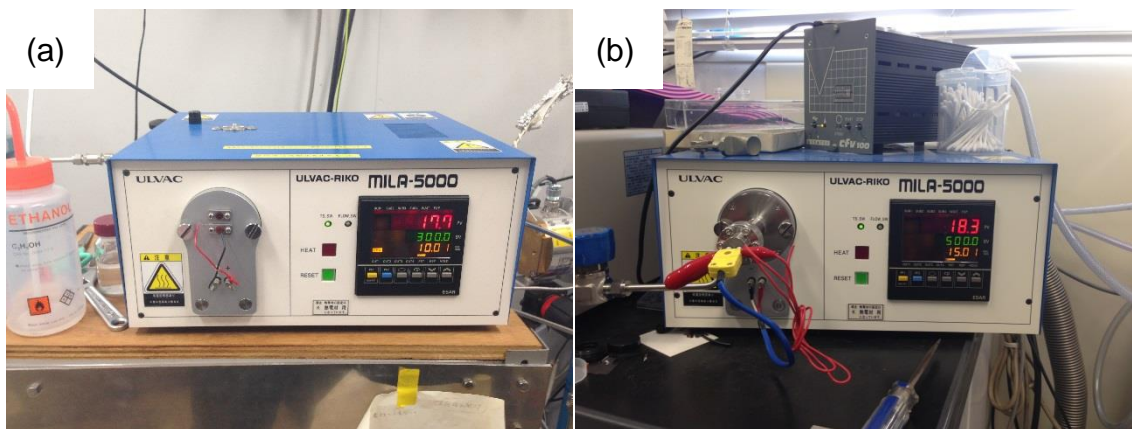


Figure 2.6 Pictures of infrared heating furnace (a) MILA-5000-P-N and (b) MILA-5000-UHV.

2.4 Conductivity Measurement Chamber

The conductivity of samples was measured in a conductivity measuring chamber (Figure 2.7). Graphene is sensitive to adsorbents [4] so annealing of graphene is necessary and the conductivity of graphene should be measured in vacuum. Thus I constructed a conductivity measurement chamber. Figure 2.8 shows the picture of sample stage. The tantalum wire heater is set under the sample stage. This heater can heat to about 300 °C. The base pressure is $\sim 1.0 \times 10^{-4}$ Pa.

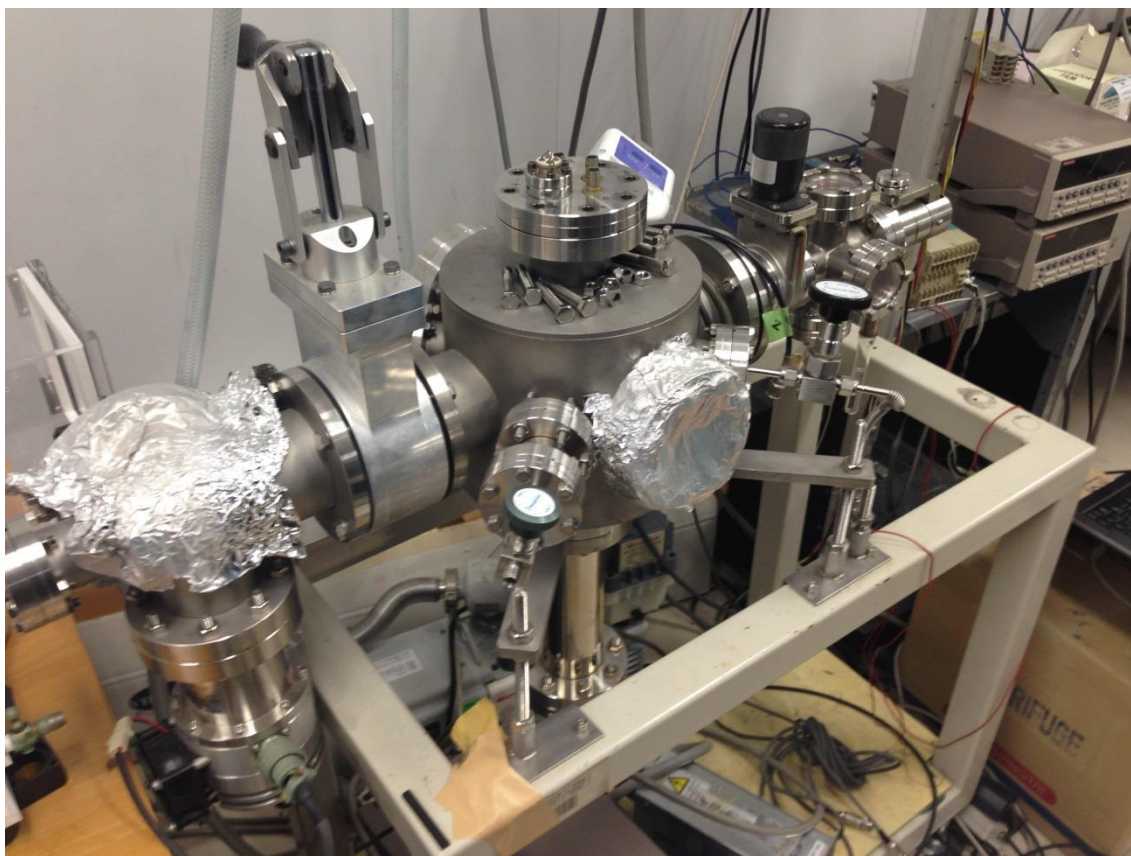


Figure 2.7 Picture of the conductivity measuring chamber.

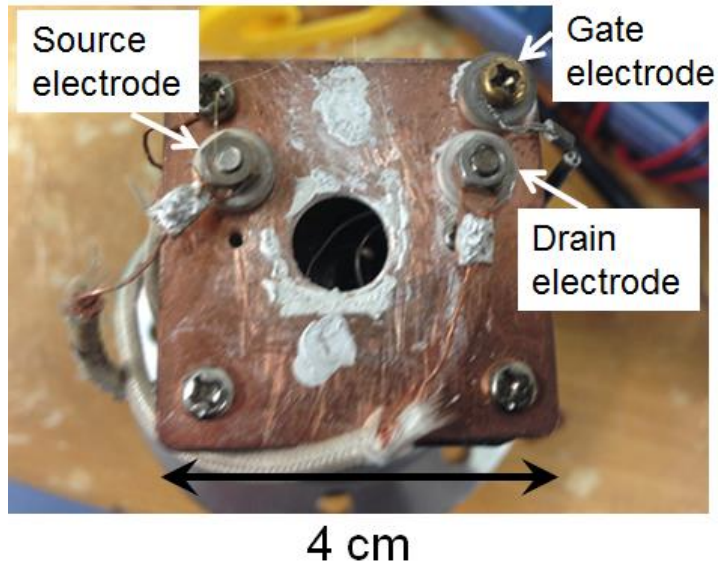


Figure 2.8 Picture of sample stage.

2.5 Other Equipment

Graphene is hydrophobic but GO is hydrophilic due to its oxygen functional groups [5]. So, GO can be dispersed to water and other polar solvents such as methanol. Surface tension of water is so high that deposition of GO on SiO_2/Si substrate is difficult. So, in order to deposit GO sheets homogeneously, GO sheets were dispersed to methanol, surface tension of which is lower than that of water. In addition to that, it is required to convert a SiO_2/Si substrate from hydrophobic to hydrophilic. To make SiO_2/Si substrate, it was treated by UV/ozone cleaner (UV-1/SUMCO. Ltd. shown in Figure 2.9). The temperature during cleaning was 50 °C and cleaning time was 10 min.



Figure 2.9 Picture of UV/ozone cleaner UV-1 .

The shape of graphene sheets were measured by scanning electron microscopy (JSM-6510/JEOL Ltd. shown in Figure 2.11).



Figure 2.10 Picture of scanning electron microscopy JSM-6510.

Spin-coating was conducted by using spin coater (K-359SD-1/KYOWARIKEN. CO. LTD shown in Figure 2.11).



Figure 2.11 Picture of spin coater K-359SD-1.

Centrifugation was conducted by using centrifuge (CN-2060/AS ONE Corporation shown in Figure 2.12).



Figure 2.12 Picture of centrifuge CN-2060.

References

- [1] Malard, L. M.; Pimenta, M. a.; Dresselhaus, G.; Dresselhaus, M. S. *Phys. Rep.* **2009**, 473, 51–87.
- [2] Krauss, B.; Lohmann, T.; Chae, D.-H.; Haluska, M.; von Klitzing, K.; Smet, J. *Phys. Rev. B* **2009**, 79, 1–9.
- [3] Kagi, H.; Tsuchida, I.; Wakatsuki, M.; Takahashi, K.; Kamimura, N.; Iuchi, K.; Hideki, W. *Geo. Cos. Acta* **1994**, 58, 3527-3530.
- [4] Schedin, F.; Geim, a K.; Morozov, S. V; Hill, E. W.; Blake, P.; Katsnelson, M. I.; Novoselov, K. S. *Nature Mater.* **2007**, 6, 652–5.
- [5] Paredes, J. I.; Villar-Rodil, S.; Martínez-Alonso, a; Tascón, J. M. D. *Langmuir* **2008**, 24, 10560–4.

Chapter 3

Graphene Preparation from Graphene Oxide by Annealing on Metal Surfaces

3.1 Introduction

Reduction of graphene oxide (GO) is a promising method for mass production of graphene. As mentioned in chapter 1, various reduction methods of GO has been reported [1-6] but reduced graphene oxide (rGO) is disordered due to defects and functional groups which are not removed by reduction process. Thus, to produce high-quality graphene at large scale, restoration of GO is required. Recently, our group reported that GO lattice can be restored by annealing at 1300 K on Pt (111) [7]. When GO was annealed at 1050 K on Si (100), honeycomb lattice was restored in some areas but the other areas remained disordered. On the other hand, when GO was annealed at 1300 K on Pt (111), most of honeycomb lattices in GO sheets were restored. However this reduction method has a problem that it is difficult to transfer restored GO sheets from a Pt (111) to insulating substrate such as SiO₂/Si. For applications of graphene to FET device, it is necessary to transfer graphene sheets to insulating substrate and a metal substrate which is supporting graphene sheets should be etched. Though platinum can be etched with aqua regia, it is so expensive that etching process is undesirable for industrial application. Generally, graphene is formed on Cu or Ni in CVD process [8-11]. So, I expected that GO sheets can be restored by catalysis of these metals and tried restoration of GO sheets by annealing on Cu and Ni. These metals are inexpensive and suitable for transfer process. In particular, Ni is expected as a catalyst of graphene restoration due to the good lattice match between graphene and Ni (111) face as shown in Figure 3.1. The hexagonal lattice constant is 2.497 Å for Ni (111) and 2.46 Å for

graphene.

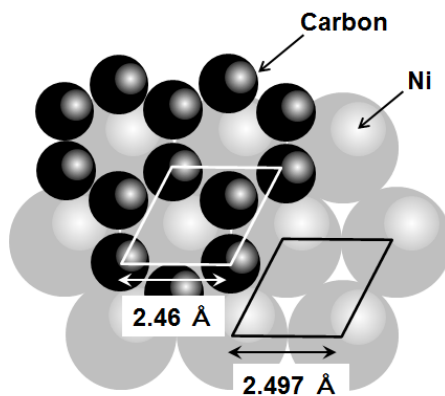


Figure 3.1 Schematic model of graphene on the Ni (111) surface.

In this study, I performed restoration of GO by two methods as follows. First, I tried to repair the defects of GO by annealing of GO sheets which was deposited on a metal foil. Second, I deposited a metal film on GO sheets and annealed it. Regarding this reduction method, dependence of the shape of graphene on the quantity of GO, the kind of metal overlayer and annealing temperature was investigated. Additionally, dependence of the shape of graphene on the thickness of Ni film and cooling rate was also investigated.

3.2 Annealing Graphene Oxide on Metal Foil

3.2.1 Experimental Method

· Synthesis of GO

GO was prepared by modified Hummers method [12, 13]. Graphite powder used in this experiment was SCB-100 (Nippon Graphite Industries, Ltd.), whose particle size was from 150 μm to 1180 μm (Figure 3.2). Graphite powder (250 mg) and NaNO_3 (188 mg) were put into concentrated H_2SO_4 (8.5 mL) and stirred by magnetic stirrer (500 rpm). The solution was cooled in an ice bath and KMnO_4 (1.13 g) was added slowly for 1h. As mentioned in section 1.4, dimanganese heptoxide (Mn_2O_7) forms by the reaction of KMnO_4 with H_2SO_4 . Dimanganese heptoxide is highly explosive, so it should be added slowly under cooling condition. Stirring was continued for 2h in an ice bath and then an ice bath was removed. The solution was stirred for 1 day at room temperature and it became very viscous and could not be stirred further. This viscous substance was left for 4 days and then it was added into 25 mL of 5 wt.% sulfuric acid aqueous solution slowly with stirring over 1 h and further stirred for 2 h. Then, 30 wt.% H_2O_2 (0.7 mL) was added and the mixture was stirred for 2 h at room temperature. Hydrogen peroxide reduces the residual manganese compound and the color of solution changed to yellow. The yellow color was due to pristine graphite oxide [14]. After that, the suspension was centrifuged at 1000 rpm for 10 min and the supernatant liquid was removed. Then, 3 wt.% H_2SO_4 /0.5 wt.% H_2O_2 aqueous solution was added to the bottom solid and it was dispersed. The dispersion liquid was centrifuged at 3000 rpm for 20 min. These washing processes, which consist of addition of H_2SO_4 / H_2O_2 aqueous solution, dispersion and centrifugation, were repeated 15 times. Next, deionized water was added into the bottom solid and the suspension was centrifuged (4000 rpm, 50 min) twice. After that, deionized water was added and the bottom solid was dispersed. The dispersion liquid was centrifuged at 4000 rpm for 70 min. These washing processes, which consist of addition of deionized water, dispersion and centrifugation, were repeated 20 times. Then the methanol was added to the bottom solid. Through this process, GO/methanol suspension was obtained. The lateral sizes of GO sheets were about 50 μm (Figure 3.3). This synthetic process was summarized in flow chart as

shown in Figure 3.4.



Figure 3.2 Picture of graphite powder (SCB-100) compared with one yen coin.

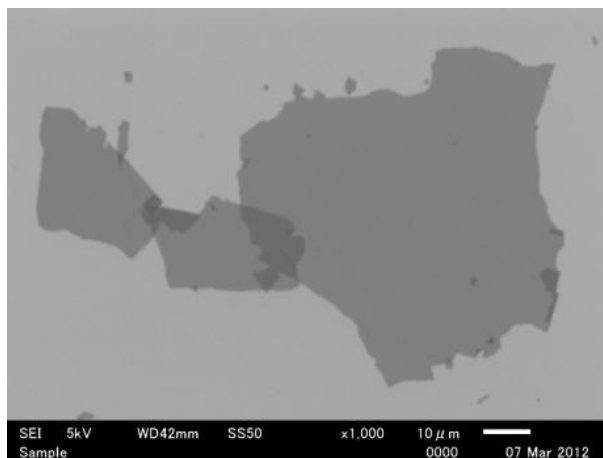


Figure 3.3 SEM image of GO sheets synthesized by modified Hummers method. The scale bar is 10 μm .

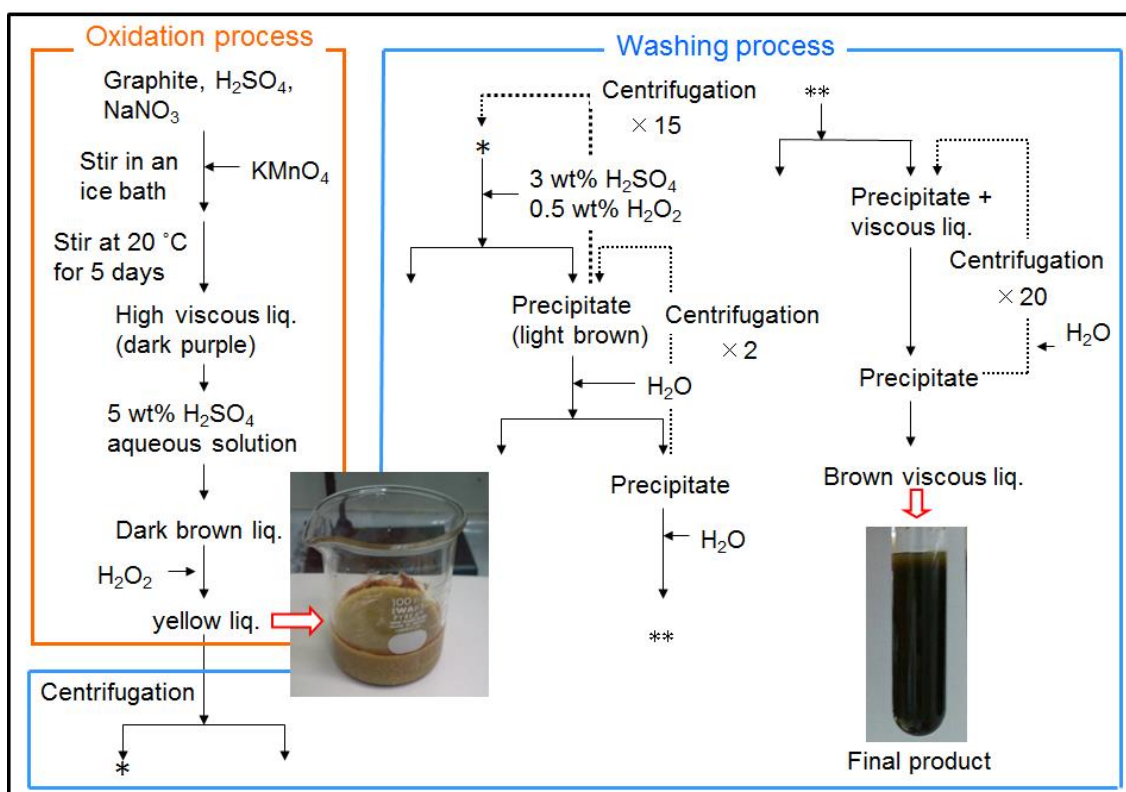


Figure 3.4 Synthesis process of GO.

· Reduction of GO by Annealing on Metal Foils

Figure 3.5 illustrates the process of GO reduction by annealing on metal foils. First, GO sheets were deposited by spin coating method (3000 rpm, 1 min) from methanol suspension on a metal foil (Cu and Ni). Then the sample was set in the infrared heating furnace and annealed at 800 or 900 °C for 30 min in Ar atmosphere. After that, PMMA (Poly(methyl methacrylate)) was deposited by spin coating method (3000 rpm, 1 min) from 2 wt.% PMMA/acetone solution on GO/metal. Next, the metal foil was etched with 0.3 mol/L FeCl₃ aqueous solution. After etching, PMMA/GO was put onto a SiO₂/Si substrate and heated at 70 °C to evaporate water and stick PMMA and SiO₂ together. Finally, PMMA was removed. In the case of Cu, PMMA was removed by washing with acetone. In the case of Ni, PMMA was removed by annealing at 1000 °C in vacuum.

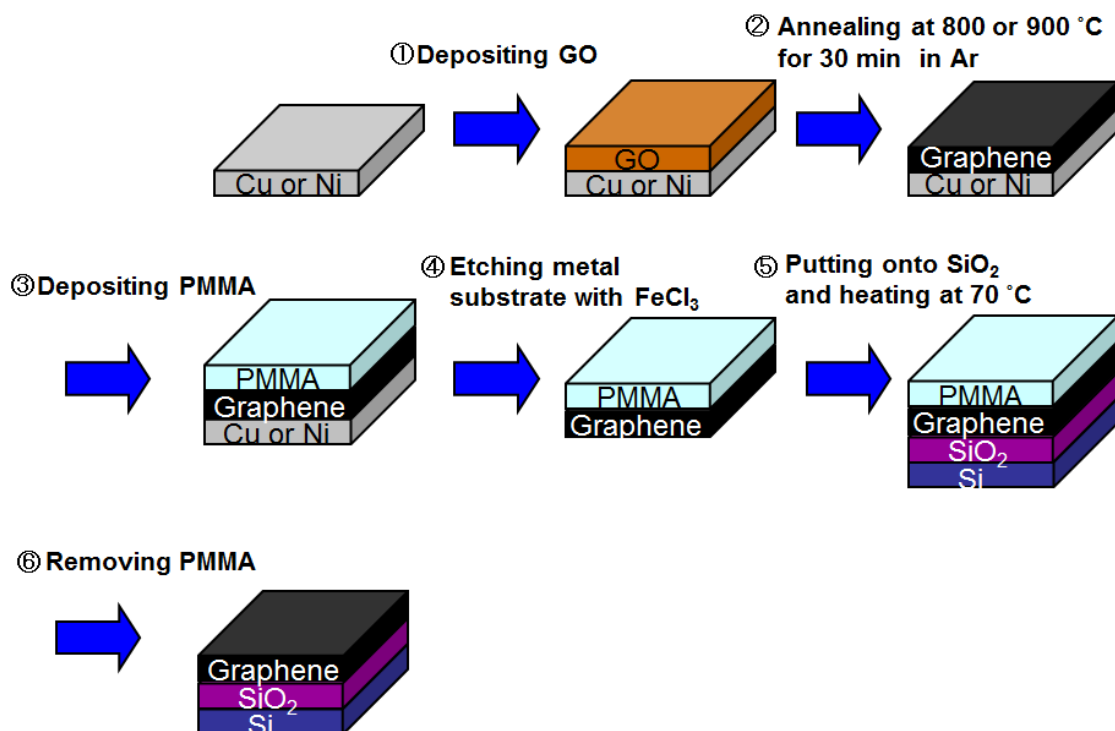


Figure 3.5 Reduction process by annealing of GO on metal foils

3.2.2 Results and Discussion

Figure 3.6(a) is SEM image of GO deposited on a Cu foil before annealing and Figure 3.6(b) is SEM image of GO after annealing at 900 °C and transfer to SiO₂ substrate, which is denoted by rGO (Cu, 900). The shape of rGO (Cu, 900) was almost similar to that of the original GO sheet. So, GO was transferred successfully. Figure 3.7 shows Raman spectra of GO before annealing and rGO (Cu, 900). Raman spectrum of rGO (Cu, 900) is similar to that of GO before annealing. In other words, the FWHM of G band and D band are broad, the D band intensity is high and the 2D band is not observed. This result suggests that GO was not restored by annealing on Cu foil. When GO was annealed at 1000 °C on Cu foil, Cu foil melted and GO sheets disappeared.

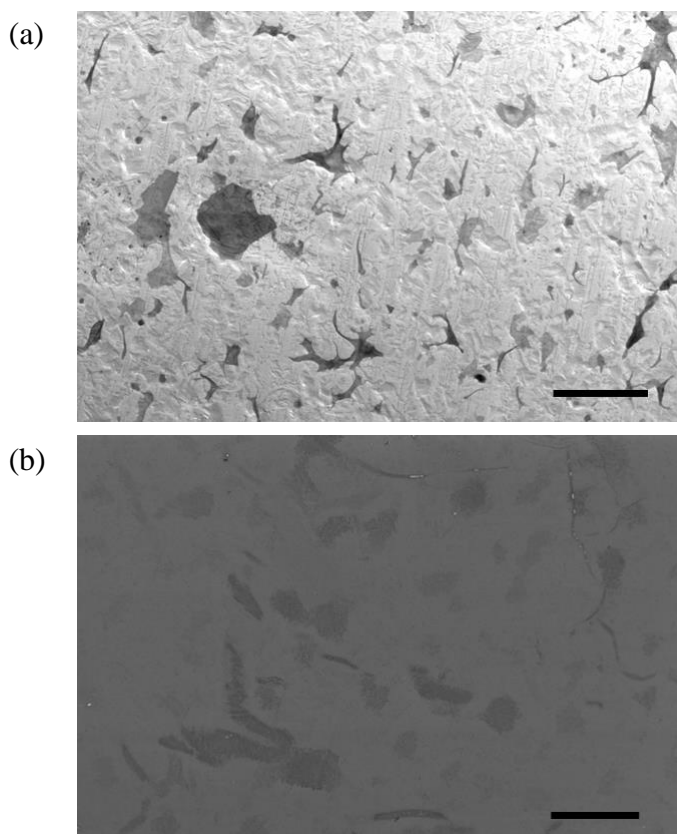


Figure 3.6 SEM images of GO (a) deposited on Cu foil before annealing, (b) after annealing at 900 °C and transfer to SiO₂. The scale bar is (a) 100 μm and (b) 50 μm.

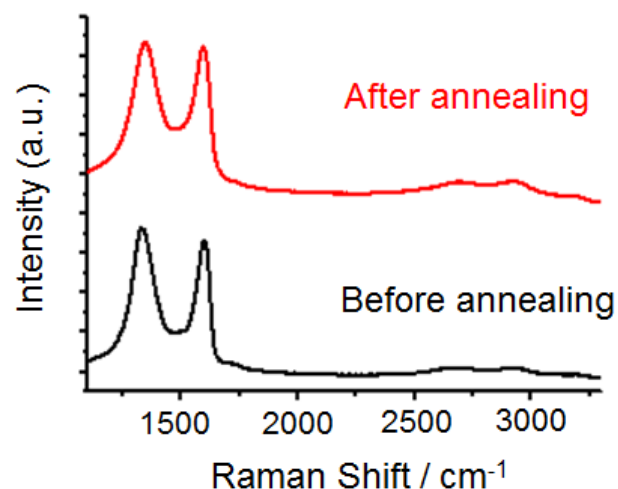


Figure 3.7 Raman spectra of GO before annealing (bottom) and after annealing at 900 °C on Cu foil and transfer to a SiO₂ substrate (top).

In the same way, GO was annealed on a Ni foil in Ar atmosphere. In the following rGO (Ni, T) denotes the sample which was formed by annealing at T °C on Ni foil and transferred to a SiO₂ substrate. In the case of rGO (Ni, 900), GO sheets disappeared. Figure 3.8 shows SEM image and optical microscope image of rGO (Ni, 800). Many wrinkle-like materials are observed. Figure 3.9 shows Raman spectra of rGO (Ni, 800), rGO (Ni, 700) and as grown GO. Compared with rGO (Ni, 800) and GO, FWHM of G band, FWHM of D band and the D band intensity of rGO (Ni, 800) are similar to that of GO but 2D band with weak intensity is observed in rGO (Ni, 800). 2D band of rGO (Ni, 700) is also observed but the intensity of it is weaker than that of rGO (Ni, 800). These results indicate that GO was restored by annealing on Ni film and effective temperature is 800 °C. Possibly, this restoration is due to carbon solution. Carbon solubility to Ni is about 0.4 % at 800 °C [15] and that to Cu is about 0.01 % at 900 °C [16]. The difference of carbon solubility might produce these results. However, in this method, most of GO sheets disappeared due to Ni evaporation. To avoid evaporation of GO sheets, I performed annealing GO at the interface between a Ni layer and SiO₂.

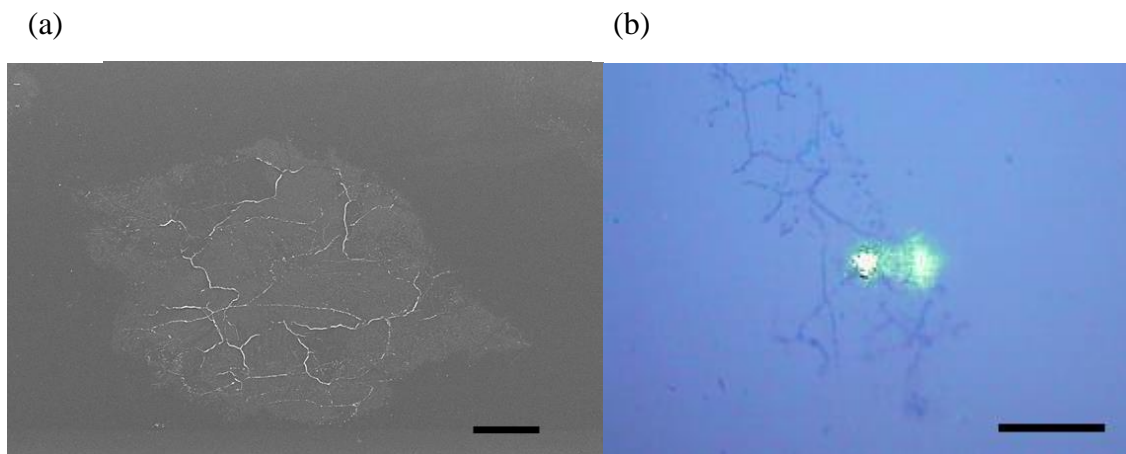


Figure 3.8 (a) SEM image and (b) optical microscope image of rGO (Ni, 800). All scale bars are equal to 20 μm.

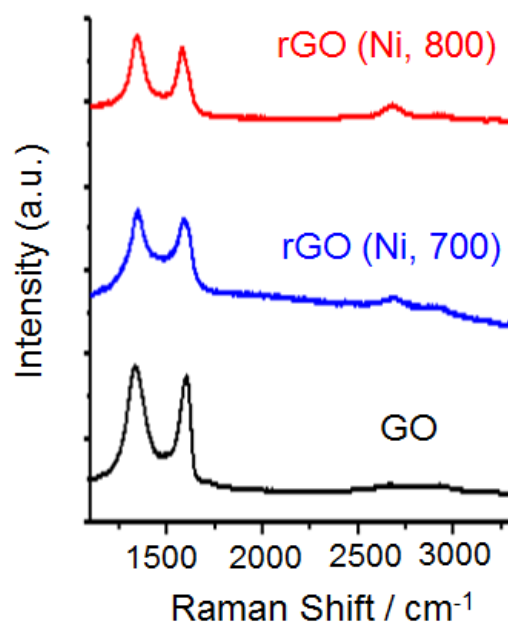


Figure 3.9 Raman spectra of GO (black), rGO (Ni, 700) (blue) and rGO (Ni, 800) (red).

3.3 Annealing Graphene Oxide between a Ni Layer and SiO₂

3.3.1 Experimental Method

Figure 3.10 illustrates the process of annealing GO between a 100 nm Ni layer and SiO₂. First, GO sheets were deposited by spin-coating method (3000 rpm, 1 min) from methanol suspension on SiO₂ substrate, which was made hydrophilic by UV-ozone treatment. Then a 100 nm Ni film was deposited on GO/SiO₂/Si substrate by vacuum evaporation method as mentioned in section 2.1. After that the sample was set in the infrared heating furnace and heated at 800 °C for 10 min in vacuum. Finally, a Ni film was etched with 0.3 mol/L aqueous solution and the sample was washed with deionized water and methanol.

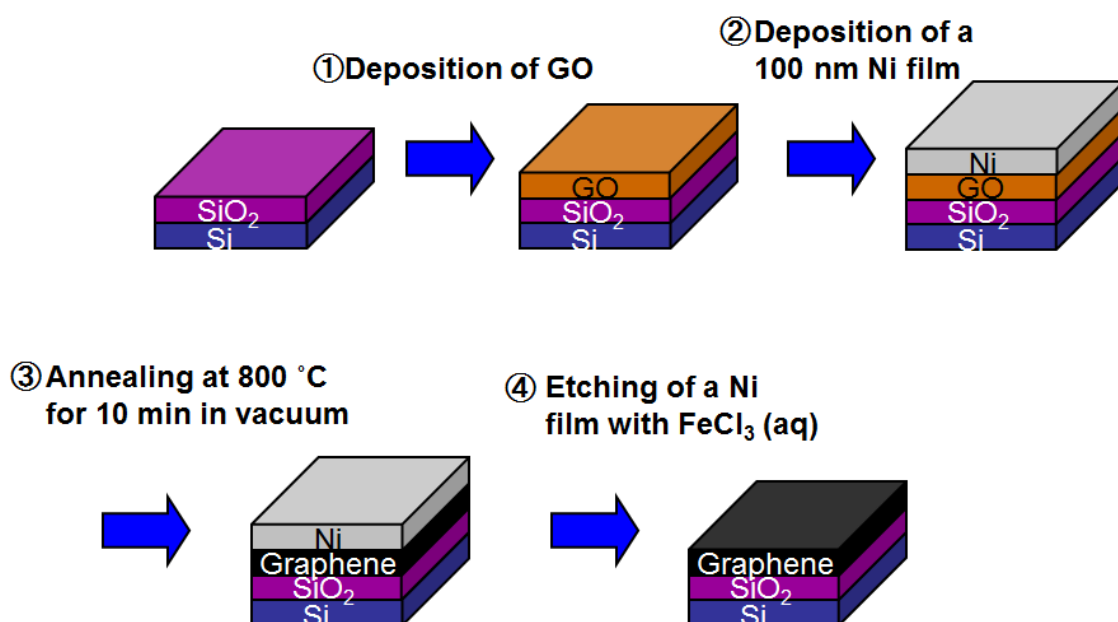


Figure 3.10 Reduction process by annealing of GO between a Ni layer and SiO₂.

3.3.2 Results and Discussion

Figure 3.11 shows the SEM image of GO annealed at 800 °C between a Ni layer and SiO₂ after etching and washing. The area circled by green line is where a Ni film was not deposited and in this area, rGO sheets were observed (sample A). In the area circled by blue line, large area sheets were observed (sample B). In the area circled by red line, threadlike materials were observed (sample C). Figure 3.12(a)-(c) show SEM images of sample A, B and C respectively. Sample A is rGO sheet with the similar shape and size of as grown GO sheet. The lateral size of sample A is about 50 μm. Sample B is the large sheet with lateral size of about 1 mm and this is about 20 times of the lateral size of original GO sheet. Judging from the contrast of SEM image, sample B may be thick. The thickness of this sample is discussed below. Sample C is the threadlike material with lateral size of about 10 μm and length of more than 1 mm. In sample C, twisted and branched structure is observed. Sample B was formed near the boundary of the area where a Ni film was deposited and not deposited. On the other hand, sample C was formed in the area where is far from the boundary.

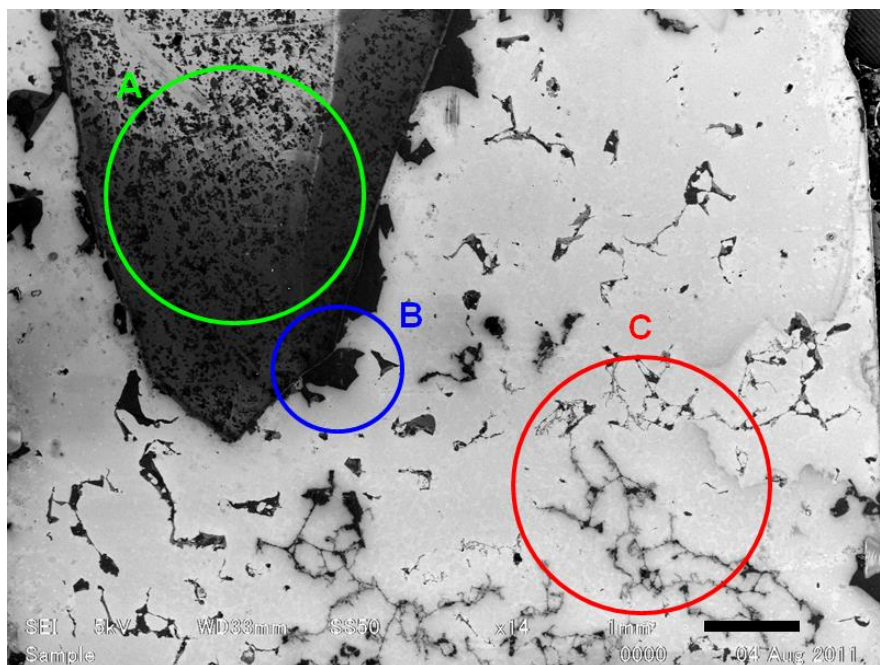


Figure 3.11 SEM image of GO after annealing at 800 °C between a Ni layer and SiO₂ after etching and washing.

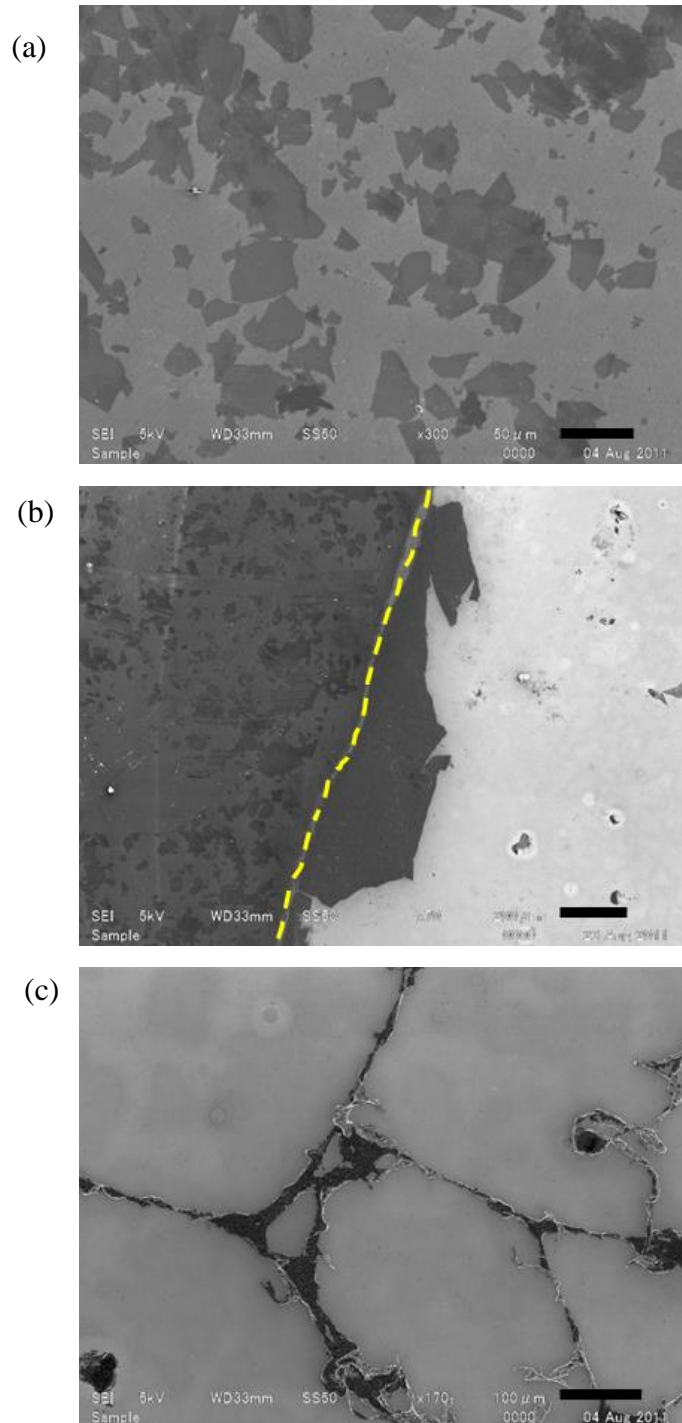


Figure 3.12 (a)-(c) SEM images of sample A, B and C respectively. The yellow dash line is a boundary of the area where a Ni film was deposited and not deposited. The scale bar of (a)-(c) is 50 μm , 200 μm and 100 μm respectively.

To evaluate the quality of these samples, Raman spectroscopy was conducted on these samples. Figure 3.13 (a)-(c) show the optical microscopic images of sample A, B and C. Figure 3.13 (d) shows Raman spectra of sample A, B and C together with that of GO. Raman spectrum of sample A is similar to that of GO, so sample A was not restored. On the other hand, Raman spectra of sample B and C are different from that of GO. In sample B and C, the intensity ratio of D band and G band; I_D/I_G is small, G band and D band sharpened, G band show red shift and 2D band can be observed. These results indicate that sample B and C were restored GO, which is suitable for being called graphene than GO. Raman spectra were measured at 5 points for each sample. The G band shift, FWHM of G band; Γ_G , I_D/I_G and I_{2D}/I_G of each sample are plotted as shown in Figure 3.14 (a)-(d) respectively. The G bands of sample A are at around 1600 cm^{-1} , on the other hand, that of sample B and C are at around 1580 cm^{-1} , which are close to the position of monolayer graphene on SiO_2 substrate [17]. About FWHM of G band, Γ_G of sample A have width of about $60\text{-}70\text{ cm}^{-1}$. Γ_G of sample B and C have width of about $20\text{-}50\text{ cm}^{-1}$, $30\text{-}60\text{ cm}^{-1}$ respectively. These widths are broader than that of pristine graphene ($\sim 14.2\text{ cm}^{-1}$ [17]) but sharper than that of GO, which is similar to that of sample A. The intensity ratio I_D/I_G of sample A, B and C are around 1.8, 0.1-1.1 and 0.2-0.9 respectively. It is reported that the crystallite size of graphene can be calculated by using an equation (3.1) [18]:

$$L_a(\text{nm}) = (2.4 \times 10^{-10}) \lambda_l^4 \left(I_D/I_G \right)^{-1} \quad (3.1)$$

where L_a is the crystalline size in nm units and λ_l is the laser line wavelength in nm unites. In this experiment, λ_l is 532 nm. From the I_D/I_G ratio and this equation, L_a of sample A, B and C are about 10 nm, 17-192 nm and 21-96 nm respectively. Compared with pristine graphene, sample B and C are more defective and its crystalline sizes are small. However, the crystalline size of about 100 nm was restored by this method. About the 2D band intensity, I_{2D}/I_G ratios of sample A are nearly zero. Those of sample B and C vary widely and are about 0.4-1.8. These results suggest that monolayer, bilayer and multilayer graphene exist in sample B and C. For industrial application of graphene, threadlike graphene of sample C is not suitable and it is desirable to obtain

monolayer or bilayer graphene selectively. It is necessary to clarify the reduction mechanism of GO in order to high-quality thin graphene sheet. Thus, I investigated the dependence of the shape of graphene on the quantity of GO, the kind of metal overlayer and annealing temperature.

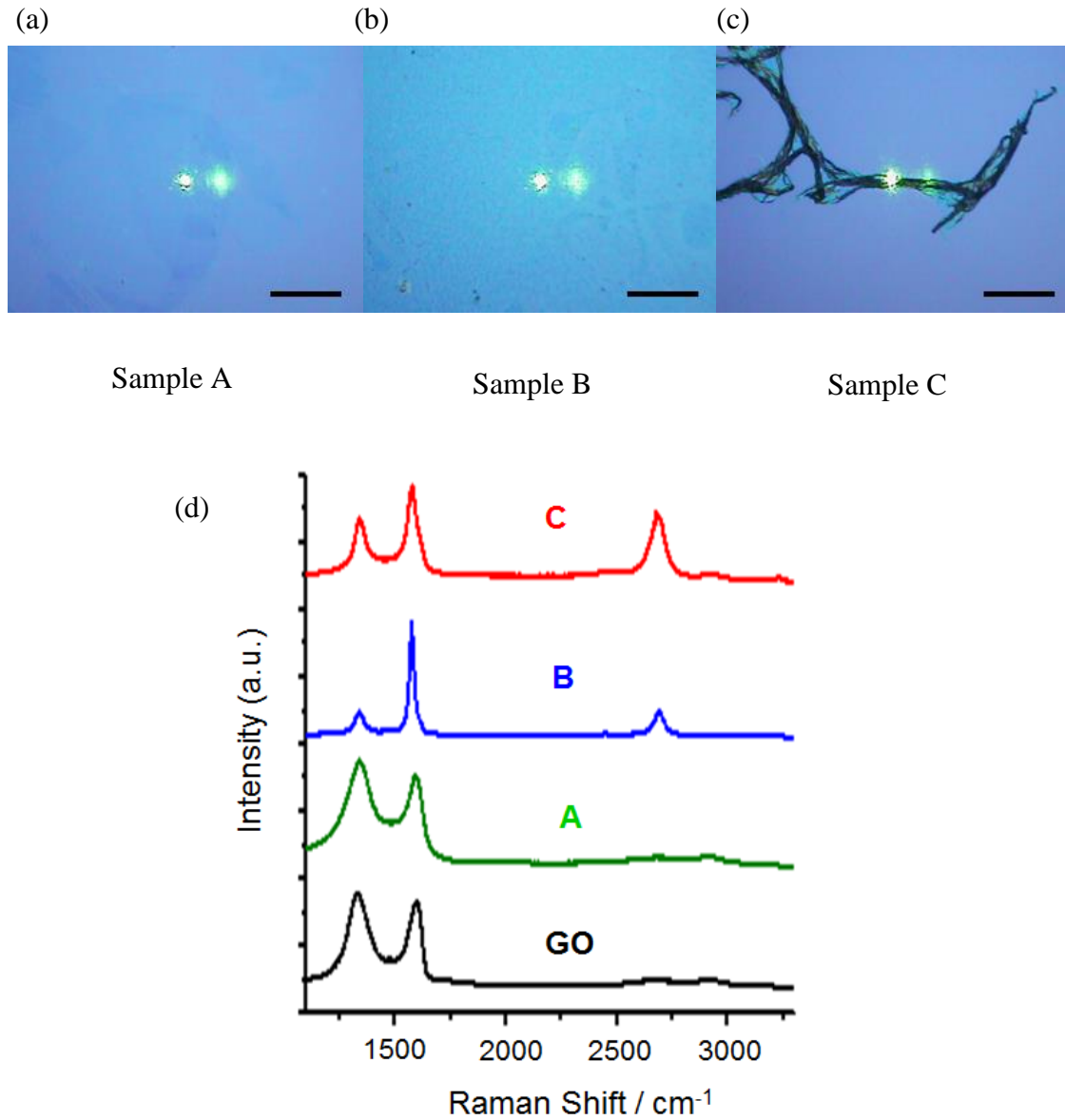


Figure 3.13 (a)-(c) Optical microscopic images of sample A, B and C at measurement point. All scale bars are equal to 20 μm . (d) Raman spectra of GO, sample A, B and C.

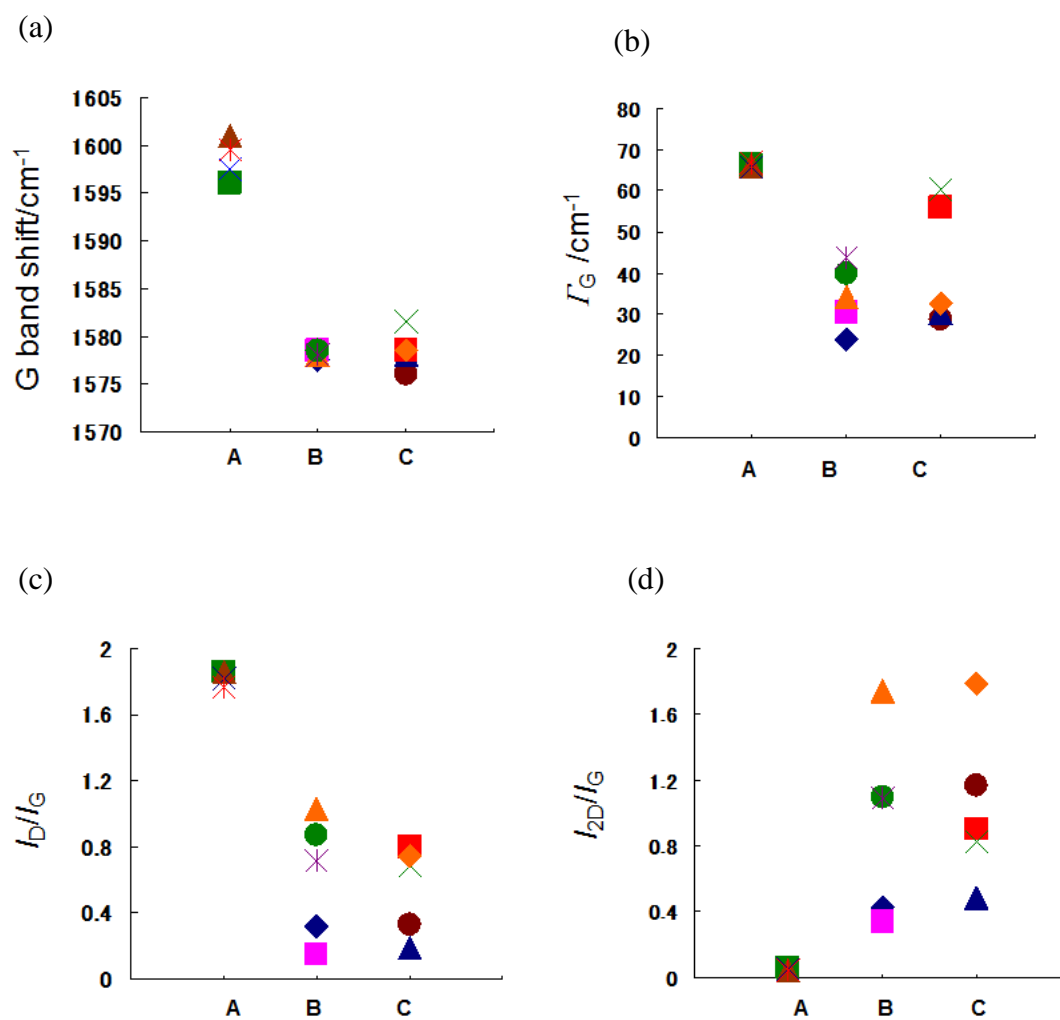


Figure 3.14 (a) G band shift, (b) GG, (c) I_D/I_G and (d) I_{2D}/I_G of GO, sample A, B and C.

3.4 Dependence of the Shape of Graphene on the Quantity of Graphene Oxide, the Kind of Metal Overlayer and Annealing Temperature

3.4.1 Experimental Method

To clarify the reduction mechanism of GO, I changed GO reduction conditions, which were the quantity of GO, the kind of metal overlayer and annealing temperature, and investigated the factor to decide the shape of graphene by examining what kind shape of graphene formed under each condition. Figure 3.15 illustrates the reduction process and conditions of GO. First, GO sheets were deposited on a SiO₂/Si substrate, which was made hydrophilic by UV-ozone treatment. The quantity of GO was adjusted by following methods; spin-coating of 1 drop of GO/methanol suspension or casting of 10 drops of it. Then a metal film was deposited on the sample. The kind of metal overlayer was 100 nm Ni film or 50 nm Pd film. When the thickness of Pd film was 100 nm, the Pd film was peeled when the sample was annealed. So the thickness of Pd film is 50 nm. Then the sample was set the infrared heating furnace and annealed for 10 min in vacuum. The annealing temperature was 800 °C or 1000 °C. After annealing, the sample was cooled to room temperature at about 30 °C/s. After that a metal film was etched. Nickel and palladium films were etched with FeCl₃ aqueous solution and HNO₃ aqueous solution respectively. Finally, the sample was washed with deionized water and methanol. The shape of graphene was observed by SEM and the quality of graphene was evaluated by Raman spectroscopy. In the following, Gr (1 drop (10 drops), Ni (Pd), 800 (1000)) denotes the sample which was formed by depositing 1 drop (10 drops) of GO suspension and Ni (Pd) overlayer and annealing at 800 (1000) °C.

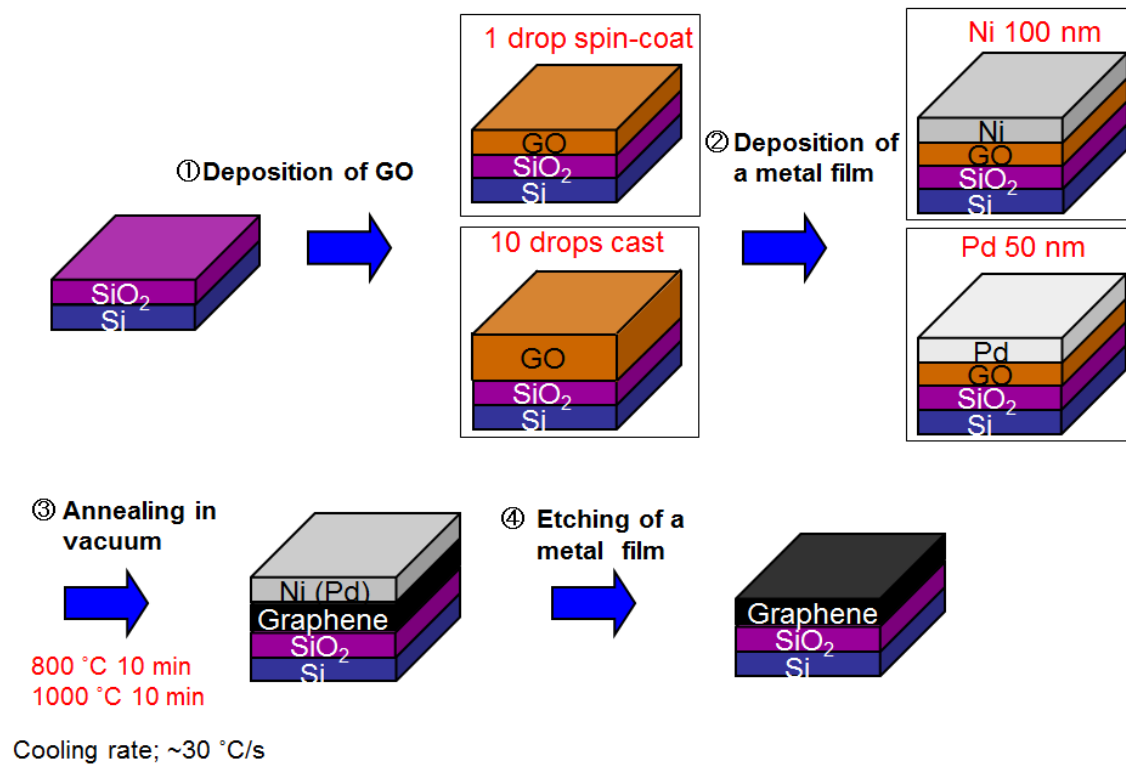


Figure 3.15 Reduction process and conditions of GO. The quantity of GO, the kind of metal overlayer and annealing temperature were changed.

3.4.2 Results and Discussion

First, influence of the quantity of GO sheets which was deposited on a SiO₂ substrate on the shape of graphene was investigated. Figure 3.16 (a) and (b) show SEM image of Gr (10 drop, Ni, 800). From SEM images, only large area graphene with the lateral size of about 50-100 μm was observed and threadlike graphene was not observed. Figure 3.16 (c) is optical microscope image and (d) is Raman spectrum measured at the circled point in (c). From Raman spectrum, the I_D/I_G ratio is low (0.10) and 2D band can be observed but the I_{2D}/I_G ratio is less than 1 (0.55). These results indicate that large area graphene sheets with a few defects were formed and they were multilayer. To investigate the distribution of defects, I_D/I_G mapping was measured. Figure 3.17 shows I_D/I_G mapping of (a) Gr (10 drops, Ni, 800) and (b) Gr (1 drop, Ni, 800). Compared with these mapping, I_D/I_G of Gr (10 drops, Ni, 800) is lower than that of Gr (1 drop, Ni, 800). In addition to this, I_D/I_G of Gr (1 drop, Ni, 800) is lacking in uniformity and varies considerably with location but that of Gr (10 drops, Ni, 800) is uniform.

Influence of the kind of metal overlayer on the shape of graphene was investigated. Figure 3.18 (a) and (b) show SEM images of Gr (1 drop, Pd, 800). Only threadlike graphene is observed and large area graphene was not observed. The diameter of this sample is about 1 μm and this is smaller than that of Gr (1 drop, Ni, 800). Figure 3.18 (c) is optical microscopic image and (d) is Raman spectrum. In this sample, the I_D/I_G ratio is 0.12 and the I_{2D}/I_G ratio is 1.06. Judging from these values, defects in this sample was very few and this threadlike graphene was bi-layer.

Influence of annealing temperature was investigated. Figure 3.19 (a)-(d) show low-magnification SEM image, high-magnification SEM image, optical microscope image and Raman spectrum of Gr (1 drop, Ni, 1000), respectively. From SEM images, only threadlike graphene was observed and large area graphene was not observed as in the case of Gr (1 drop, Pd, 800). However the diameter of Gr (1 drop, Ni, 1000) was different from that of Gr (1 drop, Pd, 800) and it was about several tens micrometers. With respect to Raman spectrum, the I_D/I_G ratio is 0.17 and the I_{2D}/I_G ratio is 1.34. These intensity ratios indicate that this threadlike graphene had a few defects and this sample was monolayer or bi-layer.

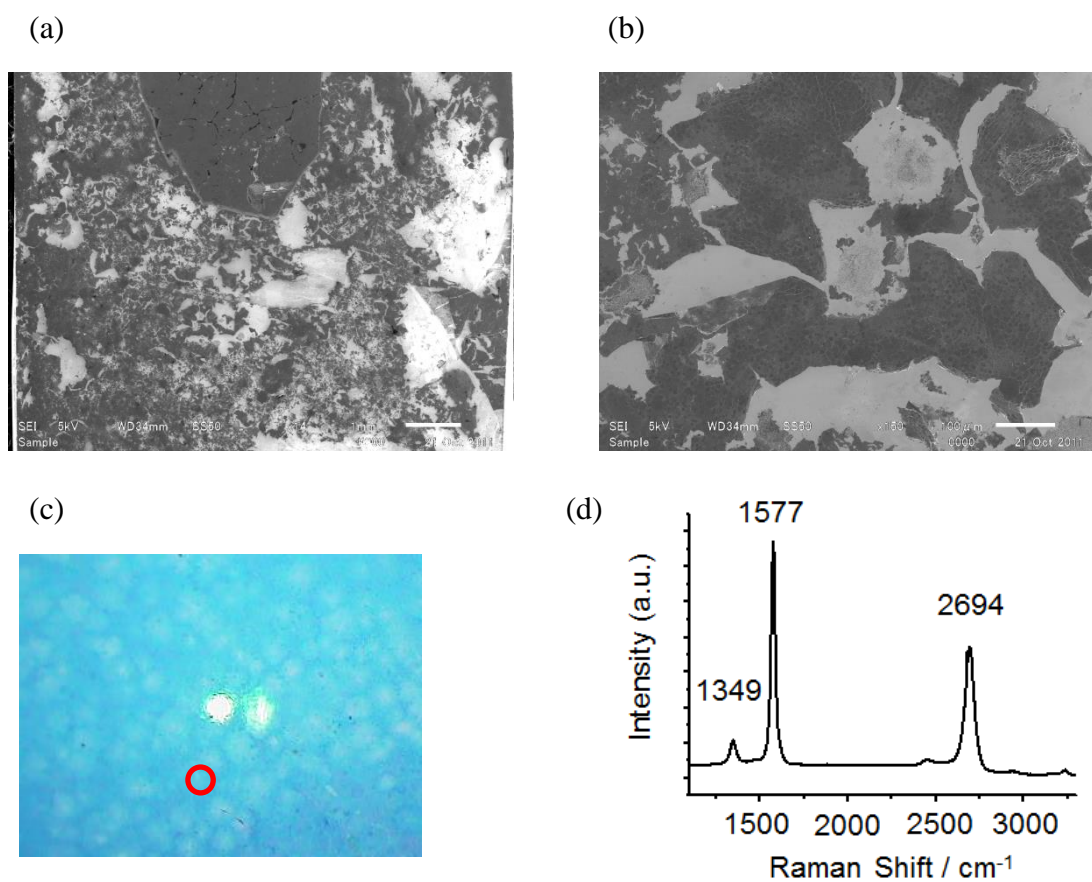


Figure 3.16 (a) low-magnification SEM image, (b) high-magnification SEM image, (c) optical microscope image and (d) Raman spectrum of Gr (10 drops, Ni, 800). Raman spectrum was measured at the circled area in (c). The scale bars are (a) 1mm and (b) 100 μm.

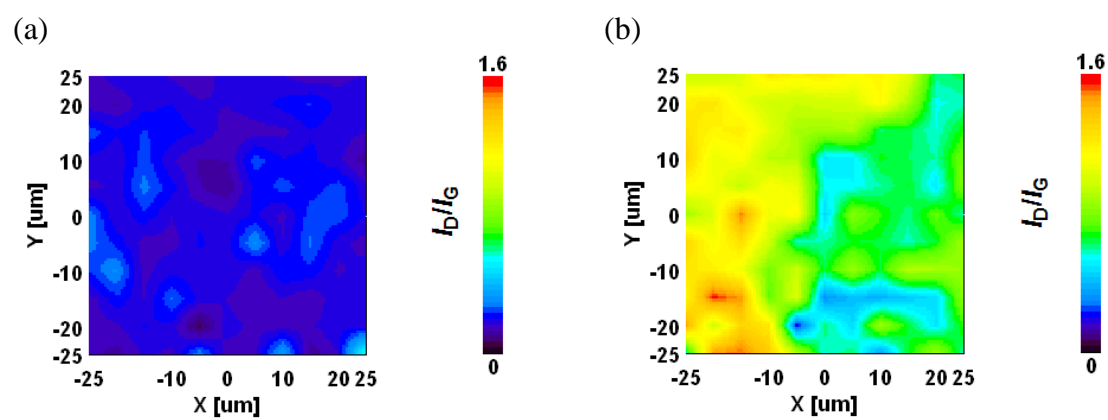


Figure 3.17 I_D/I_G mapping of (a) Gr (10 drops, Ni, 800) and (b) Gr (1 drop, Ni, 800).

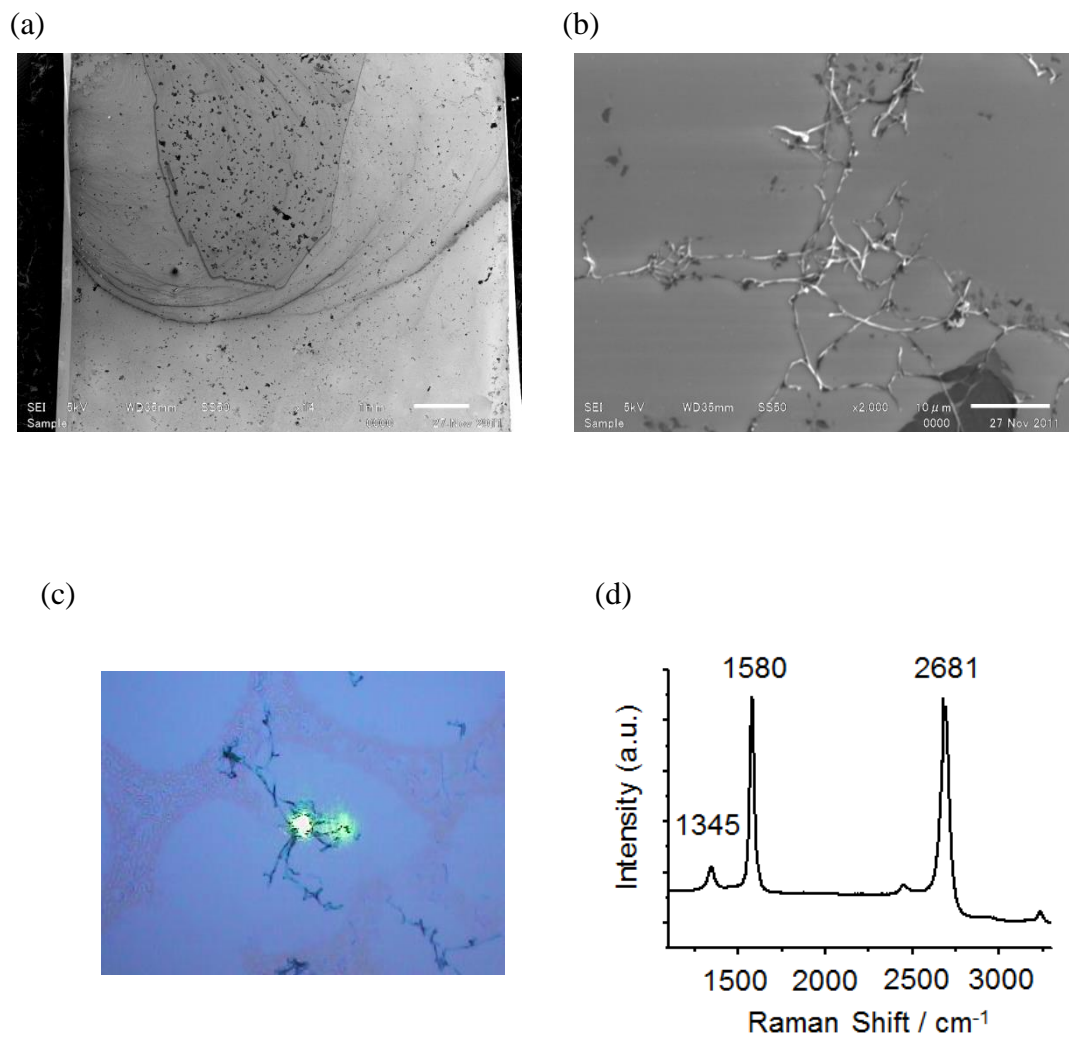


Figure 3.18 (a) Low-magnification SEM image, (b) high-magnification SEM image, (c) optical microscope image and (d) Raman spectrum of Gr (1 drop, Pd, 800). Raman spectrum was measured at the area irradiated with a laser in (c). The scale bars are (a) 1mm and (b) 10 μ m.

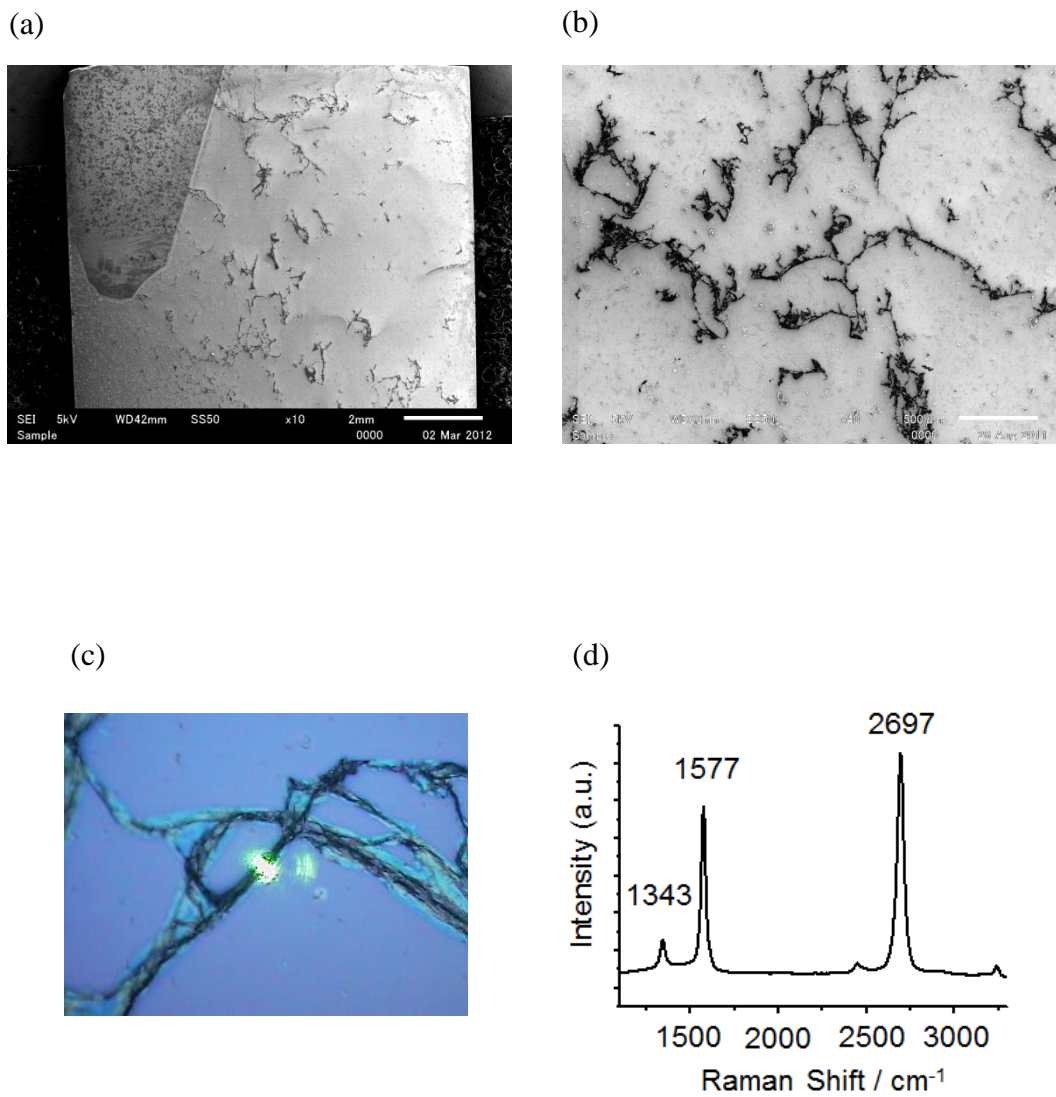


Figure 3.19 (a) Low-magnification SEM image, (b) high-magnification SEM image, (c) optical microscope image and (d) Raman spectrum of Gr (1 drop, Ni, 1000). Raman spectrum was measured at the area irradiated with a laser in (c). The scale bars are (a) 2 mm and (b) 500 μm.

When the quantity of GO was increased to 10 drops, only large area graphene was formed as seen in Gr (10 drops, Ni, 800) and when annealing temperature was increased to 1000 °C, only threadlike graphene was formed as seen in Gr (1 drop, Ni, 1000). When both of the quantity of GO and annealing temperature were increased, it was investigated whether Gr (10 drops, Ni, 1000) was large area graphene or threadlike graphene. The result is as shown in Figure 3.20. Figure 3.20 (a) and (b) show SEM images of Gr (10 drops, Ni, 1000). In Figure 3.20 (a), large area graphene is observed on the other hand, in Figure 3.20 (b), threadlike graphene was observed. Thus, both of large area graphene and threadlike graphene were formed in the case of Gr (10 drops, Ni, 1000). Figure 3.20 (e) and (f) are Raman spectra of large area graphene and threadlike graphene respectively. Figure 3.20 (c) and (d) are optical microscopy images of the area where Raman spectra of Figure 3.20 (e) and (f) were measured respectively. In Figure 3.20 (e), the I_D/I_G ratio is 0.02 and the I_{2D}/I_G ratio is 0.36. In Figure 3.20 (f), the I_D/I_G ratio is 0.18 and the I_{2D}/I_G ratio is 0.45. Judging from these values, both of large area graphene and threadlike graphene were relatively high quality but they were thick.

In the case of Gr (10 drops, Pd, 800), the results are as shown in Figure 3.21. Figure 3.21 (a) and (b) show SEM images of Gr (10 drops, Pd, 800). In the case of Gr (1 drop, Pd, 800), only threadlike graphene was formed and in the case of Gr (10 drops, Ni, 800), only large area graphene was formed. In the case of Gr (10 drops, Pd, 800), only large area graphene was formed and no threadlike graphene was observed as in the case of Gr (10 drops, Ni, 800). Figure 3.21 (c) and (d) are optical microscope image and Raman spectrum respectively. The I_D/I_G ratio is 0.43 and the I_{2D}/I_G ratio is 0.26. These values indicate that some defects existed in (10 drops, Ni, 800) and this large area graphene was thick. Figure 3.21 (e) shows I_D/I_G mapping of this sample. Compared with Figure 3.17 (b), the I_D/I_G ratio is relatively uniform but compared with Figure 3.17 (a), the I_D/I_G ratio is higher than that of Gr (10 drops, Ni, 800).

In the cases of Gr (1 drop, Pd, 1000) and Gr (10 drops, Pd, 1000), the results are shown in Figure 3.22 and Figure 3.23 respectively. From SEM images, in both cases, most of GO sheets disappeared and some GO fragments remained. Raman spectrum of Gr (1 drop, Pd, 1000), the I_D/I_G ratio is 1.42 and the I_{2D}/I_G ratio is 0.10. In the case of Gr

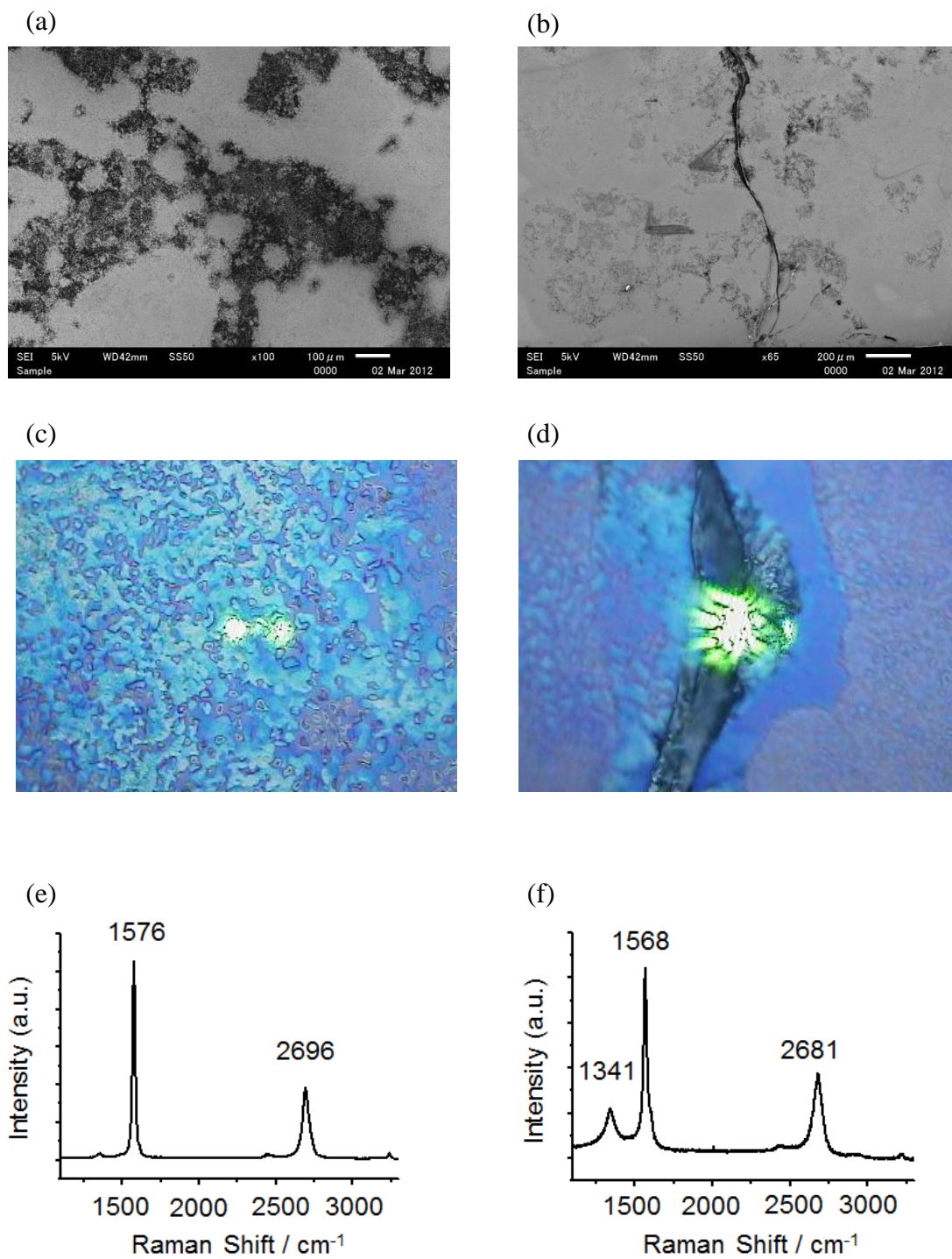


Figure 3.20 (a)(b) SEM images, (c)(d) Optical microscope images and (e)(f) Raman spectra of Gr (10 drops, Ni, 1000). (a)(c) and (e) are about large area graphene. (b)(d) and (f) are about threadlike graphene.

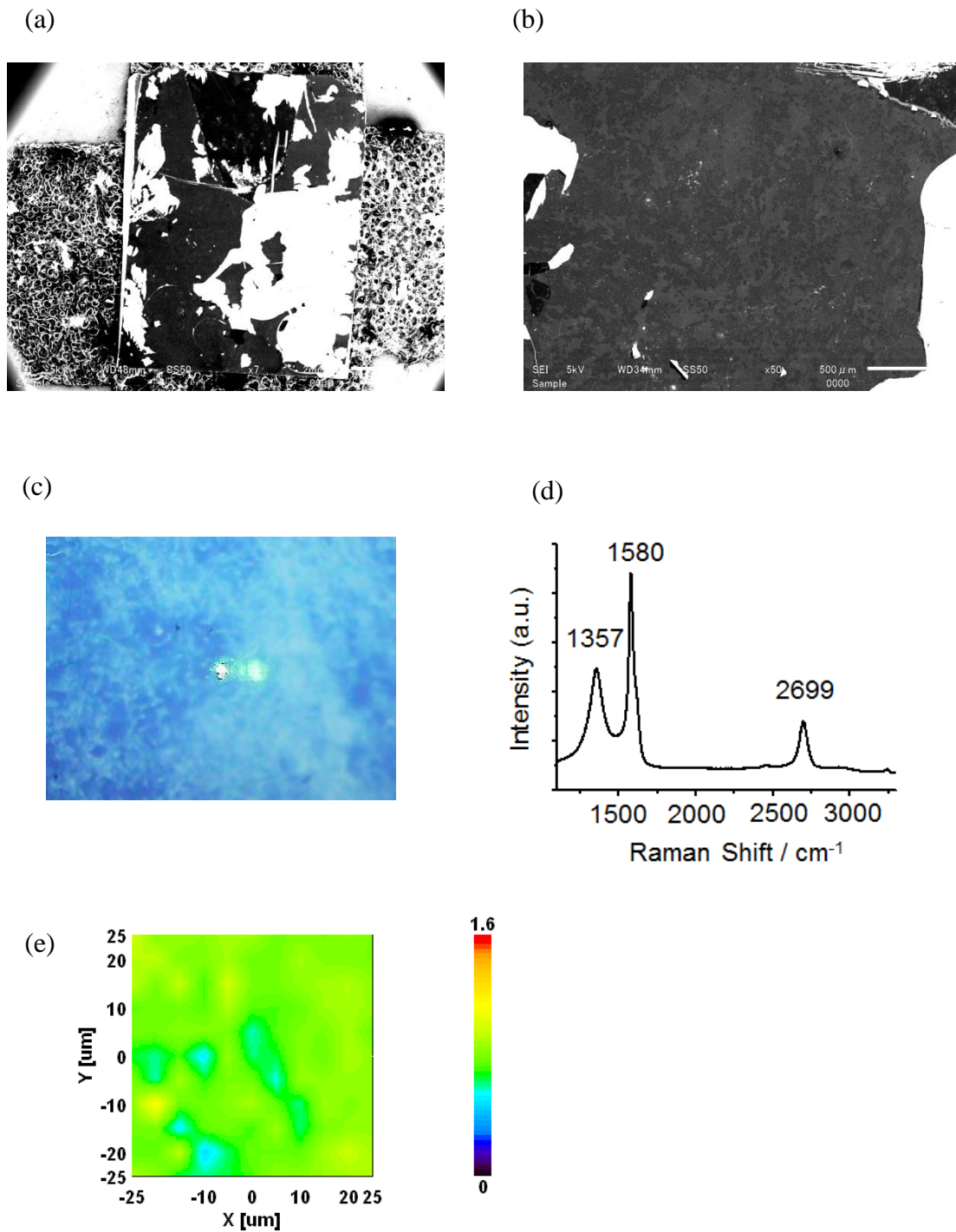


Figure 3.21 (a) Low-magnification SEM image, (b) high-magnification SEM image, (c) optical microscope image, (d) Raman spectrum and (e) I_D/I_G mapping of Gr (10 drops, Pd, 800). Raman spectrum was measured at the area irradiated with a laser in (c). The scale bars are (a) 2 mm and (b) 500 μm.

(10 drops, Pd, 1000), the I_D/I_G ratio is 1.38 and the I_{2D}/I_G ratio is 0.15. In both samples, the I_D/I_G ratio is high and the I_{2D}/I_G ratio is low. These values suggest that GO was not restored. These results were due to evaporation of Pd film. When the sample after depositing a Pd film was annealed, most Pd film disappeared. Thus, most of GO sheets also disappeared and were not restored.

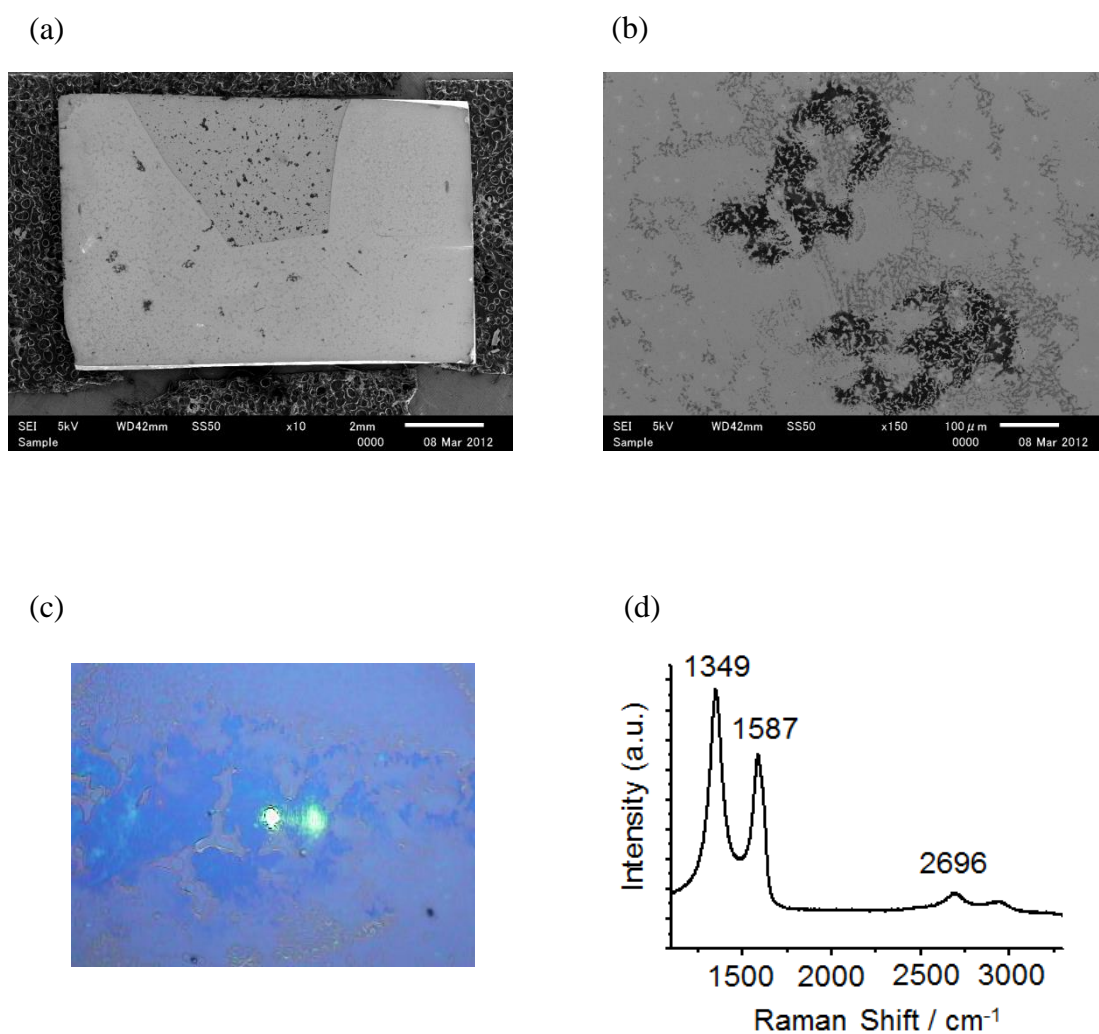


Figure 3.22 (a) Low-magnification SEM image, (b) high-magnification SEM image, (c) optical microscope image and (d) Raman spectrum of Gr (1 drop, Pd, 1000). Raman spectrum was measured at the area irradiated with a laser in (c). The scale bars are (a) 2 mm and (b) 100 μm .

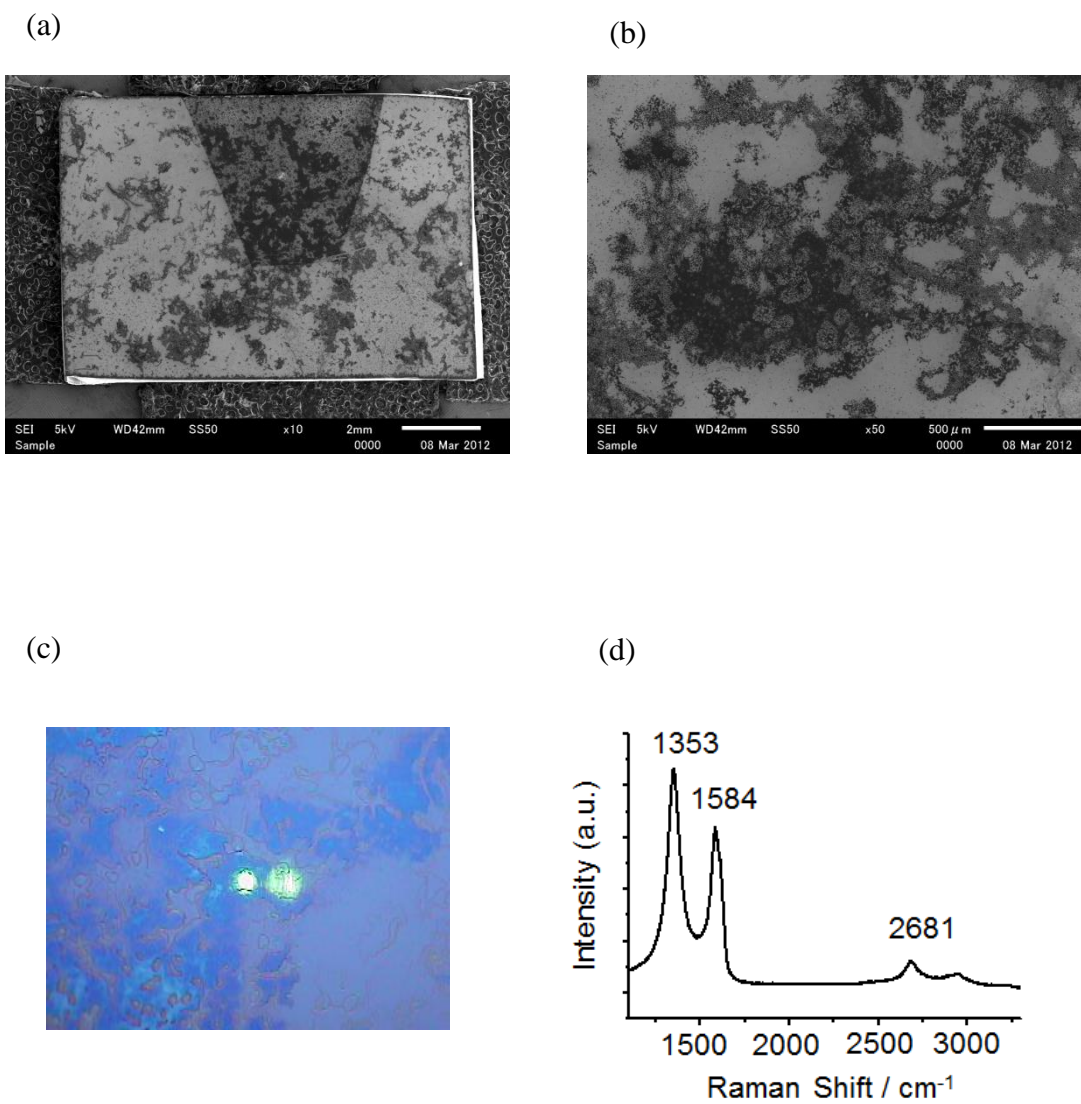


Figure 3.23 (a) Low-magnification SEM image, (b) high-magnification SEM image, (c) optical microscope image and (d) Raman spectrum of Gr (10 drops, Pd, 1000). Raman spectrum was measured at the area irradiated with a laser in (c). The scale bars are (a) 2 mm and (b) 500 μm .

These results are summarized in Table 3.1 About the quantity of GO suspension, large area graphene formed in the case of 10 drops and threadlike graphene formed in the case of 1 drop. About the kind of metal overlayer, large area graphene tended to form in the case of Ni film and threadlike graphene formed in the case of Pd film. About annealing temperature, large area graphene formed in the case of 800 °C and threadlike graphene formed in the case of 1000 °C. When the quantity of GO is high, the quantity of carbon atoms which dissolve into metal layer is high. It is reported that the carbon solubility to Pd is higher than to Ni [15, 19]. And generally, the carbon solubility to metal layer increase with temperature [15, 19]. Thus, the factor to decide the shape of graphene should be the quantity of the carbon atoms which can dissolve into a metal layer.

Table 3.1 The shapes of graphene formed under each condition.

	Ni 100 nm		Pd 50 nm	
	1 drop	10 drops	1 drop	10 drops
800 °C	Threadlike Large area	Large area	Threadlike	Large area
1000 °C	Threadlike	Threadlike Large area	GO	GO

These results and these facts suggested the reduction mechanism of GO. Figure 3.24 shows the growth mechanism model of (a) threadlike graphene and (b) large area graphene. Oxygen molecules were eliminated by annealing but the quantity of oxygen was so slight compared to Ni that oxygen might have little on the Ni film. GO between a metal film and SiO₂ substrate is decomposed and dissolve into a metal layer by annealing. When the carbon atoms dissolved into a metal layer entirely, no GO fragment remained. Then in cooling process, carbon atoms segregated. It was reported that carbon atoms which diffuse in Ni film segregate at grain boundaries preferentially [20-22]. Also in this case, carbon atoms segregated at the grain boundaries and threadlike graphene was formed as shown in Figure 3.24 (a). On the other hand, when not all carbon atoms were decomposed and dissolved into a metal layer due to high quantity of GO or low carbon solubility to a metal film, some GO fragments were left. These GO fragments should be center of graphene growth and carbon atoms segregated around the GO fragments in cooling process. As a result, large area graphene was formed as shown in Figure 3.24 (b).

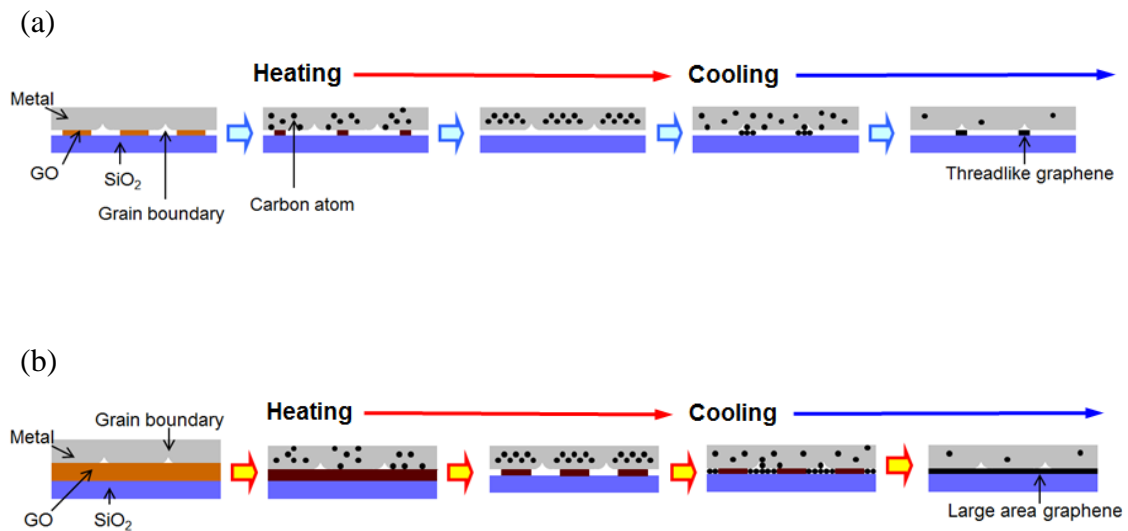


Figure 3.24 The growth mechanism model of (a) threadlike graphene and (b) large area graphene.

To obtain more information about the quality of graphene, FET measurement was performed by using the conductivity measuring chamber (section 2.4). Figure 3.25 (a) and (b) show current-bias (I_{sd} - V_{sd}) curves and current-gate voltage (I_{sd} - V_g) curve of Gr (10 drops, Ni, 800) respectively. From Figure 3.25 (b), Gr (10 drops, Ni, 800) shows bipolar characteristics. This sample was fabricated by annealing for 6 min but the quality was same as that fabricated by annealing for 10 min. From the linear region of the current-gate voltage (I_{sd} - V_g) curve, the carrier mobilities of electrons and holes can be obtained by using equation (3.2) [23].

$$\mu = \frac{L}{WC_0V_{sd}} \times \frac{d(I_{sd})}{d(V_g)} \quad (3.2)$$

where W and L are channel width and channel length respectively. C_0 is the capacitance/cm² of SiO₂. From this equation, carrier mobilities of electrons and holes were calculated to be 6.7 cm²/V·s and 5.7 cm²/V·s respectively. I tried to measure the carrier mobilities of threadlike graphene of Gr (1 drop, Ni, 800) but threadlike graphene was broken due to electric current. In the case of rGO which was reduced with hydrazine and annealed at 200 °C, carrier mobilities of electrons and holes were 1.5 cm²/V·s and 4.0 cm²/V·s respectively [24]. Thus, carrier mobilities of Gr (10 drops, Ni, 800) are higher than those of rGO but lower than those of graphene which is fabricated by mechanical exfoliation (~200,000 cm²/V·s) or CVD method (~1,000 cm²/V·s). These low carrier mobilities are due to defects or thickness. Judging from Raman spectrum, Gr (10 drops, Ni, 800) is thick and contains a few defects. So, it is required to fabricate thin graphene sheet than to reduce defects. To fabricate thin graphene sheet, the quantity of carbon atoms which dissolve into a metal film and segregate at the interface of a metal film and SiO₂ must be controlled. To do this, I investigated the dependence of the shape of graphene sheet on the thickness of Ni film and cooling rate.

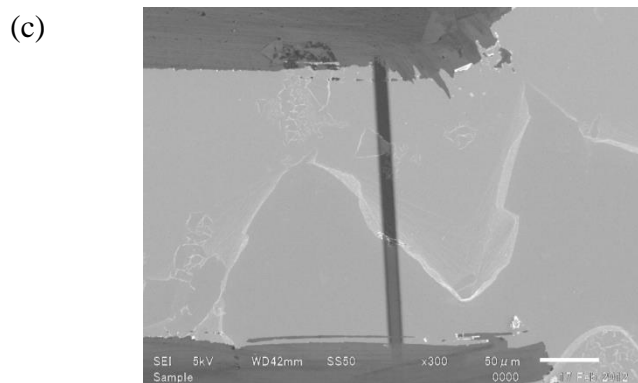
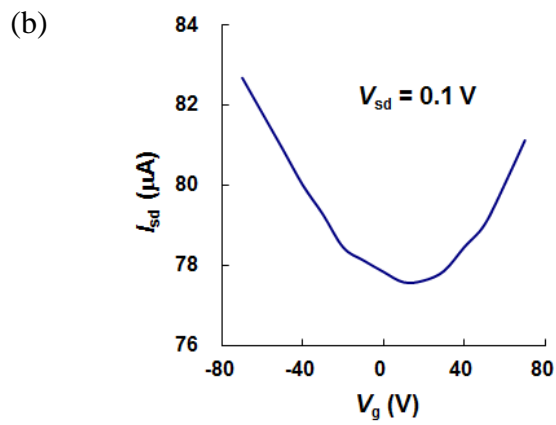
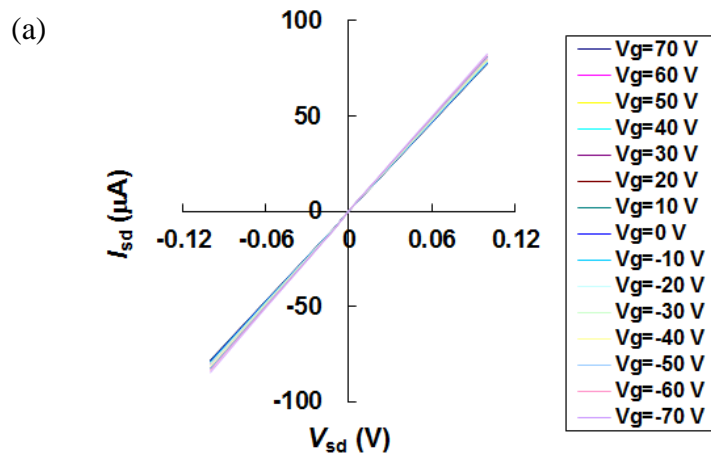


Figure 3.25 (a) Current-bias (I_{sd} - V_{sd}) curves, (b) electrical transport characteristics of Gr (10 drops, Ni, 800) and (c) SEM image of the area where FET measurement was performed.

3.5 Dependence of the Shape of Graphene on the Thickness of Ni Film and Cooling Rate

3.5.1 Experimental Method

To fabricate thin graphene sheet, I changed the thickness of Ni film and cooling rate. Figure 3.26 illustrates the reduction process of GO. In the similar way of reduction method of section 3.3.1, GO between a Ni film and SiO₂ substrate was annealed and a Ni film was etched. In this way, the thickness of Ni film was changed from 20 nm to 60 nm and cooling rate was ~30 °C/s (turn the heating switch off) or ~10 °C/s. In the following rapid cooling represents cooling rate at ~30 °C and slow cooling represents cooling rate at ~10 °C. Annealing temperature was 800 °C and annealing time was 6 min. The shape of graphene was observed by SEM and the quality of graphene was evaluated by Raman spectroscopy. In the following, Gr (X, s (r)) denotes the sample which was formed by depositing a Ni film of X nm thickness and cooling with a slow (rapid) rate.

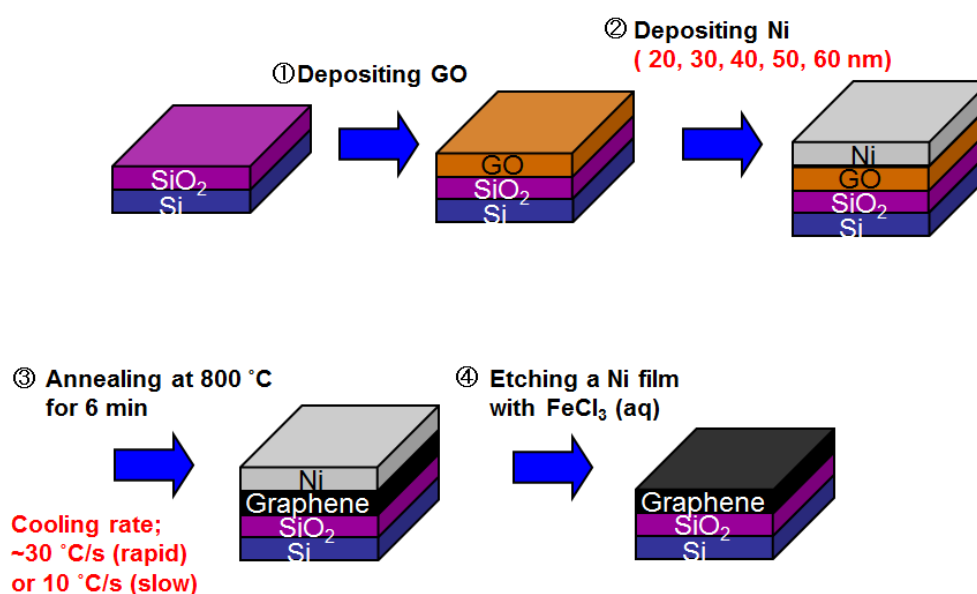


Figure 3.26 Reduction process and conditions of GO. The quantity of GO, the kind of metal overlayer and annealing temperature were changed.

3.5.2 Results and Discussion

Figure 3.27-31 show SEM images of graphene formed under each condition. When Ni film was 20-40 nm (Figure 3.27-29), the lateral sizes of graphene were about several tens μm and the shapes of graphene seems similar to that of the original GO sheets (Figure 3.3). Additionally, compared with the shape of graphene formed under rapid cooling and slow cooling, the shapes of graphene resemble each other. These results indicate that cooling rate had little effect on the shape and size of graphene in the case thin Ni film (20-40 nm). On the other hand, when Ni film was 50-60 nm (Figure 3.30 and 31), the morphologies of graphene are quite different from that of original GO sheets. In the case of Gr (50, s), circular graphene with the lateral size of approximately 50 μm was formed as shown in Figure 3.30 (a). In this sample, only circular graphene is observed and graphene whose shape resembles that of original GO sheet was not observed. In contrast, in the case of Gr (50, r), threadlike graphene with the width of approximately 1 μm and typical length of several tens μm was formed as shown in Figure 3.30 (b). In the case of Gr (60, s), graphene whose shape was like round with the lateral size of approximately 50 μm was formed as shown in Figure 3.31 (a). In the case of Gr (60, r), small graphene with the lateral size of approximately 10 μm was formed as shown in Figure 3.31 (b). Like this, the shapes of graphene formed in the case of thick Ni film (50-60 nm) were different from that of original GO sheets. Besides, the shape of graphene formed under slow cooling was different from that of graphene formed under rapid cooling. Thus, in the case of thick Ni film, cooling rate affects the shape of graphene in contrast to the case of thin Ni film. As just described, when a Ni film was thin, the shape of graphene was similar to that of original GO sheet and when a Ni film was thick, the shape of graphene was different from that of original GO sheet. The boundary in the Ni thickness is located between 40 nm and 50 nm.

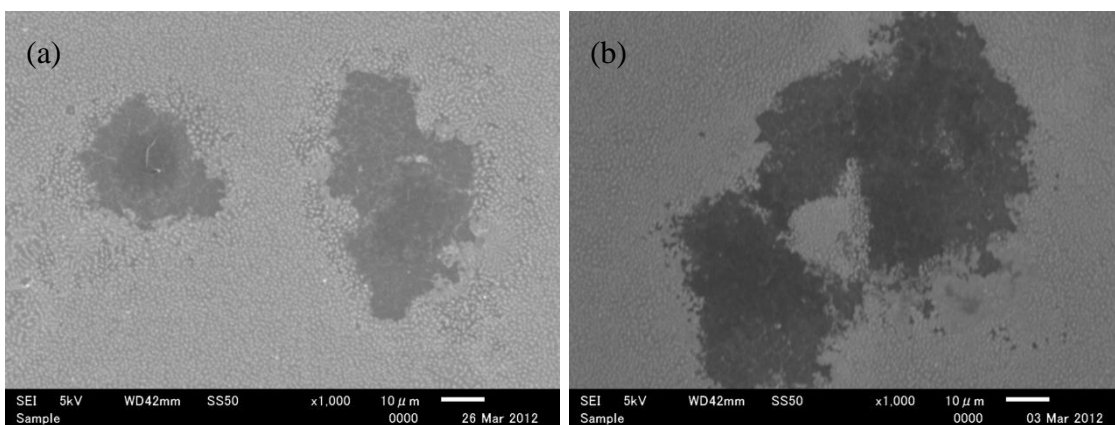


Figure 3.27 SEM images of (a) Gr (20, s) and (b) Gr (20, r).

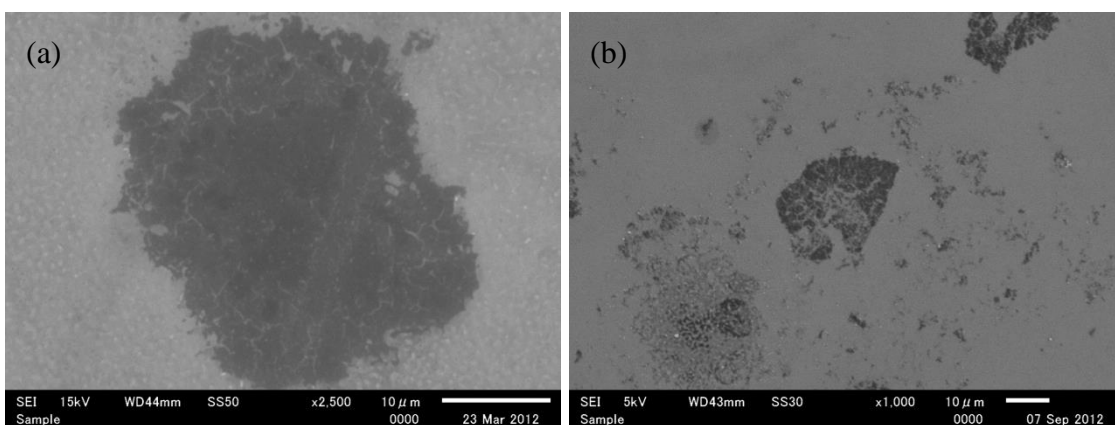


Figure 3.28 SEM images of (a) Gr (30, s) and (b) Gr (30, r).

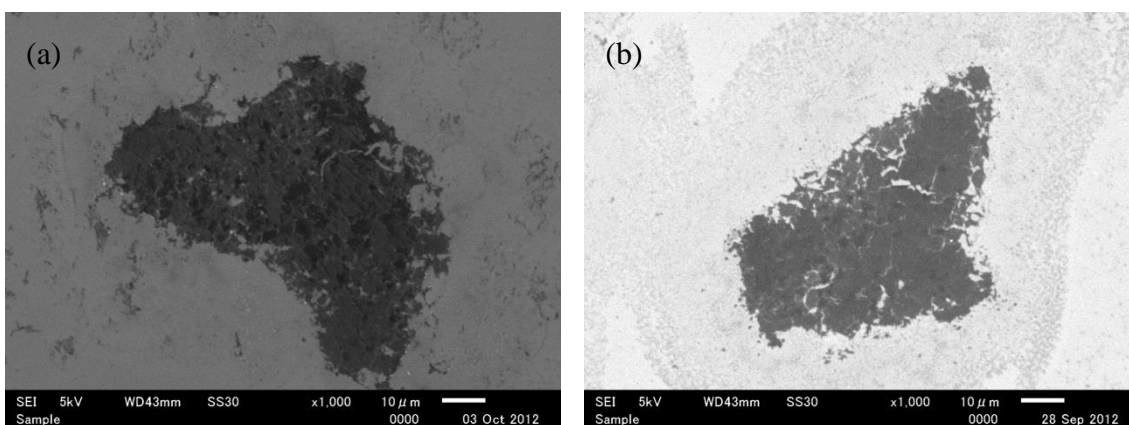


Figure 3.29 SEM images of (a) Gr (40, s) and (b) Gr (40, r).

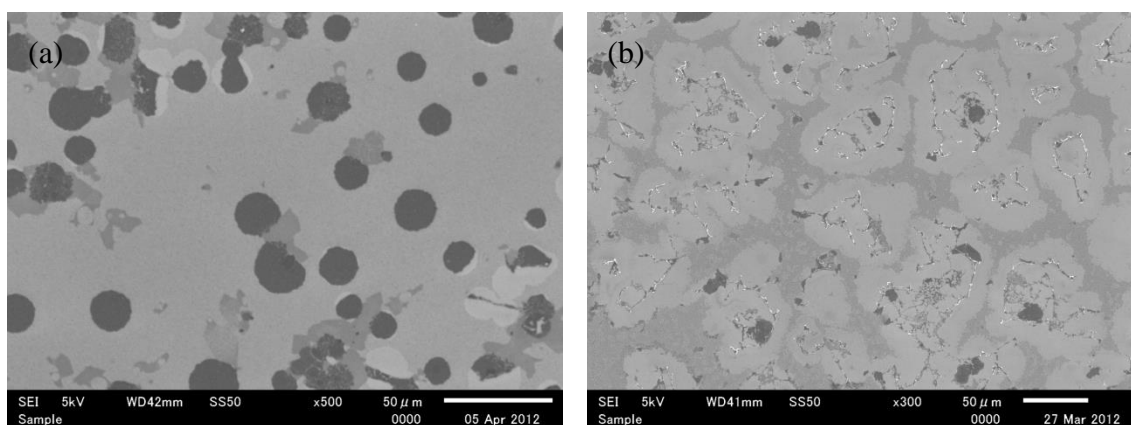


Figure 3.30 SEM images of (a) Gr (50, s) and (b) Gr (50, r).

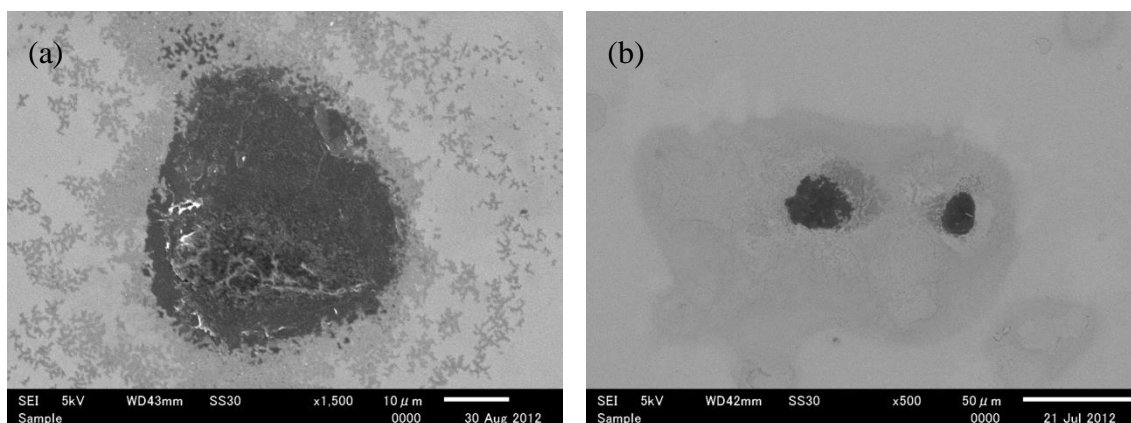


Figure 3.31 SEM images of (a) Gr (60, s) and (b) Gr (60, r).

These samples were characterized by Raman spectroscopy. Figure 3.32 (a) shows typical Raman spectra of Gr (50, s), Gr (20, s), rGO and GO. rGO was reduced by thermal annealing at 800 °C in vacuum. In Raman spectra of GO and rGO, the G band and D band are broad and the 2D band is absent. These results indicate that GO and rGO were disordered and contain many defects and sp^3 structure. In contrast, in Raman spectra of Gr (50, s) and Gr (20, s), the G band and D band become sharp and the 2D band appears. Additionally, the I_{2D}/I_G ratio is >1 and this result indicates that these graphene sheets were monolayer or bi-layer. Thus, thin graphene sheets could be obtained. As shown in Figure 3.32 (b) and (c), the I_D/I_G ratio and I_{2D}/I_G ratio were plotted as a function of the Ni film thickness respectively. Raman spectra were measured at 3–6 points for each sample. Figure 3.32 (b) shows that the I_D/I_G ratio of each Ni thickness is quite-variable but in some samples, the I_D/I_G ratio is less than 1. This means that some graphene sheets of these samples were high quality and defects of those were very few. Figure 3.32 (c) shows that the I_{2D}/I_G ratio of each Ni thickness is also quite-variable but it is larger than 1 in most of samples except the case of 60 nm Ni film. Thus, monolayer or bi-layer graphene could be obtained by changing the Ni thickness and cooling rate.

Recently, some methods of direct growth of graphene on SiO_2 by Ni catalysis have been reported [25-28]. In these methods, polymers such as PMMA were used as carbon sources and transfer process was not necessary. Graphenes prepared by these methods were high quality and thin (monolayer or bi-layer) but flammable hydrogen gas and high temperature of 1000 °C were necessary. In our method, graphene was formed at relatively low temperature of 800 °C without hydrogen gas. So, our method is more suitable for industrial applications. These advantages must be due to the structure of GO, which resembles graphene.

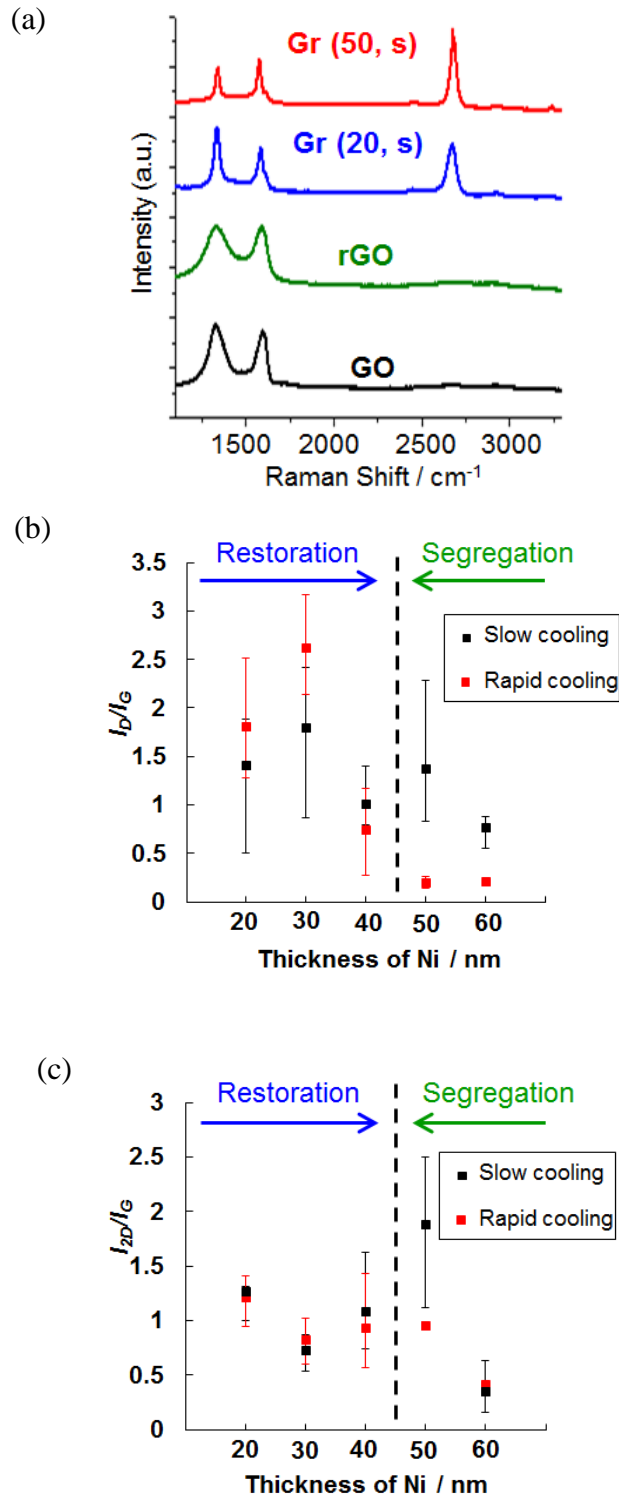


Figure 3.32 (a) Typical Raman spectra of GO, rGO, Gr (20, s) and Gr (50, s), (b), (c) I_D/I_G and I_{2D}/I_G as a function of Ni film thickness.

Judging from the shape of graphene, the reduction of GO sheets seem to occur on-site of the original GO sheets in the case of thin Ni film. On the other hand, graphene seem to form by carbon dissolution and segregation as mentioned in section 3.4 in the case of thick Ni film. To clarify this hypothesis, whether graphene sheets had formed at the original position of GO sheets was investigated by tracking the same GO sheet in the case of Gr (20, r). Figure 3.33 shows SEM images of Gr (20, r), (a) after depositing a 20 nm Ni film, (b) after annealing and (c) after etching in the same region. The region where the same GO sheet was deposited was confirmed by scratched line on the SiO₂ substrate. Figure 3.33 (a) shows that a Ni film was deposited uniformly on GO sheet and SiO₂ substrate. Figure 3.33 (b) and (c) show that graphene remained at the same position of the original GO sheet though the size became slightly smaller than that of the original GO sheet. Figure 3.33 (d) shows Raman spectrum of Gr (20, r) measured at the circled area in Figure 3.33 (c). From the 2D band, whose intensity was comparable to that of the G band, sharp D band and G band, GO sheet was restored and thin graphene sheet was formed. Thus, in the case of thin Ni film, it was confirmed that GO sheet was reduced on-site. In the case of thick Ni film, in contrast, the shape of graphene was quite different from that of the original GO sheet. In the following, I call reduction process for thin Ni film, in which the shape of graphene is similar to that of original GO sheet, restoration and reduction process for thick Ni film, in which the shape of graphene is different from that of original GO sheet, segregation.

In previous works, the effect of metal etching was not observed directly [25-28]. Figure 3.33 elucidates the effect of etching. The shape of graphene in Figure 3.33 (c) is similar to that of the gray region in Figure 3.33 (b). Thus it suggests that the effect of metal etching to the shape of graphene is not so much. However, as shown in Figure 3.33 (d), the D band intensity is higher than that of graphene fabricated by mechanical exfoliation or CVD method. This high intensity D band might be due to the incomplete restoration but it is possible that part of defects is formed by etching process.

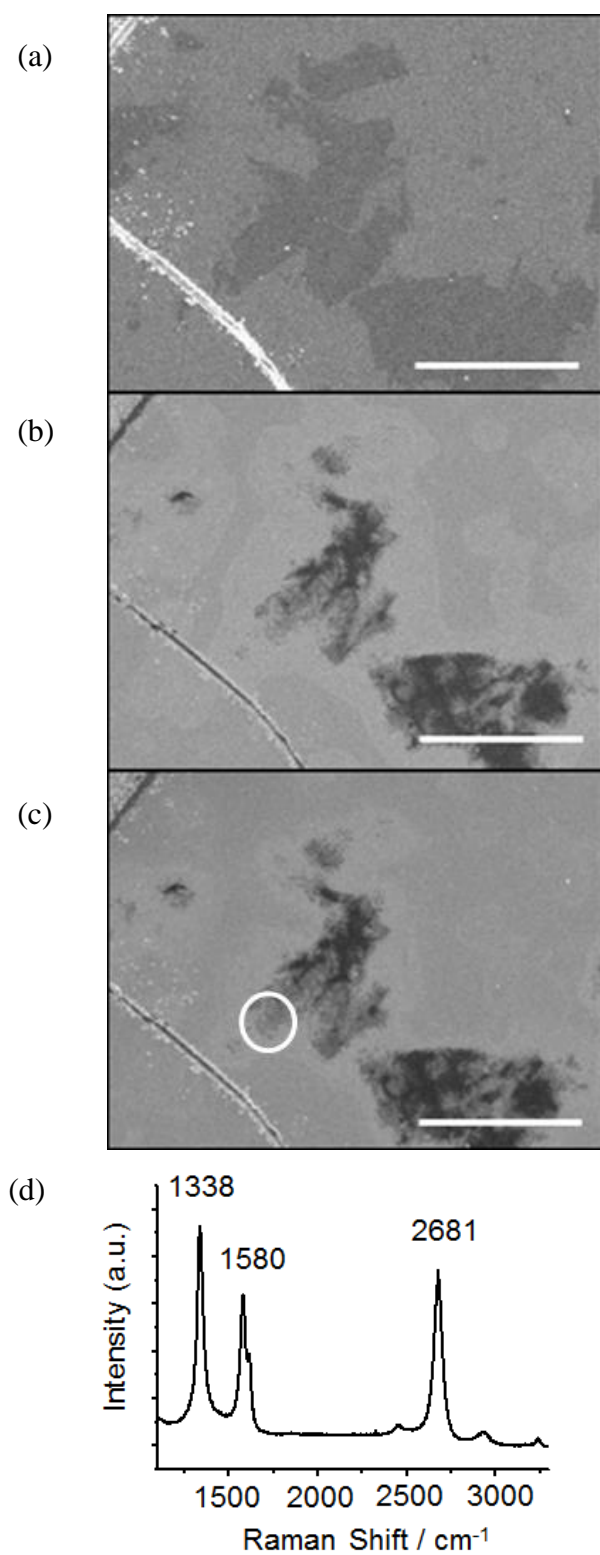


Figure 3.33 SEM images of Gr (20, r). (a) after 20 nm Ni deposition, (b) after annealing, (c) after etching. (d) Raman spectrum taken at the circle area shown in (c). All scale bars are equal to 100 μm .

As described above, the shape of graphene depends on the thickness of Ni film. When Ni film is thin, GO sheet is reduced on-site and the shape of graphene is similar to that of the original GO sheet. When Ni film is thick, GO sheet is dissolved into Ni film and segregated, so the shape of graphene does not reflect the shape of original GO sheet. In order to get insight into reduction mechanism, the distributions of defects in graphene were measured by Raman mapping of the I_D/I_G ratio for Gr (40, s) and Gr (50, s). Figure 3.34 shows I_D/I_G mapping of (a) Gr (40, s) and (b) Gr (50, s). Although the size and shape of these samples resembled each other, the distributions of the I_D/I_G ratio were quite different. In the case of Gr (40, s), the I_D/I_G ratio was uniform totally. In contrast, in the case of Gr (50, s), the I_D/I_G ratio was high at the edge. These differences suggest that the reduction mechanism depends on the thickness of Ni film.

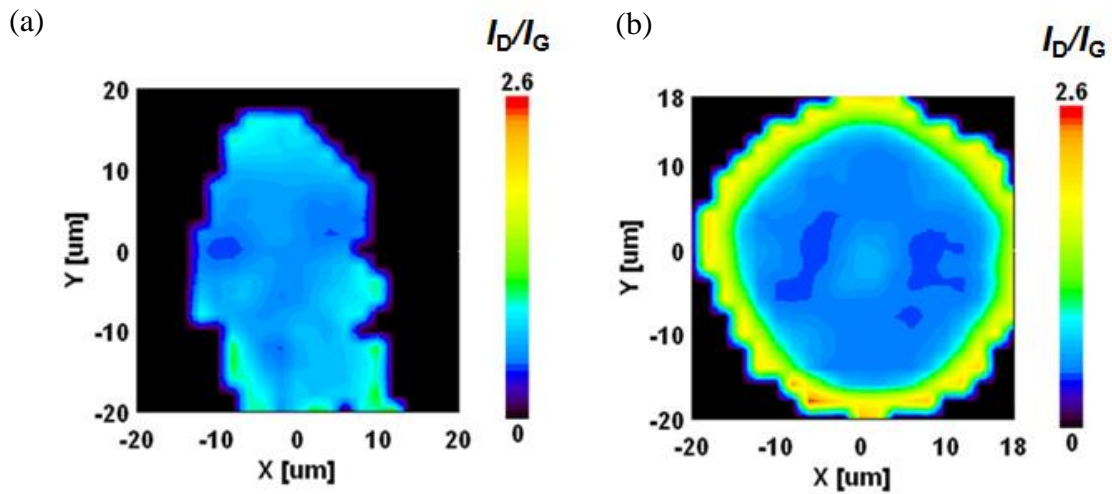


Fig. 3.34 I_D/I_G mapping of (a) Gr (40, s) and (b) Gr (50, s).

Based on these results, the reduction mechanism of GO sheet between a Ni film and SiO₂ substrate will be discussed. In the case of graphene growth from solid carbon sources such as PMMA and amorphous carbon etc., the carbon sources are decomposed and dissolve into a Ni layer. In the case of GO sheet, ease of decomposition is considered to differ according to whether the region is ordered or disordered. In the region where sp² and sp³ structure is disordered or functionalized with oxygen groups, GO sheet would be likely to dissociate fast as compared to that in ordered sp² structure [29]. Another key factor of the reduction mechanism is carbon solubility to a Ni film. It was reported that carbon solubility to Ni is about 0.4 % at 800 °C [15]. From this, the thickness of Ni film necessary for all carbon atoms of a monolayer graphene to dissolve at 800 °C is evaluated to be 80 nm. In this experiment, initial coverage of GO sheet was smaller than unity. Thus thickness of Ni film in which all carbon atoms can dissolve was between 40 nm and 50 nm, which was less than 80 nm.

Figure 3.35 (a) shows the reduction mechanism model of GO sheet in the case of thin Ni film. GO in disordered region would decompose into carbon atoms preferentially and the isolated carbon atoms can be dissolved into the Ni film until the limit of solubility. When the Ni film was thin, part of carbon atoms could not be dissolved into the Ni layer. Those remaining carbon atoms around GO sheets would suppress further decomposition of GO sheets. In this case, the ordered sp² regions of GO sheets remained at the original position. In cooling process, the carbon atoms which dissolved into the Ni film segregated at the interface between the Ni film and SiO₂ substrate. These segregated carbon atoms would repair the defects and vacancies of GO sheets as shown in Figure 3.34 (a). Thus disordered region of GO sheet decomposed preferentially by Ni catalysis. On the other hand, ordered region remained at the original position and they worked as a template for transformation from GO to graphene during cooling process. Thus, the shape of graphene was similar to that of the original GO sheet and cooling rate had little effect on the shape of graphene.

Figure 3.35 (b) shows the reduction mechanism model of GO sheet in the case of thick Ni film. When the Ni film was thick, the shape of graphene was quite different from that of the original GO. This should be because all GO sheets decomposed into

carbon atoms and once all carbon atoms dissolved into the Ni film. First, disordered region in GO sheets was decomposed during annealing process at 800 °C but these isolated carbon atoms were incorporated into the Ni film entirely and the density of isolated carbon atoms between the Ni film and SiO₂ substrate decreased to zero. Then, ordered region was also decomposed. Thus, all GO sheets decomposed into carbon atoms and dissolved into the Ni film. In cooling process, the carbon atoms which diffused into the Ni film were segregated at the interface between the Ni film and SiO₂ substrate and graphene was formed in a similar way of CVD graphene grown on Ni [30]. In the case of rapid cooling, duration of carbon segregation is short so that the segregation occurred mainly at such defective sites as grain boundaries and threadlike graphene was formed. On the other hand, in the case of slow cooling, duration of carbon segregation is long so that the carbon atoms could diffuse laterally at the Ni/SiO₂ interface and circular graphene was formed.

Difference of defects distribution in Figure 3.34 can be explained by these reduction mechanisms. In the case of restoration process, disordered region was decomposed and ordered region remained at the original position. In cooling process, the dissolved carbon atoms segregated at the defective site of GO sheets. Thus defects and vacancies were repaired and the ordered region remained unchanged. This process makes the defects density uniform as shown in Figure 3.34 (a). On the other hand, in the case of segregation process with slow cooling process, graphene was grown by segregated carbon atoms and periphery of graphene is corresponded to growth front, which contains many defects [31]. Thus the I_D/I_G ratio in peripheral region is higher than that in inside region as shown in Figure 3.34 (b).

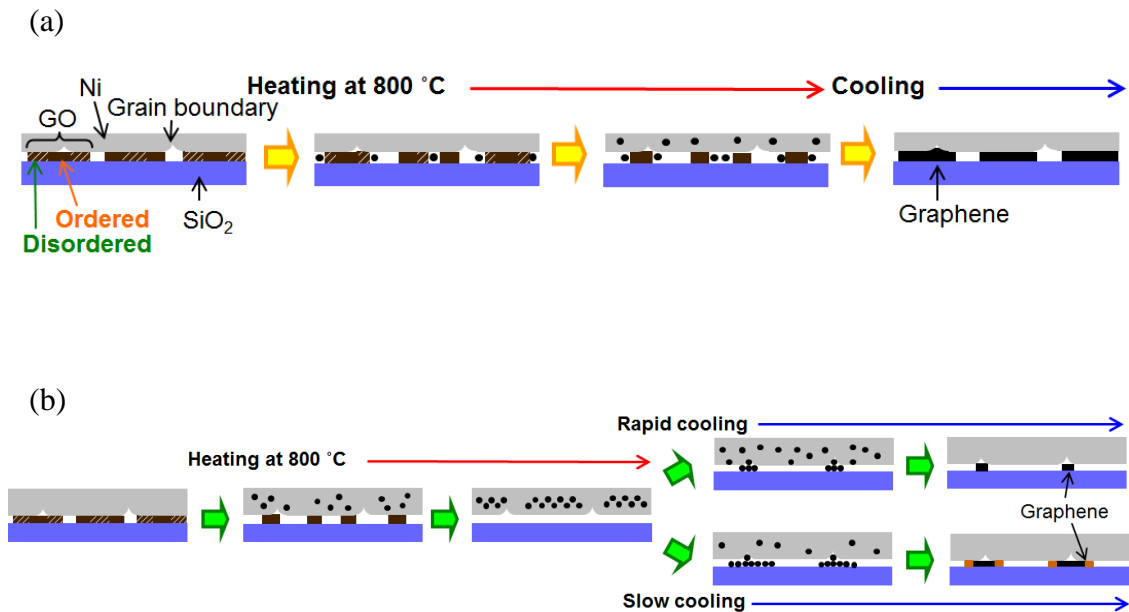


Figure 3.35 The reduction mechanism model of GO sheet in the case of (a) thin Ni film and (b) thick Ni film.

3.6 Conclusions

I have succeeded in restoration of defects in GO by using catalysis of Ni. When GO sheets were deposited on a Ni film and annealed at 800 °C, they were slightly restored but most of them disappeared due to Ni evaporation. In order to avoid disappearance of GO sheets, a Ni film was deposited on GO sheets and GO was annealed between a Ni film and SiO₂ substrate. As a result, 2 types of graphene; large area graphene with the lateral size of about 1mm and threadlike graphene with the width of about 10 μm, were obtained at the area where a Ni film was deposited. The qualities of these 2 types of graphene were evaluated by Raman spectroscopy. In both of large area graphene and threadlike graphene, the D, G band become sharp and 2D band appears. These results indicate that GO sheet was restored by this method.

In order to clarify the reduction mechanism of GO sheet, three reduction conditions, which were the quantity of GO, the kind of metal overlayer and annealing temperature,

were changed. When the carbon atoms dissolved into a metal film entirely, they were segregated preferentially at grain boundaries. Thus threadlike graphene was formed. On the other hand, when the carbon atoms did not dissolve into a metal film, some GO fragments were left. In cooling process, they were segregated around the GO fraction and large area graphene was formed.

To obtain thin graphene sheet, the thickness of Ni film and cooling rate were changed. When Ni film was thin, part of carbon atoms could not dissolve into Ni film and suppressed decomposition of GO sheets. In cooling process, carbon atoms were segregated and repaired the defects of GO sheets. Thus, graphene with the similar shape of the original GO sheets was formed and cooling rate had little effect on the shape of graphene. When Ni film was thick, all carbon atoms dissolved into a Ni film and no GO fragment was left. In cooling process, carbon atoms were segregated. In the case of rapid cooling, duration of segregation was short. So carbon atoms were segregated preferentially at grain boundaries and threadlike graphene was formed. In contrast, in the case of slow cooling, duration was long. So carbon atoms diffused laterally and circular graphene was formed. Judging from I_{2D}/I_G ratio, these graphene sheets were thin.

In the case of graphene growth from polymers or amorphous carbon, flammable hydrogen gas and high temperature of more than 1000 °C were necessary. However in this method, graphene was formed without hydrogen gas at relatively low temperature of 800 °C. This should be because the structure of GO sheet resembles that of graphene sheet. Thus, this method is suitable for industrial applications.

References

- [1] Stankovich, S.; Dikin, D. a.; Piner, R. D.; Kohlhaas, K. A.; Kleinhammes, A.; Jia, Y.; Wu, Y.; Nguyen, S. T.; Ruoff, R. S. *Carbon* **2007**, 45, 1558–1565.
- [2] Shin, H.-J.; Kim, K. K.; Benayad, A.; Yoon, S.-M.; Park, H. K.; Jung, I.-S.; Jin, M. H.; Jeong, H.-K.; Kim, J. M.; Choi, J.-Y.; Lee, Y. H. *Adv. Funct. Mater.* **2009**, 19, 1987–1992.
- [3] Fan, X.; Peng, W.; Li, Y.; Li, X.; Wang, S.; Zhang, G.; Zhang, F. *Adv. Mater.* **2008**, 20, 4490–4493.
- [4] Fernández-Merino, M. J.; Guardia, L.; Paredes, J. I.; Villar-Rodil, S.; Solís-Fernández, P.; Martínez-Alonso, A.; Tascón, J.M. D. *J. Phys. Chem. C* **2010**, 114, 6426–6432.
- [5] Chen, J. L.; Yan, X. P. *J. Mater. Chem.* **2010**, 20, 4328–4332.
- [6] Pei, S.; Zhao, J.; Du, J.; Ren, W.; Cheng, H.-M. *Carbon* **2010**, 48, 4466–4474.
- [7] Obata, S.; Tanaka, H.; Saiki, K. *Appl. Phys. Express* **2011**, 4, 025102.
- [8] Li, X.; Cai, W.; An, J.; Kim, S.; Nah, J.; Yang, D.; Piner, R.; Velamakanni, A.; Jung, I.; Tutuc, E.; Banerjee, S. K.; Colombo, L.; Ruoff, R. S. *Science* **2009**, 324, 1312–4.
- [9] Reina, A.; Jia, X.; Ho, J.; Nezich, D.; Son, H.; Bulovic, V.; Dresselhaus, M. S.; Kong, J. *Nano Lett.* **2009**, 9, 30–5.
- [10] Kim, K. S.; Zhao, Y.; Jang, H.; Lee, S. Y.; Kim, J. M.; Kim, K. S.; Ahn, J.-H.; Kim, P.; Choi, J.-Y.; Hong, B. H. *Nature* **2009**, 457, 706–10.

- [11] Terasawa, T.; Saiki, K. *Carbon* **2012**, 50, 869–874.
- [12] Hummers, W. S.; Offeman, R. E. *J. Am. Chem. Soc.* **1958**, 80, 1339.
- [13] Hirata, M.; Gotou, T.; Horiuchi, S.; Fujiwara, M.; Ohba, M. *Carbon* **2004**, 42, 2929–2937.
- [14] Dimiev, A.; Kosynkin, D. V.; Alemany, L. B.; Chaguine, P.; Tour, J. M. *J. Am. Chem. Soc.* **2012**, 134, 2815–22.
- [15] Eizenberg, M.; Blakely, J. M.; *Surf. Sci.* **1979**, 82, 228–236.
- [16] Mclellan, R. B. *Scrip. Metallurgica* **1969**, 3, 389–391.
- [17] Wang, Y. Y.; Ni, Z. H.; Yu, T.; Shen, Z. X.; Wang, H. M.; Wu, Y. H.; Chen, W.; Wee, A. T. S. *J. Phys. Chem. C* **2008**, 112, 10637–10640.
- [18] Pimenta, M. A.; Dresselhaus, G.; Dresselhaus, M. S.; Cançado, L. G.; Jorio, A.; Saito, R. *Phys. Chem. Chem. Phys.* **2007**, 9, 1276–91.
- [19] Hamilton, J. C.; Blakely, J. M. *Surf. Sci.* **1980**, 91, 199–217.
- [20] Kwak, J.; Chu, J. H.; Choi, J.-K.; Park, S.-D.; Go, H.; Kim, S. Y.; Park, K.; Kim, S.-D.; Kim, Y.-W.; Yoon, E.; Kodambaka, S.; Kwon, S.-Y. *Nature Commun.* **2012**, 3, 645.
- [21] Fisher, J. C. *J. Appl. Phys.* **1951**, 22, 74–77.
- [22] Balluffi, R. W.; Blakely, J. M. *Thin Solid Films* **1975**, 25, 363–392.
- [23] Wang, H.; Robinson, J. T.; Li, X.; Dai, H. *J. Am. Chem. Soc.* **2009**, 131, 9910–1.

- [24] Joung, D.; Chunder, a; Zhai, L.; Khondaker, S. I. *Nanotechnology* **2010**, *21*, 165202.
- [25] Byun, S.-J.; Lim, H.; Shin, G.-Y.; Han, T.-H.; Oh, S. H.; Ahn, J.-H.; Choi, H. C.; Lee, T.-W. *J. Phys. Chem. Lett.* **2011**, *2*, 493–497.
- [26] Shin, H.-J.; Choi, W. M.; Yoon, S.-M.; Han, G. H.; Woo, Y. S.; Kim, E. S.; Chae, S. J.; Li, X.-S.; Benayad, A.; Loc, D. D.; Gunes, F.; Lee, Y. H.; Choi, J.-Y. *Adv. Mater.* **2011**, *23*, 4392–7.
- [27] Yan, Z.; Peng, Z.; Sun, Z.; Yao, J.; Zhu, Y.; Liu, Z.; Ajayan, P. M.; Tour, J. M. *ACS Nano* **2011**, *5*, 8187–8192.
- [28] Peng, Z.; Yan, Z.; Sun, Z.; Tour, J. M. *ACS Nano* **2011**, *5*, 8241–7.
- [29] Bagri, A.; Mattevi, C.; Acik, M.; Chabal, Y. J.; Chhowalla, M.; Shenoy, V. B. *Nature Chem.* **2010**, *2*, 581–7.
- [30] Yu, Q.; Lian, J.; Siriponglert, S.; Li, H.; Chen, Y. P.; Pei, S.-S. *Appl. Phys. Lett.* **2008**, *93*, 113103.
- [31] Yu, Q.; Jauregui, L. A; Wu, W.; Colby, R.; Tian, J.; Su, Z.; Cao, H.; Liu, Z.; Pandey, D.; Wei, D.; Chung, T. F.; Peng, P.; Guisinger, N. P.; Stach, E. a; Bao, J.; Pei, S.-S.; Chen, Y. P. *Nature Mater.* **2011**, *10*, 443–9.

Chapter 4

Reduction of Graphene Oxide by Radical Treatment

4.1 Introduction

Graphene oxide is oxidized form of graphene functionalized with oxygen functional groups such as hydroxyl group, epoxy group and carboxylic acid group as described in chapter 1. Due to these functional groups, GO can be dispersed to various solvents [1] and functionalized with other functional groups. Because GO has these excellent properties, it has been expected as a promising material for large area applications such as transparent electrode, polymer composite and drug delivery system etc. Above all, GO has been expected as a precursor of graphene. By reduction of GO, functional groups are removed and GO convert to graphene. However, there are problems that some functional groups remains and defects, which was formed in oxidation process, are not repaired. These remained functional groups and defects degrade the electrical properties of graphene, so the novel reduction method which can remove functional groups entirely and repair the defects is needed.

To date, various reduction methods in solution phase have been reported [2-7]. In these methods, functional groups were removed effectively but defects were not repaired. In vapor phase or vacuum process, some restoration methods have been reported. For example, CVD repair [8], plasma restoration [9] and alcohol vapor restoration [10] were reported. By these methods, defects were repaired and disordered lattices were restored. However, for industrial applications, the suitable process is not vapor phase or vacuum process but solution process. In these ways, it is considered that the key factor to repair the defects of GO should be free radicals. Thus, reduction of GO by free radicals in solution process is desirable.

Recently, Na-Na Chai *et al.* reported that GO was reduced by heating at 100 °C with

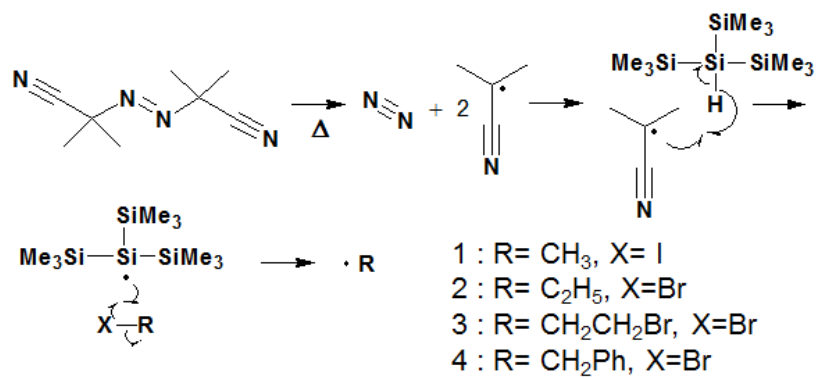
benzoyl peroxide (BPO) in DMF [11]. In this method, BPO was thermally decomposed and benzyl radicals were produced. These benzyl radicals react with the sp^3 carbon atoms of GO, which was functionalized with oxygen groups, and GO was reduced. However, some functional groups and defects remained as similar results of other reduction methods. Possibly, this incomplete reduction was because benzyl radical was so large that it could not reach the defect site of GO.

In this work, I investigated the dependence of reactivity with GO on the size of free radicals by using methyl radical, ethyl radical and benzyl radical. Additionally, I used bromoethyl radical to investigate the effect of halogen group.

4.2 Experimental Method

4.2.1 Radical Treatment of GO Suspension

GO was synthesized by modified Hummers method [12, 13] as described in section 3.2.1. Radical treatment of GO was carried out as follows. First, GO was dispersed in DMF and 0.5 mg/mL GO/DMF suspension was prepared. Then 10 mg (0.06 mmol) of azobisisobutyronitrile (AIBN), 50 μ L (0.16 mmol) of tris(trimethylsilyl)silane (TTMSS) and 75 μ L of alkyl halide or benzyl halide (1~4 in Scheme 1) were added to the 2.0 mL of GO / DMF suspension and the mixture was heated at 80 °C for 2 h. The amounts of substance of radical sources 1-4 were 1.20, 0.96, 0.87 and 0.63 mmol respectively. According to previous study, the content of oxygen contained in GO was approximately 2.25 atom% [12]. This content corresponds to 0.02 mmol and this amount of substance is much smaller than that of radical sources 1-4. Thus, these radical sources were used excessively relative to oxygen in GO. Scheme 4.1 depicts a mechanism of generation of free radical and Figure 4.1 shows a schematic diagram of radical reduction of GO. In the following, radical treated GO is described as rtGO.



Scheme 4.1 Mechanism of free radical generation.

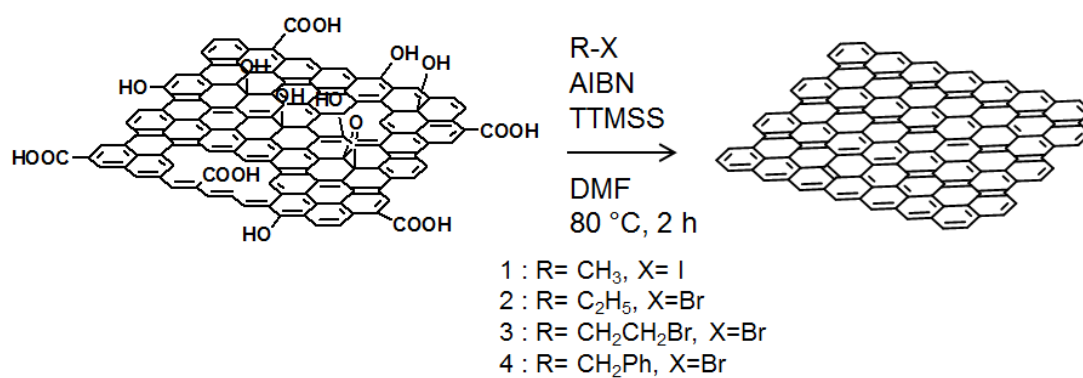


Figure 4.1 Conversion from GO (left) to graphene (right) by radical reduction.

4.2.2 Sample Preparation for Raman Spectroscopy

In order to measure Raman spectra of one-layer rtGO sheet, radical treatment of one-layer GO sheet was carried out as shown in Figure 4.2. First, one-layer GO sheets were deposited by spin-coating method (3000 rpm, 1 min) from GO/methanol suspension on a SiO₂/Si substrate, which was made hydrophilic by UV-ozone treatment (chapter 2). Then this GO/SiO₂/Si sample was immersed into 2 mL of DMF. Next, one of radical sources (1-4 in Scheme 4.1), AIBN and TTMSS were added. The quantities of these reagents were equal to as described in section 4.2.1. After that the mixture was heated at 80 °C for 2h. Finally, the sample was washed with deionized water and methanol several times. For comparison, one-layer rGO was also prepared by similar method. GO/ SiO₂/Si was immersed into 2 mL of DMF and 75 μL of hydrazine monohydrate was added. Then the mixture was heated at 80 °C for 2h and washed with water and methanol several times.

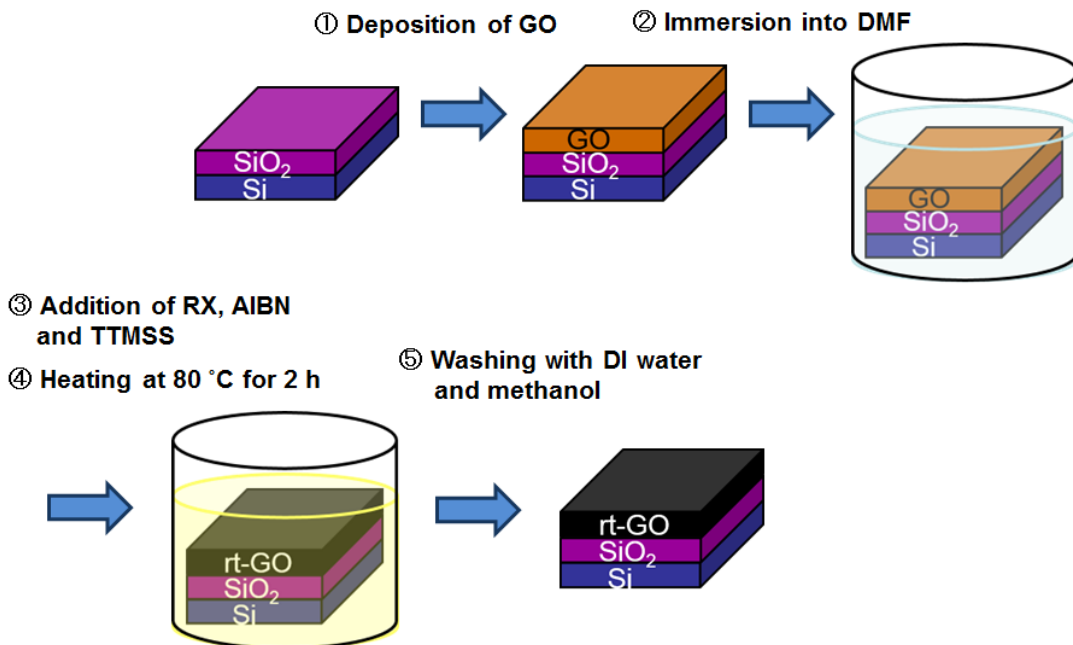
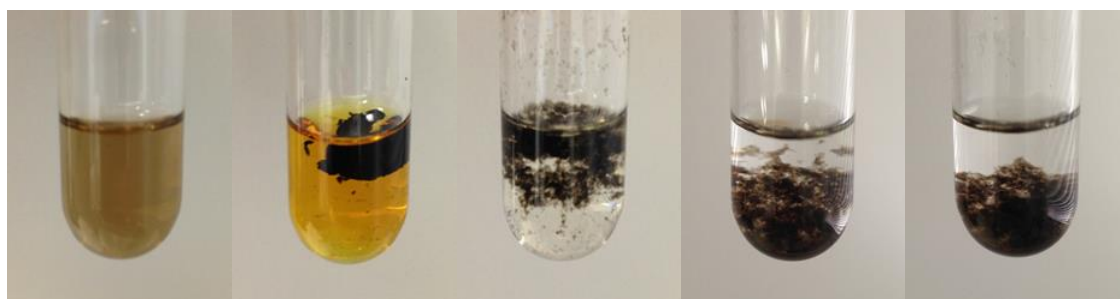


Figure 4.2 Preparation of one-layer rtGO sheet.

4.3 Results and Discussion

Figure 4.3 shows photographs of GO suspension before and after the radical treatment. Before the radical treatment, the color of GO suspension was brown and the GO sheets dispersed uniformly. After the radical treatment, the color of GO changed to black and GO sheets aggregated as shown in Figure 4.3 (b)-(e). These phenomena were seen in other reduction methods [14]. Thus these results indicate that GO could be reduced by free radicals, which were methyl radical, ethyl radical, bromoethyl radical and benzyl radical. The solution treated with CH_3I (Figure 4.3 (b)) was yellow due to iodine formed by decomposition of CH_3I .

The qualities of rtGO were evaluated by Raman spectroscopy. The samples for Raman spectroscopy were prepared by the method as described in section 4.2.2. Figure 4.4 shows Raman spectra of GO, rGO, rtGO treated with CH_3I , $\text{C}_2\text{H}_5\text{Br}$, $\text{BrC}_2\text{H}_4\text{Br}$ and PhCH_2Br . Raman spectrum of rGO is shown for comparison. In the spectra of rtGO, 2D band intensities are very weak. Judging from these Raman spectra, rtGO was less restored than graphene formed by Ni catalysis described in chapter 3. To analyze these Raman spectra in detail, peak fitting was carried out. As shown in Figure 4.5, the peaks at around 1100-1700 cm^{-1} can be deconvoluted into three different peaks, which are G band, D band and D^{**} band. The G band is located at around 1590 cm^{-1} and originates from graphite structure. The D band is located at around 1350 cm^{-1} and originates from defects or edges [15]. The D^{**} band is located at around 1500 cm^{-1} and some researchers have attributed this peak to amorphous carbon [16]. The FWHM of G band; Γ_G , the FWHM of D band; Γ_D and the peak intensity ratio of the D^{**} band to that of the G band; $I_{\text{D}^{**}}/I_G$ are plotted for each reducing agent as shown in Figure 4.6. The reducing agents are arranged in order of the number of carbon atoms. The Γ_G of rGO and rtGO are similar to each other (except PhCH_2Br) but smaller than that of GO. This indicates that rtGO were reduced to an equal degree of rGO, which was reduced by hydrazine. In contrast, the Γ_D and $I_{\text{D}^{**}}/I_G$ of each sample is different from each other. Both the Γ_D and $I_{\text{D}^{**}}/I_G$ are considered to relate with the crystallinity [17]. According to Figure 4.6, the crystallinity of rtGO treated with iodomethane and 1,2-dibromoethane are better than that of rGO reduced with hydrazine. Judging from the Γ_D and $I_{\text{D}^{**}}/I_G$, the



(a) GO (b) CH_3I (c) $\text{C}_2\text{H}_5\text{Br}$ (d) $\text{BrC}_2\text{H}_4\text{Br}$ (e) PhCH_2Br

Figure 4.3 Photos of (a) GO suspension and rtGO treated with (b) CH_3I , (c) $\text{C}_2\text{H}_5\text{Br}$, (d) $\text{BrC}_2\text{H}_4\text{Br}$ and (e) PhCH_2Br .

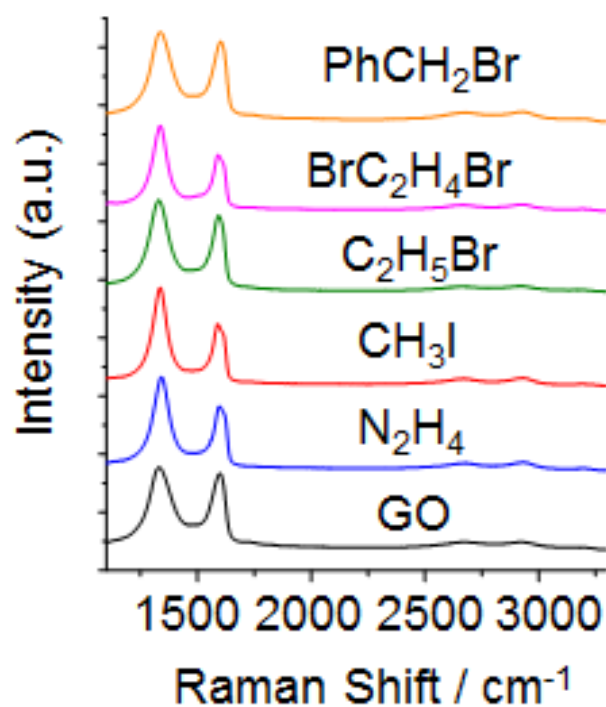


Figure 4.4 Raman spectra of GO, rGO treated with N_2H_4 , rGO treated with CH_3I , $\text{C}_2\text{H}_5\text{Br}$, $\text{BrC}_2\text{H}_4\text{Br}$ and PhCH_2Br (from bottom to top).

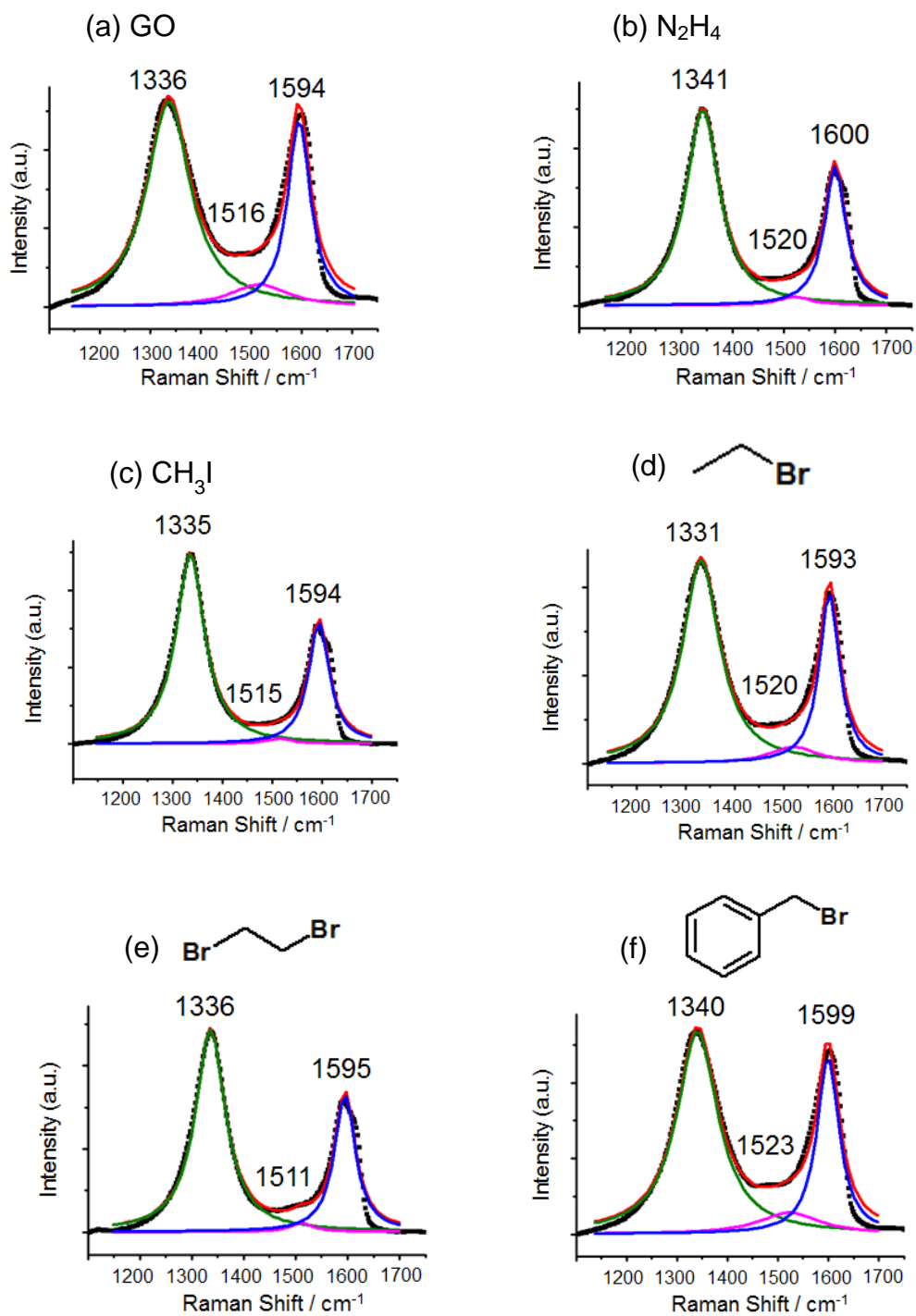


Figure 4.5 Raman spectra of GO (a), rGO reduced with hydrazine (b), and rtGOs reduced with iodomethane (c), bromoethane (d), 1,2-dibromoethane (e) and α -bromotoluene (f). Figures denote the wavenumbers of D, D**, and G bands.

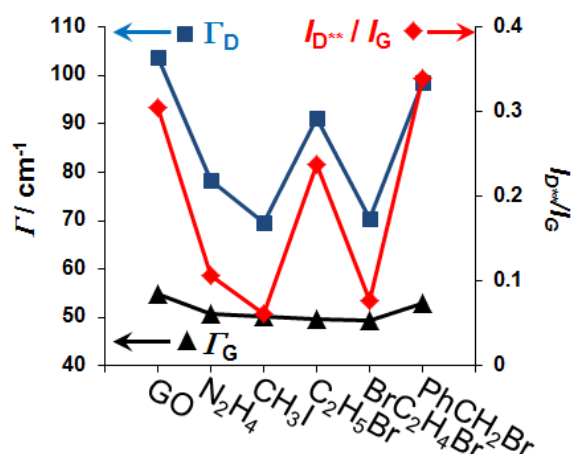
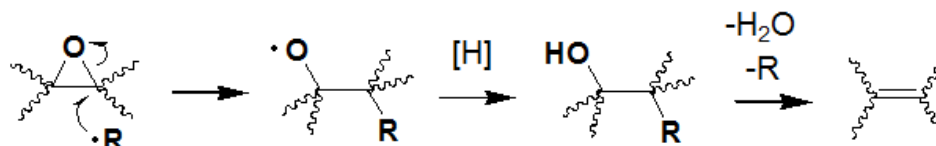
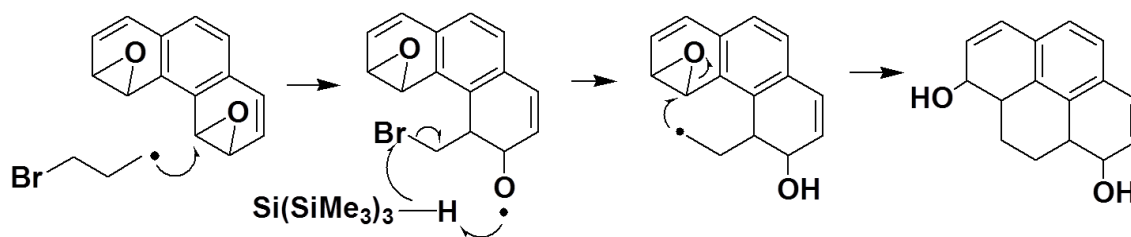


Figure 4.6 Γ_G , Γ_D and the $I_{D^{**}}/I_G$ ratio for each reducing agent.

improvement of the crystallinity were achieved as following order; $\text{CH}_3\text{I} > \text{BrC}_2\text{H}_4\text{Br} > (\text{N}_2\text{H}_4) > \text{C}_2\text{H}_5\text{Br} > \text{PhCH}_2\text{Br}$. The radical reduction mechanism might be similar to phenyl radical reduction mechanism [11] as shown in Scheme 4.2. Radical sources with smaller number of carbon atoms seem advantageous for removing oxygen groups and sp^3 or amorphous part in GO. This should be because a smaller molecule should be easier to reach the defects and functional groups. However, in the cases of $\text{BrC}_2\text{H}_4\text{Br}$ and $\text{C}_2\text{H}_5\text{Br}$, the larger molecule improved the crystallinity of GO more effectively. Since a $\text{BrC}_2\text{H}_4\text{Br}$ molecule has two bromo groups, a radical reaction is expected to occur twice per molecule as shown in Scheme 4.3. Thus, $\text{BrC}_2\text{H}_4\text{Br}$ restored GO effectively.



Scheme 4.2 Reduction mechanism of GO by using free radicals.



Scheme 4.3 Reaction of GO with bromoethyl radical.

To obtain more information about the crystallinity of rtGO, FET measurement was carried out in the similar way as described in section 3.4.2. Figure 4.7 (a) shows current-bias (I_{sd} - V_{sd}) curves and (b) shows the current-gate voltage (I_{sd} - V_g) curve of rtGO treated with CH_3I before annealing. In Figure 4.7 (b), current-gate voltage curve shows bipolar characteristics and from the linear region, carrier mobilities of electrons and holes were obtained by using equation (3.2). Carrier mobilities of electrons and holes were calculated to be $1.4 \text{ cm}^2/\text{V}\cdot\text{s}$ and $2.0 \text{ cm}^2/\text{V}\cdot\text{s}$ respectively. In order to eliminate the effect of adsorbent, this sample was annealed at $300 \text{ }^\circ\text{C}$. Figure 4.8 shows current-bias curves and current-gate voltage curve of this sample after annealing. Carrier mobilities of electrons and holes were calculated to be $3.5 \text{ cm}^2/\text{V}\cdot\text{s}$ and $1.7 \text{ cm}^2/\text{V}\cdot\text{s}$ respectively. This electron mobility is higher than that of rGO which was reduced with hydrazine and annealed at $300 \text{ }^\circ\text{C}$ (electron mobility; $3.0 \text{ cm}^2/\text{V}\cdot\text{s}$) [18]. Thus, this radical reduction method is effective for improving crystallinity of GO.

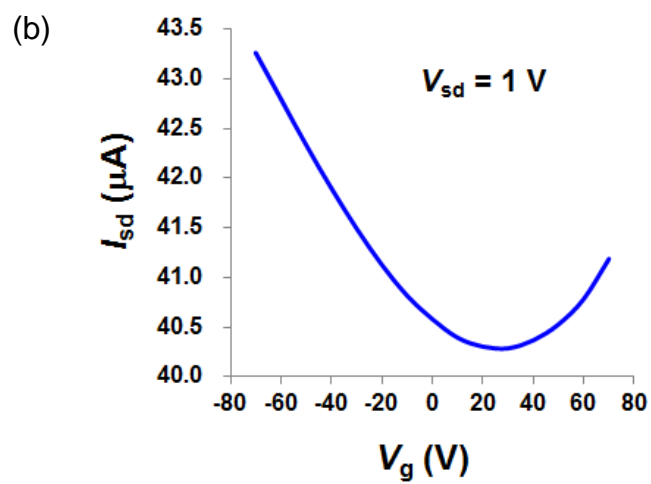
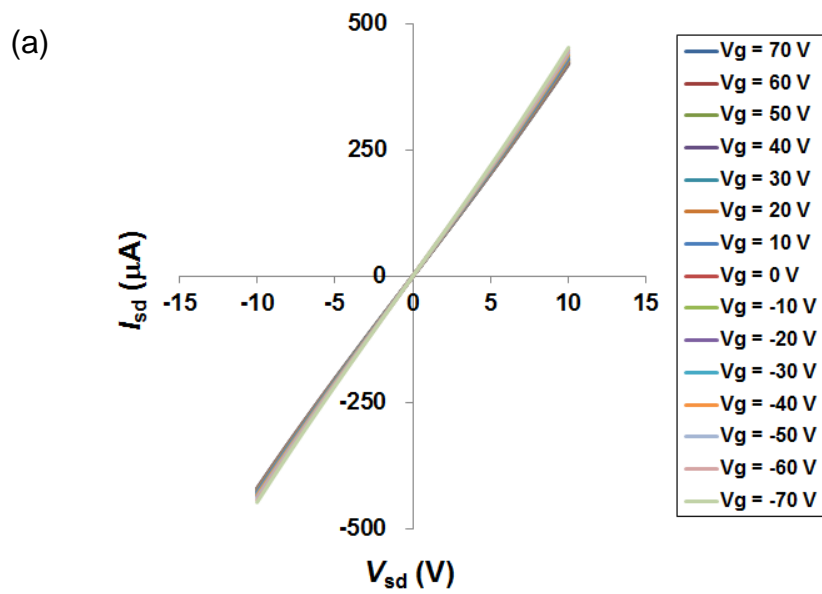


Figure 4.7 (a) Current-bias (I_{sd} - V_{sd}) curves, (b) current-gate voltage (I_{sd} - V_g) curve of rtGO treated with CH_3I before annealing.

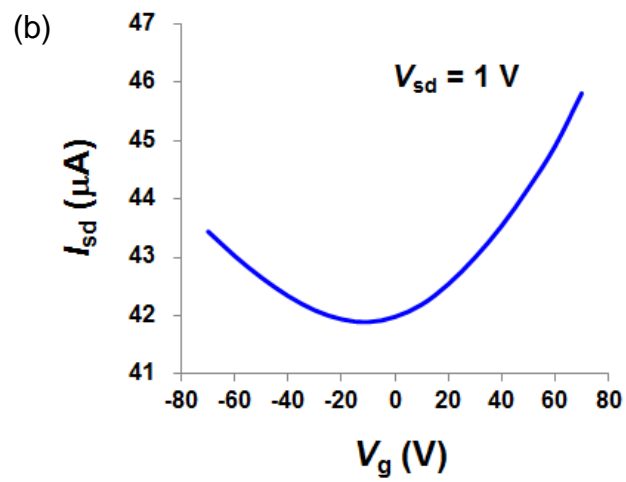
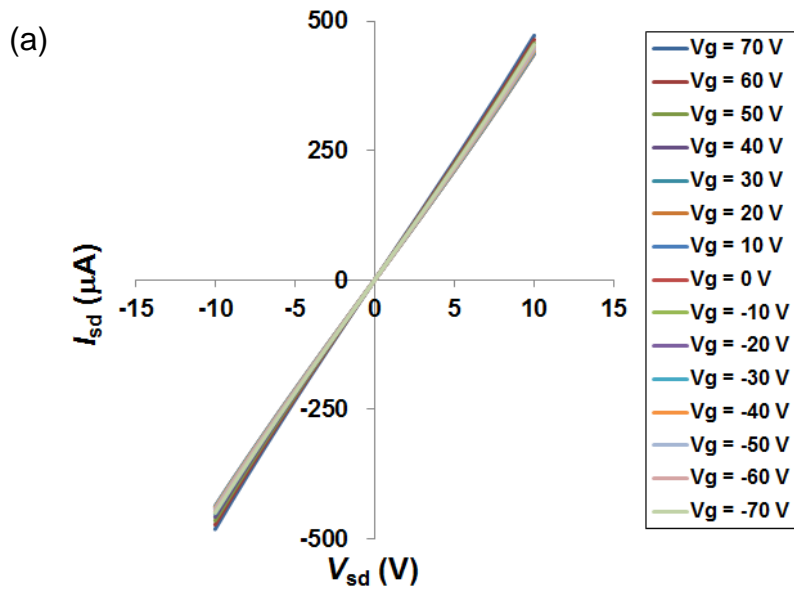


Figure 4.8 (a) Current-bias (I_{sd} - V_{sd}) curves, (b) electrical transport characteristics of rtGO treated with CH_3I after annealing.

4.4 Conclusions

In this study, I reduced GO by four different radical species. The radical sources were iodomethane, bromoethane, 1,2-dibromoethane and α -bromotoluene. In all cases, GO suspension changed from brown to black and aggregated. These phenomena indicate that GO was reduced. Raman spectra of these samples except for α -bromotoluene show very weak 2D band but D and G bands are sharper and $I_{D^{**}}/I_G$ ratio is smaller than those of GO. Judging from the FWHM of D band and the $I_{D^{**}}/I_G$ ratio, improvement of the crystallinity were achieved as following order; $\text{CH}_3\text{I} > \text{BrC}_2\text{H}_4\text{Br} > (\text{N}_2\text{H}_4) > \text{C}_2\text{H}_5\text{Br} > \text{PhCH}_2\text{Br}$. Iodomethane improved the crystallinity of GO most effectively because smaller molecules should be easier to reach the defects or sp^3 regions. 1,2-Dibromoethane reduced GO more effectively than bromoethane. Probably, this is because 1,2-dibromoethane molecule has two bromo groups and reacts with GO twice. The electron mobility of rGO treated with iodomethane and annealed at 300 °C was $3.5 \text{ cm}^2/\text{V}\cdot\text{s}$. This value was higher than that of rGO reduced with hydrazine and annealed at 300 °C. Thus, this reduction method facilitates the large scale production of graphene since radical reduction can be performed in solution process at relatively low temperature of 80 °C proceeds more effectively and safely than hydrazine reduction.

References

- [1] Paredes, J. I.; Villar-Rodil, S.; Martínez-Alonso, A.; Tascon, J. M. D. *Langmuir* **2008**, 24, 10560.
- [2] Stankovich, S.; Dikin, D. a.; Piner, R. D.; Kohlhaas, K. A.; Kleinhammes, A.; Jia, Y.; Wu, Y.; Nguyen, S. T.; Ruoff, R. S. *Carbon* **2007**, 45, 1558–1565.
- [3] Shin, H.-J.; Kim, K. K.; Benayad, A.; Yoon, S.-M.; Park, H. K.; Jung, I.-S.; Jin, M. H.; Jeong, H.-K.; Kim, J. M.; Choi, J.-Y.; Lee, Y. H. *Adv. Funct. Mater.* **2009**, 19, 1987–1992.
- [4] Fan, X.; Peng, W.; Li, Y.; Li, X.; Wang, S.; Zhang, G.; Zhang, F. *Adv. Mater.* **2008**, 20, 4490–4493.
- [5] Fernández-Merino, M. J.; Guardia, L.; Paredes, J. I.; Villar-Rodil, S.; Solís-Fernández, P.; Martínez-Alonso, A.; Tascón, J. M. D. *J. Phys. Chem. C* **2010**, 114, 6426–6432.
- [6] Chen, J. L.; Yan, X. P. *J. Mater. Chem.* **2010**, 20, 4328–4332.
- [7] Pei, S.; Zhao, J.; Du, J.; Ren, W.; Cheng, H.-M. *Carbon* **2010**, 48, 4466–4474.
- [8] López, V.; Sundaram, R. S.; Navarro, C. G.; Olea, D.; Burghard, M.; Herrero, J. G.; Zamora, F.; Kern, K. *Adv. Mater.* **2009**, 21, 4683–4686.
- [9] Cheng, M.; Yang, R.; Zhang, L.; Shi, Z.; Yang, W.; Wang, D.; Xie, G.; Shi, D.; Zhang, G. *Carbon* **2012**, 50, 2581–2587.

- [10] Su, C.-Y.; Xu, Y.; Zhang, W.; Zhao, J.; Liu, A.; Tang, X.; Tsai, C.-H.; Huang, Y.; Li, L.-J. *ACS Nano* **2010**, 4, 5285–92.
- [11] Chai, N.-N.; Zeng, J.; Zhou, K.-G.; Xie, Y.-L.; Wang, H.-X.; Zhang, H.-L.; Xu, C.; Zhu, J.-X.; Yan, Q.-Y. *Chem. Euro. J.* **2013**, 19, 5948–54.
- [12] Hummers, W. S.; Offeman, R. E. *J. Am. Chem. Soc.* **1958**, 80, 1339.
- [13] Hirata, M.; Gotou, T.; Horiuchi, S.; Fujiwara, M.; Ohba, M. *Carbon* **2004**, 42, 2929–2937.
- [14] Stankovich, S.; Piner, R. D.; Chen, X.; Wu, N.; Nguyen, S. T.; Ruoff, R. S. *J. Mater. Chem.* 2006, 16, 155.
- [15] Ferrari, A. C. *Solid State Commun.* **2007**, 143, 47.
- [16] Jawhari, T.; Roid, A.; Casado, J. *Carbon* **1995**, 33, 1561–1565.
- [17] Ivleva, N. P.; Messerer, A.; Yang, X.; Niessner, R.; Pöschl, U. *Environ. Sci. Technol.* **2007**, 41, 3702–3707.
- [18] Obata, S.; Tanaka, H.; Saiki, K. *Carbon* **2013**, 55, 126–132.

Chapter 5

Reduction and Sulfuration of Graphene Oxide by Solution Process

5.1 Introduction

Recently, heteroatom doped graphene has been paid much attention. By doping heteroatoms, electronic structure of graphene can be tuned. To date, various elements have been doped to graphene such as N, B, P, I and S [1-5]. Especially, S-doped graphene, whose structure model is shown in Figure 5.1, is expected to have remarkable properties. For example, theory calculation predicted that the band gap of graphene is opened by sulfur doping [6] and NO₂ molecules adsorbed S-doped graphene preferentially [7]. For these properties, applications of S-doped graphene to electronic device and gas sensor have been expected. Moreover, it has been reported that S-doped graphene exhibited high oxygen-reduction reaction (ORR) activity. In fuel cells, Pt/C is used as a catalytic electrode of ORR but platinum is too expensive and methanol crossover degrades the catalytic activity of Pt/C. So, an alternative catalytic electrode of Pt/C is required and S-doped graphene is a candidate material. S-doped graphene was fabricated by various methods, which were annealing GO at 600-1050 °C with benzyl disulfide [5], CVD process by using hexane in the presence of sulfur [8] and annealing GO at 600 °C or 1000 °C with H₂S, CS₂ or SO₂ [9]. However, these methods are vapor phase process and high temperature of more than 600 °C is required. For industrial applications, solution phase preparation of S-doped graphene is desirable. Therefore, I tried S-doping of GO by solution process. In this experiment, ammonium polysulfide ((NH₄)₂S_x) was used as a sulfur doping source.

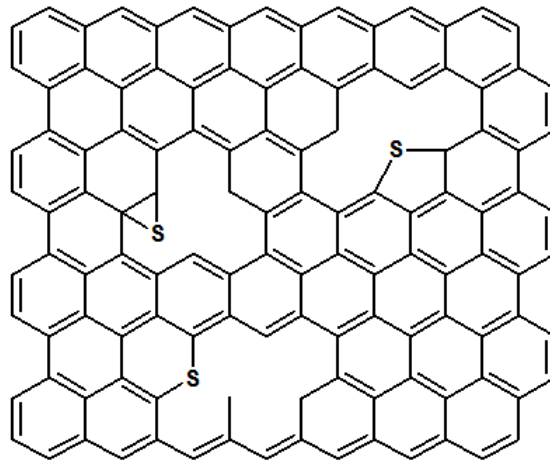


Figure 5.1 Structure model of S-doped graphene.

5.2 Experimental Methods

5.2.1 Preparation of Sulfurated Graphene

Figure 5.2 is the flow chart of preparation of sulfurated graphene (SG). First, 0.5 mL of GO aqueous solution (4 mg/mL) was dropped into 5 mL of $(\text{NH}_4)_2\text{S}_x$ and the mixture was left at room temperature for 2 h. Then the mixture was filtrated and washed with deionized (DI) water and methanol 5 times respectively. The dried SG powder was added to methanol and dispersed by sonication. After that, SG was deposited on a Si substrate by drop casting method from SG/methanol dispersion liquid. This sample was measured by X-ray photoelectron spectroscopy (XPS).

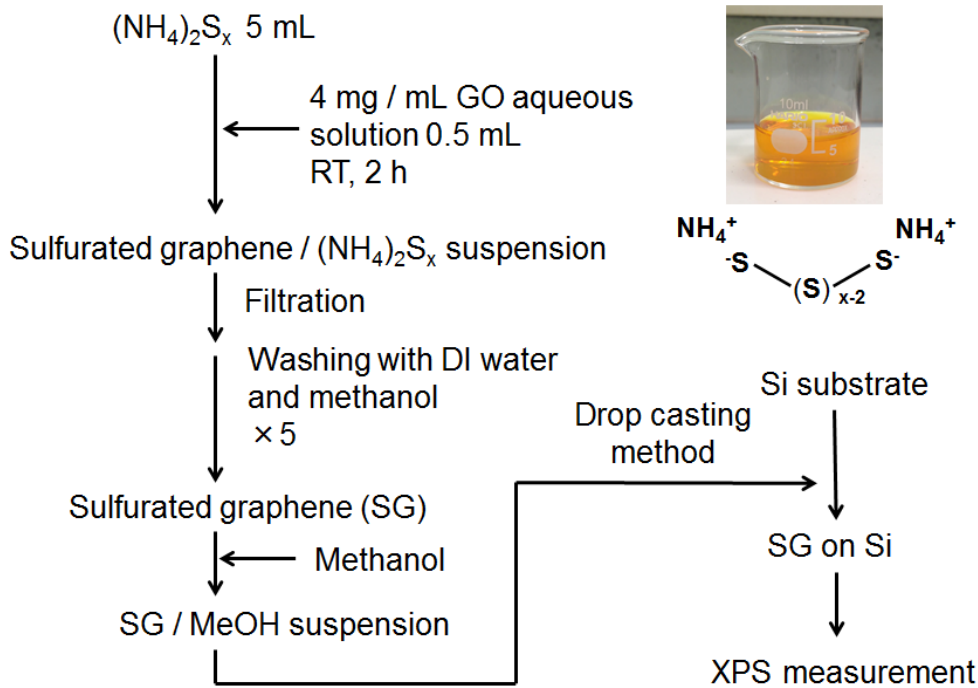


Figure 5.2 Flow chart of sulfurated graphene preparation.

The inset shows the picture of $(\text{NH}_4)_2\text{S}_x$.

5.2.2 Sample Preparation for Raman Spectroscopy

In order to measure Raman spectra of monolayer SG, sulfuration of monolayer GO sheet was carried out as shown in Figure 5.3. First, one-layer GO sheets were deposited by spin-coating method (3000 rpm, 1 min) from GO/methanol suspension on a SiO_2/Si substrate which was made hydrophilic by UV-ozone treatment (chapter 2). Then, PMMA was deposited on GO by spin-coating method (3000 rpm, 1 min). This sample was floated on $(\text{NH}_4)_2\text{S}_x$ and left at room temperature for 2 h. The oxide film of SiO_2 substrate was etched by $(\text{NH}_4)_2\text{S}_x$. Therefore, PMMA/GO was peeled from SiO_2 substrate and floated on $(\text{NH}_4)_2\text{S}_x$. In this operation, GO sheet was sulfurated and GO converted to SG. Next, PMMA/SG was floated on DI water and washed several times. After that, PMMA/SG was transferred onto another SiO_2 substrate and dried by heating at 80 °C for a few minutes. Finally, PMMA was removed by acetone.

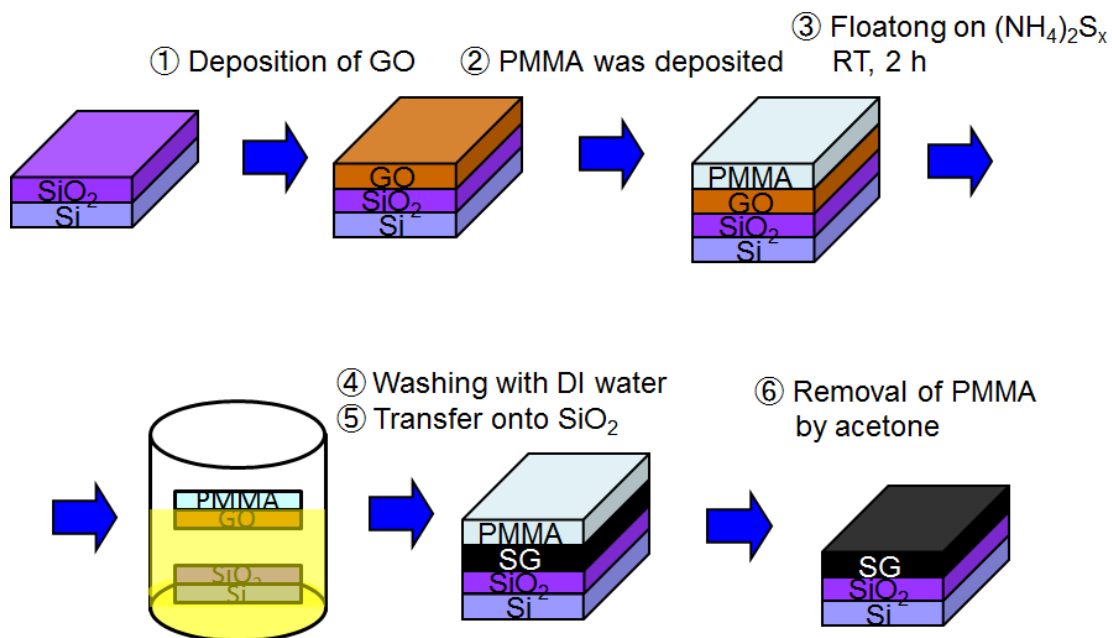


Figure 5.3 Preparation of monolayer SG sheet.

5.3 Results and Discussion

Figure 5.4 are photos of (a) GO aqueous solution before treatment with $(\text{NH}_4)_2\text{S}_x$, (b) GO aqueous solution after treatment with $(\text{NH}_4)_2\text{S}_x$ and (c) SG dispersed in methanol after washing. By treatment with $(\text{NH}_4)_2\text{S}_x$, GO changed from brown to black and aggregated. As described in section 4.3, these phenomena can be observed when GO is reduced [10]. Therefore, GO was reduced by treatment with $(\text{NH}_4)_2\text{S}_x$. It was reported that GO was reduced when the pH of GO suspension is high (>11) [11]. However, GO was reduced with $(\text{NH}_4)_2\text{S}_x$ even when the pH was ~ 9 as shown in Figure 5.5. Therefore, the reduction of GO with $(\text{NH}_4)_2\text{S}_x$ did not depend on the pH. $(\text{NH}_4)_2\text{S}_x$ molecule is decomposed by light and heat, and H_2S , which has a strong reducing ability, was formed. Probably, this H_2S caused the reduction of GO.

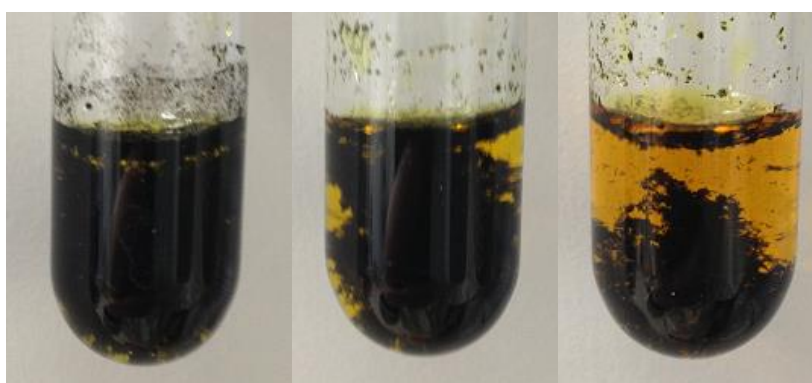


(a)

(b)

(c)

Figure 5.4 Photos of (a) GO aqueous solution, (b) SG in $(\text{NH}_4)_2\text{S}_x$ and (c) SG in methanol.



pH

~9

~10

~11

Figure 5.5 Photos of GO treated with $(\text{NH}_4)_2\text{S}_x$ under conditions of pH ~9 to ~11.

In order to confirm S-doping of GO, XPS spectra were measured as shown in Figure 5.6 (a). Strong C1s peak and O1s peak are observed. This O1s peak is due to the oxygen functional groups in SG and oxygen molecule adsorbed on the surface of SG. Figure 5.6 (b)-(d) show high-resolution XPS spectra of C1s, S2p and N1s respectively. In Figure 5.6 (b), the C1s peak is broad, which indicates that carbon atoms were functionalized with various functional groups. In Figure 5.6 (c), S2p peak can be observed, which indicates that sulfur existed in SG. This spectrum can be deconvoluted into 3 single peaks. The peaks at 164.2 eV and 165.4 eV correspond to S2p_{3/2} and S2p_{1/2} peaks of C-S-C or elemental sulfur. The broad peak at 168.7 eV should arise from some oxidized sulfur (SO_x) [12, 13]. In addition to sulfur, nitrogen also existed as shown in Figure 5.6 (d). This spectrum can be fitted with one single peak. The peak at 401.0 eV corresponds to nitrogen of amide binding or graphitic doped nitrogen [14]. It was reported that an aryl alkyl ketone reacts with (NH₄)₂S_x and converts to amide (Willgerodt reaction) [15]. Probably, GO have alkyl ketone and amide binding was formed by Willgerodt reaction. The content of S; S/C and N; N/C were 3.8 atom% and 1.9 atom% respectively. The probable S-doping mechanism is shown in Figure 5.7. The oxygen functional groups of GO are removed and dangling bonds are formed. These dangling bonds react with (NH₄)₂S_x and sulfur atoms are incorporated into GO sheets.

In order to evaluate the crystallinity of SG, Raman spectra were measured. The samples for Raman spectroscopy were prepared as described in section 5.2.2. Figure 5.8 (a) shows Raman spectrum of monolayer SG. This Raman spectrum is similar to that of reduced GO and radical treated GO (section 4.3) and 2D band is very weak. As shown in Figure 5.8 (b), this spectrum can be deconvoluted to 3 peaks; G band, D band and D** band. The D** band is considered to arise from amorphous carbon [16]. Five samples of monolayer SG were measured. The $I_{D^{**}}/I_G$ ratios were 0.08 ± 0.02 and FWHM of D band were $77 \pm 3 \text{ cm}^{-1}$. These values are comparable to those of radical treated GO (section 4.3). Thus, in addition to sulfuration, treatment with (NH₄)₂S_x improved the crystallinity of GO.

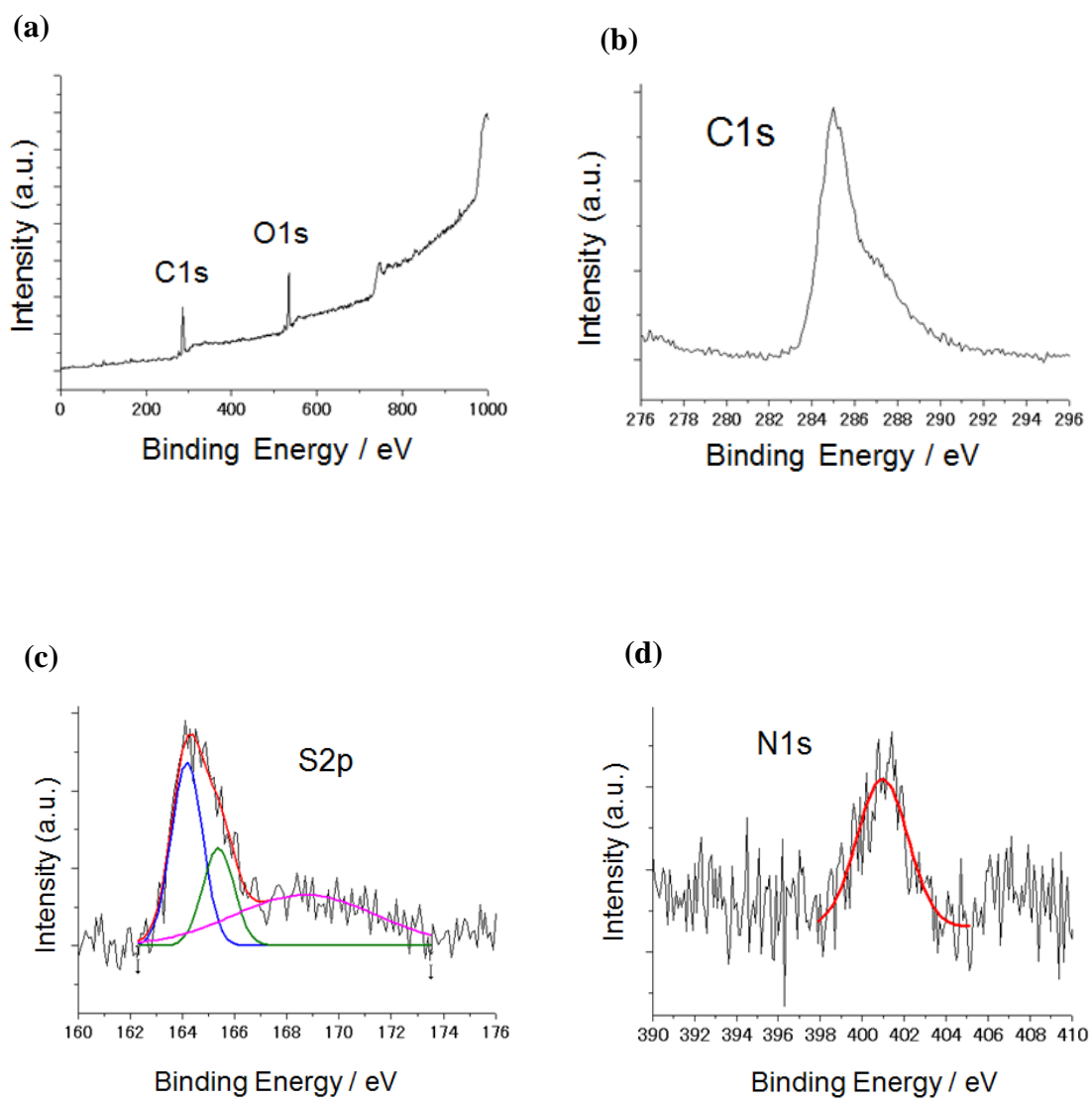


Figure 5.6 (a) XPS spectrum of SG. High resolution XPS spectra of (a) C1s, (b) S2p and (c) N1s.

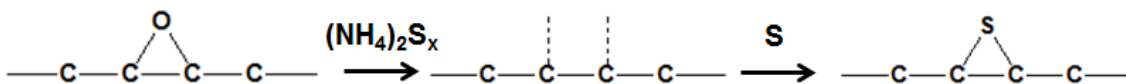


Figure 5.7 Sulfur doping mechanism of GO by $(\text{NH}_4)_2\text{S}_x$.

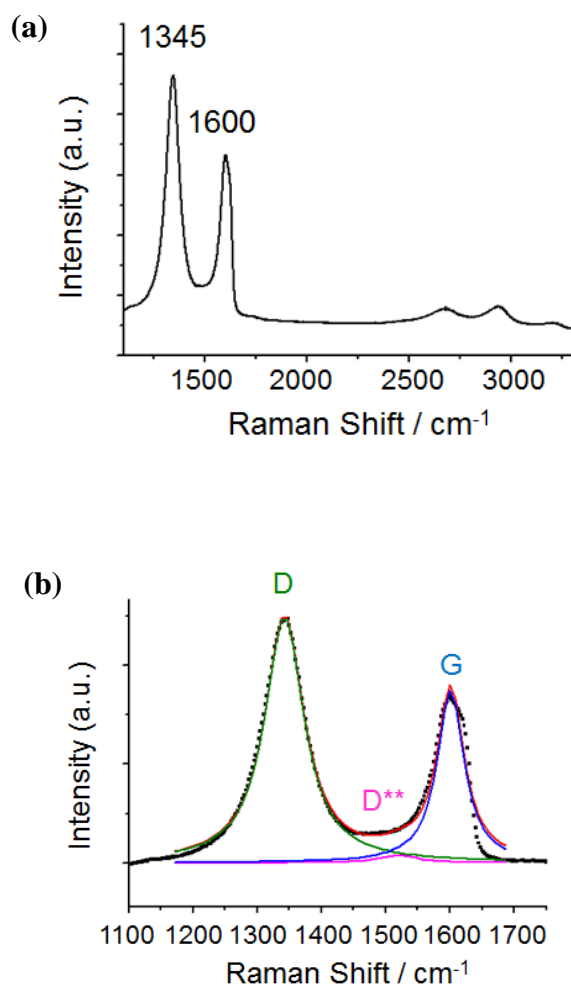


Figure 5.8 (a) Raman spectrum of monolayer SG. (b) Peak fitting of Raman spectrum of monolayer SG.

5.4 Conclusions

In this study, I conducted the sulfuration and reduction of GO by treatment with $(\text{NH}_4)_2\text{S}_x$. When GO aqueous suspension was dropped and left at room temperature, GO changed from brown to black and aggregated. These phenomena indicate that GO was reduced. The existence of sulfur was confirmed by XPS measurement. S2p peaks can be observed and deconvoluted to C-S-C peak or elemental sulfur and oxidized sulfur. In addition to sulfur, nitrogen also existed. The N1s peak can be fitted with one single peak and this may be attributed to the amide binding. The content ratio of S to C was 3.8 atom% and N to C was 1.9 atom%. By Raman spectroscopy, the crystallinity of SG was evaluated. The $I_{\text{D}^{**}}/I_{\text{G}}$ were 0.08 ± 0.02 and FWHM of D band were $77 \pm 3 \text{ cm}^{-1}$. These values indicate that the crystallinity of GO was improved by treatment with $(\text{NH}_4)_2\text{S}_x$.

This process can be conducted in solution process at room temperature. Therefore, this method opens up the opportunity for mass production of graphene and S-doped graphene.

References

- [1] Wang, X.; Li, X.; Zhang, L.; Yoon, Y.; Weber, P. K.; Wang, H.; Guo, J.; Dai, H. *Science* 2009, 324, 768–71.
- [2] Sheng, Z.-H.; Gao, H.-L.; Bao, W.-J.; Wang, F.-B.; Xia, X.-H. *J. Mater. Chem.* 2012, 22, 390-5.
- [3] Liu, Z.-W.; Peng, F.; Wang, H.-J.; Yu, H.; Zheng, W.-X.; Yang, J. *Angew. Chem. Int. Ed.* 2011, 50, 3257–61.
- [4] Yao, Z.; Nie, H.; Yang, Z.; Zhou, X.; Liu, Z.; Huang, S. *Chem. Commun.* 2012, 48, 1027–9.
- [5] Yang, Z.; Yao, Z.; Li, G.; Fang, G.; Nie, H.; Liu, Z.; Zhou, X.; Chen, X.; Huang, S. *ACS Nano* 2012, 6, 205–211.
- [6] Denis, P. A. *Chem. Phys. Lett.* 2010, 492, 251–257.
- [7] Dai, J.; Yuan, J.; Giannozzi, P. *Appl. Phys. Lett.* 2009, 95, 232105.
- [8] Gao, H.; Liu, Z.; Song, L.; Guo, W.; Gao, W.; Ci, L.; Rao, A.; Quan, W.; Vajtai, R.; Ajayan, P. M. *Nanotechnology* 2012, 23, 275605.
- [9] Poh, H. L.; Šimek, P.; Sofer, Z.; Pumera, M. *ACS Nano* 2013, 7, 5262-5272.
- [10] Stankovich, S.; Piner, R. D.; Chen, X.; Wu, N.; Nguyen, S. T.; Ruoff, R. S. *J. Mater. Chem.* 2006, 16, 155.
- [11] Fan, X.; Peng, W.; Li, Y.; Li, X.; Wang, S.; Zhang, G.; Zhang, F. *Adv. Mater.* 2008,

20, 4490–4493.

[12] Herrmann, I.; Kramm, U. I.; Radnik, J.; Fiechter, S.; Bogdanoff, P. J. *Electrochem. Soc.* 2009, 156, B1283.

[13] Kim, J. Y.; Reucroft, P. J.; Taghiei, M.; Pradhan, V. R.; Wender, I. *Energy & Fuels* 1994, 8, 886–889.

[14] Li, X.; Wang, H.; Robinson, J. T.; Sanchez, H.; Diankov, G.; Dai, H. J. *Am. Chem. Soc.* 2009, 131, 15939–44.

[15] McMillan, F. H.; King, J. A. J. *Am. Chem. Soc.* 1948, 70, 4143–4150.

[16] Jawhari, T.; Roid, A.; Casado, J. *Carbon* 1995, 33, 1561–1565.

Chapter 6

Concluding Remarks

In this thesis, I have developed three types of reduction methods of graphene oxide (GO), which were annealing on Ni surface, reaction with free radical and treatment with $(\text{NH}_4)_2\text{S}_x$.

Annealing on Metal Surfaces (Chapter 3)

Reduction of GO is a promising method for mass production of graphene but there is a problem that defects and a few functional groups remained in reduced graphene oxide (rGO). To repair the defects of GO, I annealed GO on metal surfaces.

First, GO was deposited on a Ni foil and annealed at 800 °C under Ar atmosphere. From Raman spectra, the crystallinity of this sample was improved. However, most of GO sheets disappeared because of Ni evaporation. In order to avoid the disappearance of GO, a Ni film was deposited on GO sheets and I annealed GO sheets at the interface of Ni and SiO_2 . In this method, threadlike graphene with the width of approximately 10 μm and large area graphene with the lateral size of about 1 mm were formed.

In order to clarify this reduction mechanism, I changed reduction conditions, which were the quantity of GO, the kind of metal overlayer and annealing temperature. In this experiment, the factor to decide the shape of graphene was investigated by examining what kind of the shape of graphene was formed under each condition. As a result, the factor to decide the shape of graphene was the quantity of the carbon atoms which can dissolve into a metal layer. When all carbon atoms dissolved, threadlike graphene was formed. On the other hand, when not all carbon atoms dissolved and some GO fragments were left, large area graphene was formed. These 2 types of graphene were relatively high quality but thick.

Then, to fabricate thin graphene sheet, I changed the thickness of Ni film and cooling rate. In the case of thin Ni film, graphene with the similar shape of the original GO

sheets was formed and cooling rate had little effect. In contrast, in the case of thick Ni film, cooling rate affected the shape of graphene. In the case of rapid cooling, threadlike graphene was formed and in the case of slow cooling, circular graphene was formed. Judging from Raman spectroscopy, these graphenes were thin.

By this method, graphene can be grown on the desired position of various substrates at relatively low temperatures without use of hydrogen gas.

Reaction with Free Radicals (Chapter 4)

For industrial applications, reduction of graphene in solution process is desirable. So, I conducted reduction of GO in solution process by treatment with four different species. The radical sources were CH_3I , $\text{C}_2\text{H}_5\text{Br}$, $\text{BrC}_2\text{H}_4\text{Br}$ and PhCH_2Br . Raman spectra of GO treated with these reagent indicate that the improvement of crystallinity was achieved in the following order; $\text{CH}_3\text{I} > \text{BrC}_2\text{H}_4\text{Br} > (\text{N}_2\text{H}_4) > \text{C}_2\text{H}_5\text{Br} > \text{PhCH}_2\text{Br}$. Therefore, reduction of GO with CH_3I and $\text{BrC}_2\text{H}_4\text{Br}$ is more effective than hydrazine reduction, which is used generally.

Treatment with $(\text{NH}_4)_2\text{S}_x$ (Chapter 5)

S-doped graphene has been paid much attention for its remarkable properties. Toward mass production of S-doped graphene, I conducted the sulfuration and reduction of GO by treatment with $(\text{NH}_4)_2\text{S}_x$. From XPS spectra, the existence of sulfur was confirmed and the content of sulfur to carbon was 3.8 atom%. Judging from Raman spectra, the crystallinity of GO was improved with the treatment with $(\text{NH}_4)_2\text{S}_x$. In this method, sulfuration and reduction can be achieved in one-pot process.

In conclusion, these reduction methods can be conducted under relatively mild and safe condition as compared with previous methods and thus are considered to be suitable for mass production of graphene from graphene oxide.

Acknowledgement

I would like to express my cordial gratitude to my supervisor, Prof. Koichiro Saiki. He gave me insightful comments and tremendous support. Without his guidance and persistent help this dissertation would not have been possible.

I owe my deepest gratitude to Prof. Takehiko Sasaki for valuable advice and helpful comment.

I am deep grateful to Dr. Seiji Obata. I have had the tremendous support and considerable encouragement of him.

I would like to offer my special thanks to Dr. Gaku Imamura. His meticulous comments were an enormous help to me.

I want to thank all members of Saiki laboratory for enormous help.

Finally, I would like to show my greatest appreciation to my family for moral support and financial support.